Identification of new therapeutic compounds against carbapenemase-producing *Klebsiella pneumoniae* using a novel agar-based high-throughput microarray compound screening approach

By

Zandile Pearl Mahlangu

Thesis presented for the degree of

DOCTOR OF PHILOSOPHY

In the Department of Chemistry, Faculty of Science

University of Cape Town, South Africa

July 2023

Supervisor: Dr Vinayak Singh

Drug Discovery and Development Centre (H3D), University of Cape Town

Co-supervisors: Dr Asongwe Lionel Ateh Tantoh and Dr Kabamba Alexandre

NextGen Health, Council of Scientific and Industrial Research (CSIR)

University of Cape Town

The copyright of this thesis vests in the author. No quotation from it or information derived from it is to be published without full acknowledgement of the source. The thesis is to be used for private study or noncommercial research purposes only.

Published by the University of Cape Town (UCT) in terms of the non-exclusive license granted to UCT by the author.

University of Cape Town

Declaration

I, Zandile Pearl Mahlangu, hereby declare that the work on which this thesis is based is my original work (except where acknowledgements indicate otherwise) and that neither the whole work nor any part of it has been or is being submitted for another degree in this or any other university. I authorize the university to reproduce for the purpose of research either the whole or any portion of the contents in any manner whatsoever.

Signature ……..

Date ……....

Dedication

I dedicate this work to my father, Mr. Aaron Majosi Mahlangu, who relentlessly instilled the importance of education in me and never allowed me to think or believe for better alternative. Ngiyathokoza Mgwezane, Rhotjh'elimnyama Amanye Ayakhanya. To my mother, Mrs. Octavia Nelisiwe Mahlangu, who made it her life's mission to ensure that I never drifted from my father's vision (with a little bit of leniency), Ngiyabonga Ndosi, Khumbuza. I will forever be grateful for your selfless efforts.

Acknowledgements

First and foremost, I would like to give thanks to the higher power for giving me will power and perseverance when odds for completing this project seemed to be stacked against me.

"Makabongwe uNkulunkulu ongalahlanga umkhuleko wami nomusa wakhe kimi
Amahubo 66:20"

I wish to express my gratitude to my co-supervisor Dr Lionel Tantoh, who taught me all the fundamentals of microarray printing and gave guidance throughout the cause of this project. I would also like to thank my supervisor Dr Vinayak Singh for taking me on as a student, for the guidance, and all the valuable contributions you made towards the successful completion of this work. To my current and former second co-supervisors, Dr Kabamba Alexandre and Dr Dalu Mancama, I am truly grateful for the support and guidance. Thank you all for giving me exploratory freedom in conducting this project. And lastly, thank you for the kindness, understanding, and patience you showed me, it made the journey bearable.

I extend my deepest gratitude to the strongest pillars of my world, my parents Majosi and Nelisiwe Mahlangu, my brother Simphiwe, my sister Thokozile, and my niece Sibusisiwe for understanding the expectations of my PhD journey and making it mentally and emotionally bearable for me. Thank you boMgwezane.

I would like to thank my colleagues at NextGen Health for support, perspective and educational conversations, and the nuggets of wisdom shared throughout this journey. I'll forever be grateful for making the acquittance. I would also like to thank Dr Sekelwa Cosa and Marcelle Le Roux for coming to my aid with bacterial strains.

This project would have never been possible without the financial support from the Council of Scientific and Industrial Research (CSIR) and giving me access to their exceptional research facilities to conduct my project. I'll forever be grateful for the exposure and participation in the institution's research activities.

Table of Contents

List of abbreviations

AMR	Antimicrobial resistance
ARB	Antibiotic resistance breaker
ATCC	American Type Culture Collection
ATM	Aztreonam
BSL 2	Biosafety level two
CDC	Centers for Disease Control and Prevention
CFU	Colony forming units
CNF	Cellulose nanofiber
cP	Centipoise
CRISPR	Clustered regularly interspaced short palindromic repeats
CSTS	Colistin sulfate
CTXA	Cefotaxime acid
CV	Coefficient of variation
DMSO	Dimethyl sulfoxide
DOX	Doxycycline hyclate
ERY	Erythromycin
ESBLs	Extended-spectrum β-lactamases
FDA	U.S. Food and Drug Administration
G418 sulfate	Geneticin
GENS	Gentamicin sulfate
GPCR	G-protein coupled receptors inhibitor
HDP	High density plate
HEPA	High efficiency particulate air
HPMC	Hydroxypropyl methyl cellulose
HTS	High-throughput screening
IC_{50}	Half-maximal inhibitory concentration
INT	Iodonitrotetrazolium chloride
KANS	Kanamycin sulphate

kDa	Kilodalton
KPC	*K. pneumoniae* carbapenemase
KPC	*Klebsiella pneumoniae* carbapenemase
MDR	Multidrug-resistant
MHA	Muller Hinton agar
MIC	Minimum inhibitory concentration
NDM-1	Delhi metallo-beta-lactamase – 1
NEOS	Neomycin sulfate
NHGRI	National Human Genome Research Institute
OXA-48	Oxacillinase – 48
PBPs	Penicillin-binding proteins
PMBS	Polymyxin B sulfate
PPL	Priority pathogens list
R&D	Research and development
RFP	Red fluorescent protein channel
RGB	Red, green, and blue image
SD	Standard deviation
TIF	Tagged image file
TMP	Trimethoprim
TOB	Tobramycin
TSA	Tryptic soy agar
TSB	Tryptic soy broth
USA	United States of America
WHO	World Health Organization

List of figures

Chapter 1

Chapter 2

Chapter 3

List of tables

Chapter 1

Chapter 2

Chapter 3

Abstract

Klebsiella pneumoniae, a Gram-negative bacterium, is a common cause of hospital-acquired pneumonia, urinary tract infections (UTIs), bacteraemia, septicaemia, and wound/surgical site infections. Over the years, the pathogen developed resistance to most β-lactam antibacterial drugs used in clinical care. The most important of these drugs are carbapenems – a class of broad-spectrum antibiotics reserved for the treatment of infections caused by multidrug-resistant (MDR) bacteria. The emergence of carbapenem resistance has resulted in limited or ineffective treatment options for MDR *K. pneumoniae.* This prompted a global initiative to prioritize this pathogen for new drug discovery and development to reduce the severity of such infections. Therefore, this study aimed to develop a cost-effective high-throughput antibacterial microarray screening platform to accelerate drug screening efforts against carbapenem-resistant *K. pneumoniae*. To achieve this, an agar-based microarray assay, modeled based on the standard disc diffusion assay, was developed by optimizing the assay parameters, including the cellulose nanofiber (CNF) immobilization matrix, polymer component of the printing solution, inoculum, agar thickness, and agar concentration. The optimized parameters for effectively running the high-throughput antibacterial screen were set at 1.5% (w/v) CNF immobilization matrix into which spots were printed, 1.6% hydroxypropyl methylcellulose printing solution – serving as a binding agent for compounds, inoculum density ranging between ~1 x 10^5 and 2 x 10^5 CFU/mL, 0.8% (w/v) seeding agar which formed a ~0.4 mm layer into which printed compounds diffused into and affected bacteria, and 1.5% (w/v) plain agar which formed a ~1.6 mm layer overlaying the thin seeded agar layer. A proof-of-concept of the developed assay was demonstrated by screening a panel of 12 FDA-approved antibacterial drugs against five bacterial strains with varying degrees of drug susceptibility (i.e., *K. pneumoniae* 1705, *K. pneumoniae* 700603, *K. pneumoniae* 33495, *Staphylococcus aureus* 25923, and *Escherichia coli* 25922). Varying patterns and levels of bacterial susceptibility were observed on the platform, with three (polymyxin B sulfate, colistin sulfate, and gentamicin sulfate) and two (polymyxin B sulfate and colistin sulfate) test drugs showing antibacterial activity against *K. pneumoniae* 1705 and 700603, respectively. Drug-susceptible *K. pneumoniae* 33495, *E. coli* 25922, and *S. aureus* 25923 exhibited susceptibilities to six (polymyxin B sulfate, colistin sulfate, gentamicin sulfate, kanamycin sulphate, G418 sulfate, and tobramycin), seven (polymyxin B sulfate, colistin sulfate, gentamicin sulfate, kanamycin sulphate, G418 sulfate, tobramycin, neomycin sulfate), and five (kanamycin sulphate, neomycin sulfate, gentamicin sulfate, G418 sulfate, tobramycin) drugs, respectively. The optimised assay was used to screen a diverse library of 4154 compounds against a carbapenem-resistant *K. pneumoniae* (ATCC BAA 1705) and a drug-

susceptible *K. pneumoniae* (ATCC 33495) strains. The primary screen data was mined for antibacterial hits using an assay specific two-step data analysis method (i.e., combination of *Z*-score data analysis method and image-based analysis). The screening did not yield hits against the carbapenem-resistant *K. pneumoniae*. A secondary screen of 5% of inactive compounds, with *Z*-scores ranging between standard deviations (SD) of -1 and -2, selected from the primary screen against *K. pneumoniae* 1705 and 33495, was conducted to test the accuracy and reliability the of the two-step data analysis method and the hit selection criteria. A percentage agreement of >99% was obtained between the results obtained in the primary screen (using the agar-based microarray assay) and those obtained in the secondary screen (using the broth microdilution assay). The developed assay showed great potential as a rapid primary screening tool for anti-*K. pneumoniae* compounds.

Chapter 1

Literature review

1.1. Introduction

K. pneumoniae is a Gram-negative, nonmotile, encapsulated, lactose-fermenting, facultative anaerobic, rod-shaped bacterium that belongs to the family *Enterobacteriaceae*. *K. pneumoniae* is a widely recognised opportunistic pathogen that causes various clinical manifestations including hospital-acquired pneumonia, urinary tract infections (UTIs), bacteraemia, septicaemia, wound and surgical site infections (Podschun and Ullmann, 1998, Peleg and Hooper, 2010, Foxman, 2014), and community-acquired pyogenic liver abscesses (Lin et al., 2022). The severities of infections caused by this pathogen are commonly exhibited in the elderly, neonates, and immunocompromised patients (Munoz-Price et al., 2013). Over the years, there has been a significant increase in infections caused by MDR *K. pneumoniae*. The increased prevalence is mainly attributed to *K. pneumoniae* developing resistance against carbapenems – a class of broad-spectrum antibiotics reserved for the treatment of severe infections caused by MDR pathogens (Nordmann et al., 2009). *K. pneumoniae* has adapted and selected for carbapenemases, which are versatile β-lactamase enzymes capable of hydrolysing carbapenems (i.e., *K. pneumoniae* carbapenemase – KPC) (Jeon et al., 2015). Thus, necessitating the use of last-resort drugs (polymyxin B and colistin) for treating MDR *K. pneumoniae* infections (Petrosillo et al., 2019, Chen et al., 2022b). However, in recent years, *K. pneumoniae* has also developed resistance against colistin (Capone et al., 2013, Aghapour et al., 2019), with a noteworthy increase in prevalence (Narimisa et al., 2022, Yusof et al., 2022). To date, MDR *K. pneumoniae* is resistant to virtually all drugs in clinical care (Petrosillo et al., 2019). Carbapenem-resistant *K. pneumoniae* is currently regarded as one of the biggest threats to public health worldwide and for this reason, it was prioritized for urgent drug discovery and development (WHO, 2022a).

1.2. The discovery of antibacterial drugs and development of resistance

The discovery of penicillin was one of the most significant discoveries in medical history (McDermott and Rogers, 1982). It was the inception of the antibiotic era and lead to the discovery of powerful antimicrobial drugs that transformed modern medicine and completely changed therapy for infectious diseases (Spellberg and Gilbert, 2009). The golden age of antimicrobial discovery, spanning from the late 1920s to the late 1980s (Silver, 2011), afforded the field of medicine about 140 antimicrobial drugs (Spellberg and Gilbert, 2009), which, until the recent past, significantly alleviated the burden of infectious diseases. The breakthrough with

the discovery of penicillin was short-lived. In 1942, a year following penicillin commercialization, the first case of penicillin-resistant *Staphylococcus aureus* was reported. From this point forth, penicillin resistance increased substantially, gravely impacting the clinical management of bacterial infections (Lobanovska and Pilla, 2017). The mitigation strategy at the time was the development of new classes of antimicrobial drugs and their modifications to solve the resistance problem (Spellberg and Gilbert, 2014). However, bacterial pathogens continued to evolve and acquire new resistance and virulence mechanisms against each newly developed antimicrobial drug (Spellberg and Gilbert, 2014, Lobanovska and Pilla, 2017).

1.3. The WHO's critical and high-priority pathogens

1.3.1. ESKAPE pathogens and their resistance mechanisms

Genetic mutations are a common occurrence among bacterial species. They select traits suitable for adaptation and survival in changing natural habitats (natural selection) (Najafi and Pezeshki, 2014). However, exposure, overuse, and misuse of antibiotics in clinical care and animal husbandry accelerate the rate of bacterial genetic mutations (Michael et al., 2014). To evade and survive antibacterial activity, bacteria need to constantly evolve under unremitting selective pressure, thus resulting in the emergence of multidrug-resistant pathogens.

Bacterial species have all undergone some degree of genetic mutation (from either natural selection or selective pressure) during their lifespan (Najafi and Pezeshki, 2014). However, a panel of six MDR bacterial pathogens collectively termed "ESKAPE" — vancomycin-resistant ***E****nterococcus faecium,* vancomycin and methicillin -resistant ***S****. aureus*, carbapenem-resistant ***K****. pneumoniae,* carbapenem-resistant ***A****cinetobacter baumannii,* carbapenem-resistant ***P****seudomonas aeruginosa,* and carbapenem-resistant ***E****nterobacter* species (Rice, 2008) — rapidly evolved multidrug-resistant mechanisms (Rice, 2008), which include enzymatic inactivation of antibiotics, modification of drug targets, changing cell permeability through porin loss or increase in expression of efflux pumps, and adaptation to mechanical protection provided by biofilm formation (Santajit and Indrawattana, 2016). Hydrolytic inactivation of antibacterial drugs, mediated by enzymes coded by genes in mobile genetic elements, has become the most significant mechanism of resistance among ESKAPE pathogens, on a global scale (Egorov et al., 2018, Varela et al., 2021). The pathogens evade the lethal action of virtually all antibacterial drugs in clinical care, including drugs of last-resort (Nordmann et al., 2009, Pendleton et al., 2013, Ismail et al., 2019). This has significantly affected

infection control in clinical practice. Therefore, these pathogens are critically and highly prioritized for novel drug discovery and development.

1.3.2. Clinical and economic impact of infections caused by ESKAPE pathogens

Increasing hospital-based reports indicate that the prevalence of MDR ESKAPE pathogens diagnosis in bloodstream infections is significantly higher than that of susceptible bacteria (Ramsamy et al., 2018, Marturano and Lowery, 2019). In a study by Marturano and Lowery (Marturano and Lowery, 2019), assessing the United States of America's (USA) data set of over 1.1 million patient encounters between May 2014 and June 2018, it was discovered that ESKAPE pathogens represented 42.2% of species isolated from bloodstream infections. Delays in implementing adequate antibacterial therapy resulted in severe and prolonged infection, which led to a 3.3-day increase in hospital stay, a $5500 increase in the cost of care, and a 2.1% increase in mortality (Marturano and Lowery, 2019). These factors constitute the burden of ESKAPE infections and have a direct negative economic impact due to increased resource utilization, cost of patient care, and societal costs for lost labor supply and productivity (Founou et al., 2017, Marturano and Lowery, 2019, Zhen et al., 2019).

1.4. Challenges in antibacterial development and possible solutions

In the years that followed the golden age of antibiotic discovery, antibiotic discovery efforts declined significantly due to challenges attributed to the difficulties of discovering novel classes of antibiotics, insufficient revenue returns to drive long-term investment in antibiotic discovery and development, and regulatory barriers to market approval (Pew, 2016). The combined effect of these challenges, with much emphasis on the economic aspect of antibiotic research and development (R&D), leads key players in drug discovery to abandon antibiotic R&D (Carroll, 2015, Hu, 2018, Renwick and Mossialos, 2018, Dall, 2019, Stoner, 2020). As a result, the antibiotic pipeline has remained inadequate to handle the global crisis caused by ESKAPE pathogens (WHO, 2022a).

1.4.1. The business of antibacterial drugs

Pharmaceutical companies invest billions of dollars in the drug discovery process – from concept to market (DiMasi et al., 2016). The ultimate goal, following the successful development of a drug, is the return on the investment and earning profit (Pew, 2016), which is achieved by assigning a high cost per unit of the newly developed drug (where a low volume of prescriptions is predicted) or assigning a low cost per unit (where a high volume of prescription is predicted) (Advisory-Board, 2020). This investment recouping strategy can be

applied to drugs in other therapeutic areas, especially those developed for chronic diseases (McKenna, 2019). In contrast, the successful development of an antibacterial drug does not equate to commercial success due to (1) the unpredictable demand for the new drug: fluctuating prevalence of disease, (2) the short-term administration period, and (3) subject to antibiotic stewardship, which is aimed at preserving antibacterial activity and extend their life span (Renwick and Mossialos, 2018, IFPMA, 2021). Moreover, there is a threat of bacteria developing resistance against the newly developed drug, which may result in a complete loss of investment (WEF, 2018). The flawed economic nature and model of the business have led major pharmaceutical companies and start-up companies like Novartis, AstraZeneca, Sanofi, Allergan, Octagon, Achaogen, and Melinta to discontinue antimicrobial R&D (Carroll, 2015, Hu, 2018, Dall, 2019, Stoner, 2020).

1.4.2. Incentivizing antibacterial research and development

Combating antibacterial resistance seems impossible without effective antibacterial therapy. According to O'Neill (O'Neill, 2016), 700 000 people die each year from drug-resistant infections, this number is estimated to reach 10 million by 2050 if the problem is not addressed. Mitigating the severity of the problem requires multifaceted strategies. The most crucial strategy is amending the current business model to include pull incentives suitable for attracting investors. According to the World Economic Forum (WEF)(WEF, 2018), the current business model is mainly structured to support basic and pre-clinical antibacterial research (push incentives), however, it is insufficient to drive development through to clinical research and commercialization. Stakeholders representing public health, both large and small antibiotic developers, academic institutions, and funding organizations made a plea to policymakers for balanced incentives structured to support R&D (push) and reward successful drug development and commercialization (pull), in a manner that ensures patient access and appropriate stewardship (DRIVE-AB, 2018). The recommended incentive package includes non-refundable grants for R&D, tax incentives, reimbursement reforms, market reforms, delinking profitability of new drugs from units sold, and antibiotic susceptibility bonus (DRIVE-AB, 2018, Morel et al., 2020, IFPMA, 2021).

1.4.2.1. Initiatives implemented to support antibacterial value chain

Infectious Diseases Society of America's (IDSA's) early awareness of the magnitude and impact of antibacterial resistance was a fundamental foundation from which today's initiatives are built (IDSA, 2004, Boucher et al., 2009). The awareness fostered collaborations between the public and private sectors to

reinvigorate the antibacterial pipeline and resulted in over 50 initiatives aimed at incentivizing antibacterial R&D (Simpkin et al., 2017). The latest initiatives consist of the following:

(a) Push incentives in the form of funding schemes (grants) supporting various stages of R&D:

Early-stage R&D i.e., Combating Antibiotic Resistant Bacteria Biopharmaceutical Accelerator (CARB-X), has invested ~$361 million in 92 projects since its launch in 2016 for the development of innovative antibiotics, rapid diagnostics, vaccines, and related products addressing antibiotic resistance (CARB-X, 2021).

Projects in all stages of the antibacterial value chain i.e., Global Antibiotic Research and Development Partnership (GARDP), a collaborative initiative between WHO and Drugs for Neglected Diseases *initiative* (DND*i*), aims to raise $500 million to be used in the commercialization of at least 5 antibiotics by 2025 (Piddock, 2018).

Clinical research: AMR Action Fund is an International Federation of Pharmaceutical Manufacturers & Associations (IFPMA) initiative that seeks to support clinical research for innovative antibiotics aimed at high-priority bacterial pathogens. Collaborators of the fund pledged $1 billion intending to commercialize approximately four new antibiotics by 2030 (IFPMA, 2020).

(b) Pull incentives supporting commercialization and continuity – bills introduced and passed:

Pioneering Antimicrobial Subscriptions to End Up-surging Resistance (PASTEUR) Act of 2023: Representatives Mike Doyle and Drew Ferguson, Senators Michael Bennet and Todd Young re-introduced the PASTEUR Act to the US Senate in 2023 (the bill is yet to be passed). The major purpose of the Act will be to delink drug revenue from sales. This will be achieved by engaging in transitional subscription contracts with the government and antimicrobial developers. Thus, creating a predictable return on the investment. Antimicrobial stewardships are an integral part of the Act, drug developers are required to provide an "appropriate use" plan when they enter into the subscription contract (PASTEUR, 2023). A trial version of the PASTEUR Act was implemented in the United Kingdom in June 2020 (Mahase, 2020). The government will "pay pharmaceutical manufacturers up to £100 million to develop

and market novel antibiotics based on the assigned value to the antibiotics rather than volume of antibiotics sold" (Chang and Knight, 2020).

Developing an Innovative Strategy for Antimicrobial Resistant Microorganisms (DISARM) Act of 2019: the DISARM Act was introduced in the US House of Representatives by Senators Johnny Isakson and Robert Casey in 2019, to "encourage development and use of DISARM antimicrobial drugs" (DISARM, 2019). If passed, the act will address the issue of reimbursement following drug commercialization. No progress has been made in the process of signing this bill into law (Eisinger et al., 2023).

Generating Antibiotic Incentives Now (GAIN) Act of 2012: the GAIN Act, was passed into law in 2012 as part of the Food and Drug Administration Safety and Innovation Act (FDASIA), incentivizes antibiotic development by extending market exclusivity (patent protection) by five years for antibacterial and antifungal drugs designated as qualified infectious disease product (QIDP) and under the Federal Food, Drug, and Cosmetic Act (FD&C Act). Food and Drug Administration (FDA) granted 187 QIDP designations since the enactment of the Act to the end of 2020 (Darrow and Kesselheim, 2020).

(c) Pipeline coordinators:

AMR Industry Alliance was established "as a venue for advancing partnerships across the public and private sectors, promoting proactive industry actions and partnerships, and enabling coordination across subsectors". This ~100-member alliance is committed to promoting R&D, access, appropriate use (stewardship), and monitoring the impact of antibiotics on the environment (AMR-Industry-Alliance, 2022).

Collaborative efforts against antibacterial resistance have resulted in a great number of push incentives than pull incentives (Simpkin et al., 2017). It is therefore the responsibility of governments around the world to prioritize and accelerate the implementation of pull incentives. If packaged correctly, they will attract investors and ensure the reinvigoration of the antibiotic pipeline.

1.5. *K. pneumoniae*

K. pneumoniae is a widely recognized opportunistic pathogen that causes various clinical manifestations including hospital-acquired pneumonia, UTIs, bacteremia, septicemia, wound and surgical site infections (Podschun and Ullmann, 1998, Peleg and Hooper, 2010, Foxman, 2014), and community-acquired pyogenic liver abscesses (Chen et al., 2022a). It is the second leading cause of UTIs, accounting for 6 – 17% of all nosocomial infections (Podschun and Ullmann, 1998). In recent years it developed multiple mechanisms of antibacterial resistance which enables it to evade the activity of virtually all antibacterial drugs in clinical care (Rice, 2008), hence, it is a member of the ESKAPE panel and a critically prioritized pathogen in the global priority pathogens list (global PPL) (WHO, 2017).

1.5.1. *K. pneumoniae* virulence factors

K. pneumoniae uses various virulent mechanisms such as capsular polysaccharides, lipopolysaccharides (LPS), adhesive pilus, and siderophores to evade the host's immune defenses, colonize, and cause infection (Podschun and Ullmann, 1998):

(a) Capsular polysaccharide – *K. pneumoniae* typically expresses a large high molecular weight capsular polysaccharide, a crucial virulent factor associated with the protection of the bacterium against opsonization and phagocytosis, antibacterial peptides, and preventing deposition of complement on the bacterial surface (Cortes et al., 2002).

(b) Lipopolysaccharides (LPS) – LPS are amphipathic molecules composed of lipid A, core oligosaccharide, and long polysaccharide side chain called O (which make up the outermost component of LPS). The O antigen of the LPS confers resistance to host serum by preventing the binding of complement proteins (C1p and C3q) to the bacterial cell membrane. Thus, protecting *K. pneumoniae* from complement-mediated membrane lysis and opsonisation (Alberti et al., 1996, Doorduijn et al., 2016). They form a major component of *K. pneumoniae's* outer membrane.

(c) Adhesive pili – *K. pneumoniae* possess two morphologically and functionally distinct adhesive pili (type 1 and type 3) which facilitate adherence to target host cells, a crucial step in establishing colonization and infection (Podschun and Ullmann, 1998, Murphy et al., 2013).

(d) Siderophores – *K. pneumoniae* produces low molecular weight iron (Fe^{3+}) chelating molecules, siderophores, to acquire and solubilize ferric iron from the host which is crucial for bacterial growth and propagation within the host (Holden and Bachman, 2015, Wilson et al., 2016).

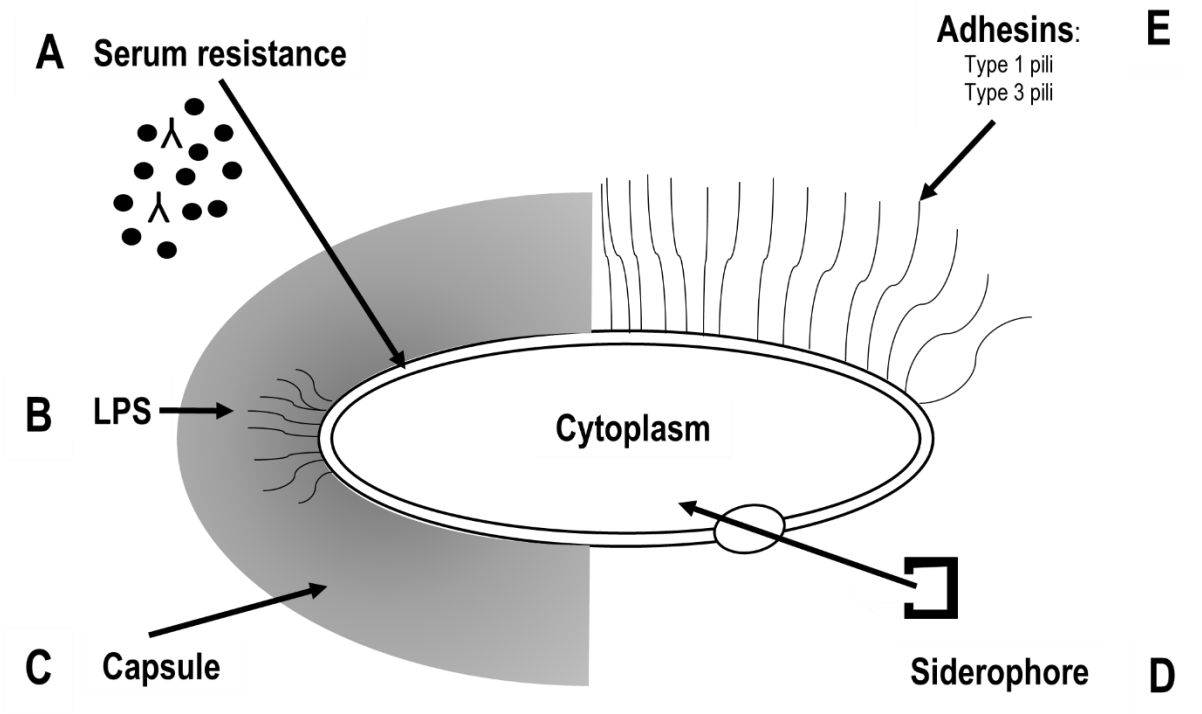

Figure 1.1. Schematic presentation of *Klebsiella* virulence factors. (A) serum resistance, (B) lipopolysaccharides (LPS), (C) capsular polysaccharide, (D) siderophores, and (E) adhesive pili (Podschun and Ullmann, 1998).

1.5.2. Carbapenems and *K. pneumoniae* carbapenemases

1.5.2.1. Clinical importance of carbapenems

Carbapenems (imipenem, ertapenem, meropenem, and doripenem) belong to the β-lactam class of antibacterial drugs (Codjoe and Donkor, 2017), showing broad-spectrum activity against both Gram-negative and Gram-positive bacteria (Brown et al., 1976, Papp-Wallace et al., 2011). This class of drugs has great potency against hydrolytic enzymes capable of hydrolyzing the four-membered β-lactam ring in both penicillin and extended-spectrum third-generation cephalosporins (β-lactamases) (Abraham and Chain, 1940, Moellering et al., 1989). They exert their potency by binding penicillin-binding proteins (PBP) (Yang et al., 1995) and prevent bacteria from completing transpeptidation (cross-linking) of peptidoglycan strands, thus preventing the synthesis of the intact bacterial cell wall (Hashizume et al., 1984, Bugg and Walsh, 1992, Papp-Wallace et al., 2011).

Carbapenems came into standard clinical use during the surge of bacteria expressing extended-spectrum beta-lactamases (ESBLs) (Elshamy and Aboshanab, 2020). These became the most effective treatment for severe infections due to their broad spectrum activity and resistance to hydrolysis by ESBLs (Papp-Wallace et al., 2011). Their antibacterial activity was incomparable to other drugs used for the same purpose at the time, hence, these were referred as drugs of last-resort (Bassetti et al., 2009). However, with excessive use, bacterial pathogens eventually developed resistance against them and clinical outcomes of MDR carbapenemase infections became virtually reflective of the pre-antibacterial era (Durante-Mangoni et al., 2019).

1.5.2.2. Resistance mechanisms of *K. pneumoniae* against carbapenems

K. pneumoniae and other members of the ESKAPE panel acquired multiple mechanisms of resistance against carbapenems including the expression of efflux pumps resulting in active expulsion of antibiotics from the periplasmic space (Padilla et al., 2010), loss of porins resulting in reduced entry of antibiotics into the bacteria's periplasmic space (Kim et al., 2007), and the inactivation of drugs by expressing hydrolytic enzymes (Rodriguez-Martinez et al., 2009). The inactivation of antimicrobial drugs by the expression of hydrolytic enzymes has become the most prevalent mechanism of resistance (Rodriguez-Martinez et al., 2009), especially the expression of carbapenemases. These enzymes represent the most versatile family of β-lactamases known to have the broadest spectrum of hydrolytic activity among all β-lactamases (Doi and Paterson, 2015, Stoesser et al., 2017). *K. pneumoniae* carbapenemase (KPC), New Delhi metallo-beta-lactamase – 1 (NDM-1), and the oxacillinase - 48 (OXA-48) carbapenemases are of clinical importance and most prevalent in *K. pneumoniae* (Nordmann and Poirel, 2014).

1.5.2.3. Molecular classification and epidemiology of *K. pneumoniae* carbapenemases

Carbapenemases most prevalent to *K. pneumoniae* belong to Amber class A β-lactamases (i.e., KPCs), class B metallo-β-lactamases (i.e., NDM-1), and class D oxacilinases (i.e., OXA-48) (Nordmann and Poirel, 2014), based on the amino acid sequence in the Ambler molecular classification system (Ambler, 1980). Class A and D β-lactamases hydrolyze their substrates by forming an acyl-enzyme through an active site serine. Hence, these are referred as serine β-lactamases. Whereas Class B β-lactamases utilize at least one active-site zinc ion to facilitate β-lactam hydrolysis (Ambler, 1980, Bush and Jacoby, 2010).

K. pneumoniae carbapenemase (KPC)

KPC-1 is the most prevalent of the three carbapenemases *in K. pneumoniae* (Nordmann et al., 2009, Munoz-Price et al., 2013). Since its first isolation in 1996 in North Carolina (United States of America USA) (Yigit et al., 2001), KPC-1 has spread worldwide with an endemic and predominant spread in the USA, some parts of South America, China, Poland, Greece, Italy, and Israel (Figure 1.2) (Munoz-Price et al., 2013). The first *bla*$_{KPC-1}$ gene encoding KPC-1 enzyme was isolated from a ~50-kb non-conjugative plasmid, an extrachromosomal double-stranded DNA that replicate independently of the host's genome (NHGRI, 2023). In recent years, it is predominantly isolated from a Tn*4401* transposon (Chen et al., 2014, Sheppard et al., 2018), which is a DNA sequence with the ability to insert into variable positions of the host genome (Bourque et al., 2018). Antibacterial hydrolysis studies conducted by Yigit et al. (Yigit et al., 2001) revealed that the spectrum of hydrolytic activity of KPC-1 was not only limited to carbapenems, but also extended to penicillins, cephalosporins, and monobactams.

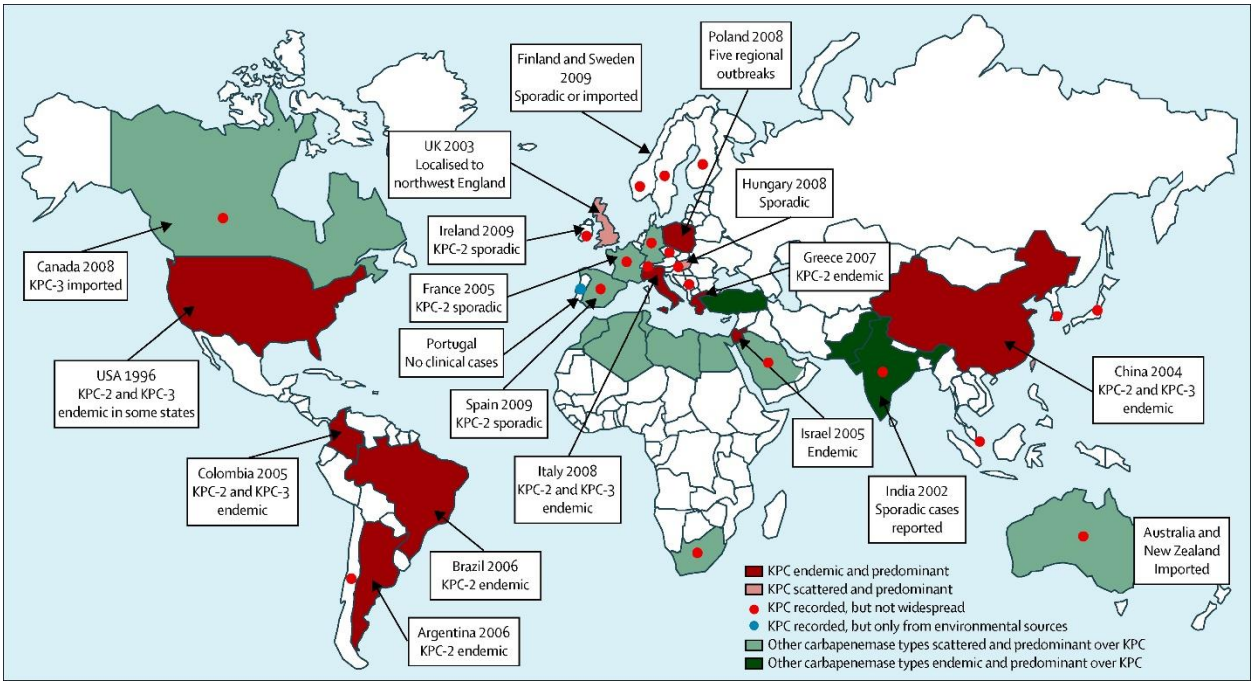

Figure 1.2. Geographical distribution of KPC producing *K. pneumonia*e (Munoz-Price et al., 2013).

New Delhi metallo-beta-lactamase – 1 (NDM-1)

NDM-1 is an Ambler class B metallo-β-lactamase. It was first identified in 2008 from a *K. pneumoniae* 05-506 strain isolated from a urine sample in New Delhi, India (Yong et al., 2009). At the time of its discovery,

NDM-1 conferred hydrolytic activity against all β-lactams except aztreonam. The *bla*$_{NDM-1}$ gene encoding for NDM-1 is located on a 180-kb plasmid along with the *bla*$_{CMY-4}$ gene and class 1 integron complex carrying several antibiotic resistance-conferring genes (Yong et al., 2009). NDM-1 has a worldwide distribution; however, the Asian continent has the highest prevalence, with 58.15% mainly distributed in China and India (Figure 1.3) (Nordmann and Poirel, 2014, Khan et al., 2017).

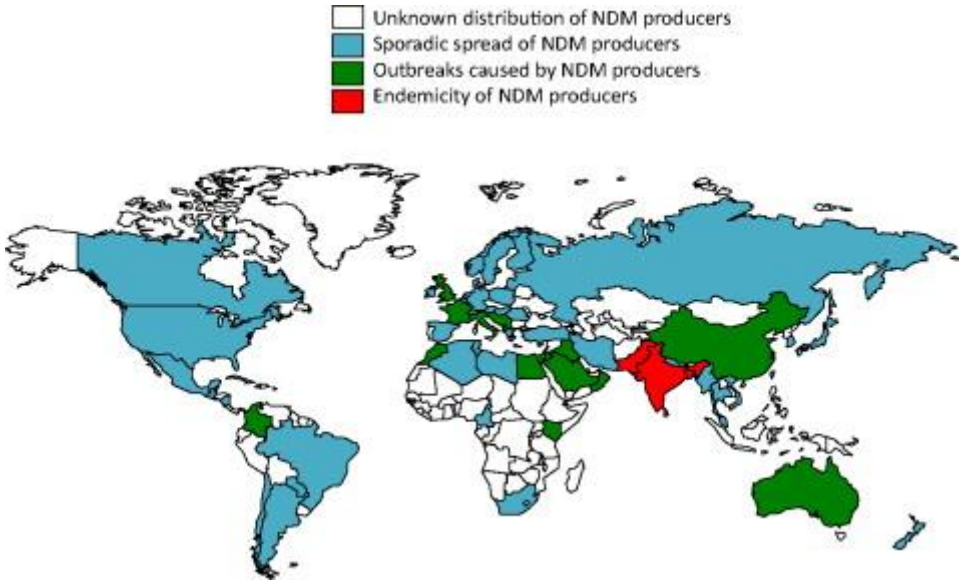

Figure 1.3. Geographical distribution of NDM producing *K. pneumonia*e (Nordmann and Poirel, 2014).

Oxacillinase – 48 (OXA-48)

The first OXA-1 enzyme, named for its affinity to isoxazolyl-type penicillins like oxacillin, was first identified in the early 1970s (Hedges et al., 1974). Since this discovery, 790 OXA-variants have been identified (Sawa et al., 2020) and given a unique number based on the chronological order in which they were discovered (June et al., 2014). Earlier OXA enzymes were characterized by their ability to efficiently hydrolyze isoxazolyl-type –lactams. However, over the years, class-D β-lactamases evolved and now have subfamilies with hydrolytic activity against carbapenems or cephalosporins (June et al., 2014). One such evolution was observed with OXA-48, the first of its kind to be isolated from a *K. pneumoniae* strain in 2001 at the Istanbul (Turkey) Faculty Hospital from the urinary tract of a 54-year-old man with a urinary tract infection and skin burns (Poirel et al., 2004). According to Poirel et al. (Poirel et al., 2004), the enzyme had strong carbapenem-hydrolyzing activity. The OXA-48 enzyme is encoded by the *bla*$_{OXA-48}$ gene located on a ~70 kb plasmid, where it is integrated through the acquisition of the Tn*1999* composite transposon which doesn't carry any other resistance genes

(Poirel et al., 2012). From its country of origin, OXA-48 has spread globally, with an endemic spread in Libya, Western Sahara, Morocco, Egypt, India, and Bangladesh; outbreaks and sporadic spread in the USA, Canada, Australia, parts of South America, and some parts of Europe and Africa (Figure 1.4) (Nordmann and Poirel, 2014).

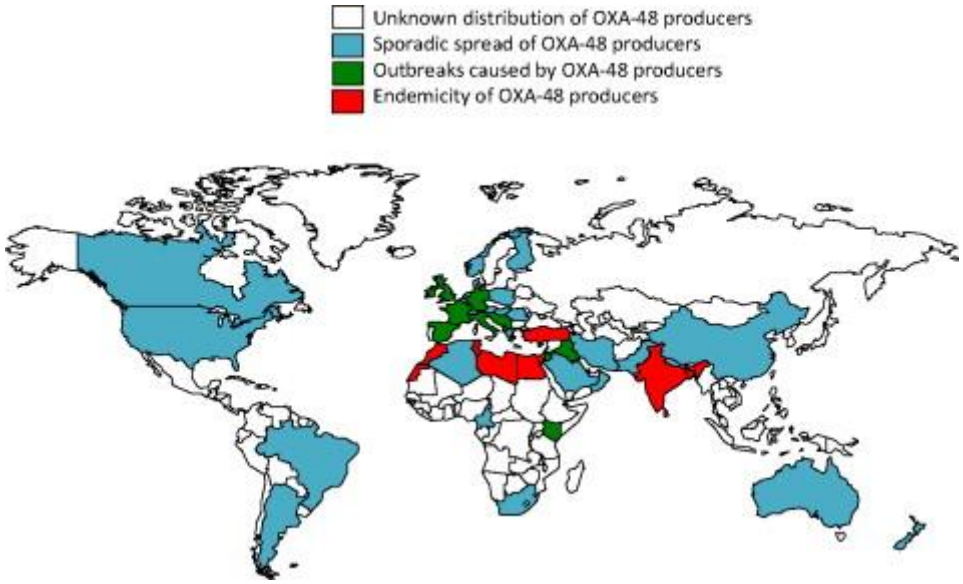

Figure 1.4. Geographical distribution of OXA-48 producing *K. pneumonia*e (Nordmann and Poirel, 2014).

1.5.2.4. Dissemination of *K. pneumoniae bla* genes

From the time of discovery in their country of origin, *K. pneumoniae bla* genes disseminated rapidly to neighboring countries and eventually acquired global status, causing outbreaks, endemic, and sporadic diseases (Nordmann et al., 2009, Munoz-Price et al., 2013). The rapid global spread of the *bla* genes is mainly attributed to their placement in mobile genetic elements (MGEs), facilitated by horizontal gene transfer (HGT), which mobilizes resistant genes from one bacterial cell to the next (Bowers et al., 2015, Potter et al., 2016). This is proven by the fact that at the time of their discovery, *K. pneumoniae bla* genes were isolated from plasmids (Yigit et al., 2001, Poirel et al., 2004, Yong et al., 2009). Transposons have also been shown to play a crucial role in the dissemination of *bla genes*, especially bla_{KPC} genes (Tang et al., 2017, Leclerc et al., 2019). The HGT is achieved through three processes including transduction (transfer of resistance genes through bacteriophages), transformation (direct uptake of naked DNA fragments released from live or dead bacteria), and conjugation (transfer of resistance genes through direct contact) (CDC, 2019). Of the three processes, conjugation is the most efficient and dominant mechanism of gene transfer utilized by *K.*

pneumoniae and the most important driver of resistance to date (Tofteland et al., 2013, Zheng et al., 2016). Positioning of *K. pneumoniae bla* genes in MGEs and the ease of spread facilitated by HGT have also enabled their spread outside the *K. pneumoniae* clonal lineage. The genes are now reported in other members of the *Enterobacteriaceae* family: *E. coli* (Govindaswamy et al., 2019), Enterobacter spp., *Proteus mirabilis* (Sheng et al., 2010), *Salmonella* spp. (Fernandez et al., 2018), and the non-fermenters: *P. aeruginosa* (Morales et al., 2018, Verma et al., 2019), and *A. baumannii* (Wasfi et al., 2021).

1.5.2.5. Clinical impact of carbapenemases

K. pneumoniae infections, once successfully treated with antibacterial drugs, have become some of the biggest global health threats of the 21st century (WHO, 2017). The evolution of *K. pneumoniae* into a multidrug-resistant pathogen, especially its resistance to carbapenems, has significantly limited treatment options for this pathogen (Petrosillo et al., 2019, Spaziante et al., 2020). As a result, infections are predisposed to cause life-threatening bacteremia (Zhang et al., 2018) and sepsis (Falcone et al., 2016), with probable outcomes such as prolonged hospital stays, high morbidity, and mortality rates (Falagas et al., 2014, Cienfuegos-Gallet et al., 2019). Falcone and colleagues reported a mortality rate of 39.6% from a retrospective study conducted on 111 patients who developed septic shock due to KPC-producing *K. pneumoniae* (Falcone et al., 2016). According to this study, the inclusion of colistin in the treatment regimen increased the chances of patient survival and resistance. Apart from some positive clinical efficacy observed, colistin was associated with inadequate serum level concentrations. This necessitated the use of high colistin concentration, which led to impaired renal function, acute kidney injury, and subsequent death. A meta-analysis study evaluating clinical outcomes in patients hospitalized with carbapenem-resistant *Enterobacteriaceae* (CRE) infections showed that infections caused by carbapenem-resistant *K. pneumoniae* and KPC-producing pathogens have mortality rates 2- to 3-fold higher than those with infections caused by carbapenem-susceptible *Enterobacteriaceae* (CSE). Delays in receipt of early appropriate empiric therapy were assumed to be the cause of this outcome (Martin et al., 2018). This finding was consistent with the study conducted by Lodise and colleagues, where they showed that “patients who received delayed appropriate therapy had longer durations of antibiotic therapy and hospital length of stay, higher costs, lower likelihood of discharge to home, and greater likelihood of the composite mortality outcome” (Lodise et al., 2019).

1.6. The current state of the antibacterial pipeline for carbapenem-resistant *K. pneumoniae*

Periodical assessment and analysis of the antibacterial pipeline are crucial in determining the effectiveness of implemented initiatives and incentives (WHO, 2022a). It also aids in identifying gaps in the antibacterial value chain that require further investment. As such, the WHO publishes annual reports on the state of the antibacterial pipeline, to determine how it responds to the global PPL (WHO, 2022a). The pipeline was assessed for its response to carbapenem-resistant *K. pneumoniae* as follows:

1.6.1. Approved drugs

Twelve antibacterial drugs received market authorization between June 2017 and November 2021, with four showing the anti-carbapenemase activity (Table 1.1) (WHO, 2022a). Vaborbactam is a β-lactamase inhibitor belonging to a novel cyclic boronate class of antibiotics with activity against KPC-2 and KPC-3 carbapenemases. It was optimized for use in combination with meropenem (carbapenem), where it functions as a resistance breaker (Castanheira et al., 2016, Lomovskaya et al., 2017).

Cefiderocol is a cephalosporin conjugated to an iron (Fe^{3+})-chelating molecule (siderophore). Lowered cell-membrane permeability, due to the loss of outer membrane porins, is one of the major virulence mechanisms in pathogenic bacteria (Fernández and Hancock, 2012). Therefore, cefiderocol takes advantage of pathogen's essential requirement for iron, by using the iron complex pathway to cross bacterial/cell membrane. Once inside the periplasmic space, it binds to PBPs, which disrupts the cell wall formation. Cefiderocol has activity against serine carbapenemases (KPC and OXA-48) and metallo-carbapenemases (NDM) (Wu et al., 2020).

Relebactam, a derivative of avibactam belonging to the diazabicyclooctane class, is a β-lactamase inhibitor approved for use in combination with cilastatin sodium (a renal dehydropeptidase inhibitor) and imipenem (a broad spectrum β-lactam antibiotic). Relebactam binds covalently to the active site of serine β-lactamases, thus preventing imipenem hydrolysis (Smith et al., 2020). This drug combination has antibacterial activity against KPCs (2 and 3) and OXA-48 carbapenemases.

Plazomicin is a semi-synthetic aminoglycoside, derived from sisomicin (Aggen et al., 2010), with an ability to evade most aminoglycoside-modifying enzymes (AMEs) of clinical importance. It exerts its antibacterial action by binding the aminoacyl-tRNA recognition site (A-site) of the 16S rRNA, where it interferes with ribosomal protein synthesis (Doi et al., 2016). Plazomicin demonstrated a wide spectrum of activity against

Enterobacteriaceae hydrolytic enzymes, including ESBLs (TEM, SHV, CTX-M, and AmpC), serine carbapenemases (KPC-2 and KPC-3), and oxacillinase (OXA-48) (Clark and Burgess, 2020).

Table 1.1. Anti-carbapenamase drugs approved between 2017 and 2021 (WHO, 2022a).

Name	Antibacterial class	Route of administration	Indications	Approval date	Market authorization holder	Innovation	Expected activity
Vaborbactam + meropenem (Vabomere)	Boronate BLI + carbapenem	Intravenous	cUTI	FDA (8/2017) EMA (11/2018)	Melinta	New chemical class	ESBL, KPC (2&3), OXA-48
Plazomicin (Zemdri)	Aminoglycoside	Intravenous	cUTI	FDA (8/2018)	Achaogen (Cipla USA/ QiLu Antibiotics, China)	—	ESBL, KPC (2&3), OXA-48
Relebactam + imipenem/ cilastatin (Recarbrio)	DBO-BLI + carbapenem/ degradation inhibitor	Intravenous	cUTI, cIAI	FDA (7/2019)	Merck Sharp and Dohme	—	ESBL, KPC (2&3), OXA-48
Cefiderocol (Fetroja)	Siderophore cephalosporin	Intravenous	cUTI	FDA (11/2019) EMA (4/2020)	Shionogi	—	ESBL, KPC (2&3), OXA-48, NDM

BLI: β-lactamase inhibitor, DBO: diazabicyclooctane, cUTI: complicated urinary tract infection, cIAI: complicated intra-abdominal infection, ESBL: extended-spectrum β-lactamase, KPC: *Klebsiella pneumoniae* carbapenemase, OXA: oxacillinase, NDM: New Delhi metallo-beta-lactamase, —: no innovation.

1.5.2. Antibacterial agents in clinical development

The recently updated clinical development pipeline has 27 “traditional” antibacterial agents targeting WHO’s priority pathogens (WHO, 2022a), with 11 showing activity against one or more *K. pneumoniae* carbapenemases (Table 1.2). Taniborbactam, a bicyclic boronate, is the only drug in phase three of development, the rest are in phase one. All drugs, except for SPR-206 (a nano-peptide analog of polymyxin) and MRX-8 (a novel polymyxin analogue), are β-lactamase inhibitors (β-lactam potentiators). Taniborbactam and VNRX-7145 (a cyclic boronate) belong to new antibacterial classes and rest of the antibacterial agents are derivatives of existing antibiotic classes.

Table 1.2. Anti-carbapenemase drugs in clinical development (WHO, 2022a).

Name	Antibiotic class	Route of administration	Clinical phase	Developer	Innovation	Expected activity
SPR-206	Polymyxin	Intravenous	1	Spero Therapeutics	—	KPC, OXA-48, NDM
ARX-1796 (oral avibactam prodrug)	DBO-BLI + ß-lactam	Oral	1	Arixa Pharmaceuticals / Pfizer11	—	KPC, OXA-48
Taniborbactam (VNRX-5133) + cefepime	Boronate-BLI + cephalosporin	Intravenous	3	VenatoRx Pharmaceuticals / GARDP	New chemical class	ESBL, KPC (2&3), OXA-48, NDM
Zidebactam + cefepime	DBO-BLI/PBP2 binder + cephalosporin	Intravenous	1	Wockhardt	—	ESBL, KPC (2&3), OXA-48
ETX0282 + cefpodoxime proxetil	DBO-BLI/PBP2 binder9 + β-lactam (cephalosporin)	Oral	1	Entasis Therapeutics	—	KPC (2&3), OXA-48
VNRX-7145 + ceftibuten	Boronate-BLI + β-lactam (cephalosporin)	Oral	1	VenatoRx Pharmaceuticals	New chemical class	ESBL, KPC (2&3), OXA-48
QPX7728 + QPX2014	Boronate-BLI + unknown	Intravenous	1	Qpex Biopharma	—	ESBL, KPC (2&3), OXA-48, NDM
QPX7728 + QPX2015	Boronate-BLI + undisclosed oral β-lactam	Oral and intravenous	1	Qpex Biopharma	—	ESBL, KPC (2&3), OXA-48, NDM
ARX-1796 (oral avibactam prodrug)	DBO-BLI + β-lactam (undisclosed)	Oral	1	Arixa Pharmaceuticals / Pfizer	—	KPC, OXA-48
OP0595 (nacubactam) + meropenem	DBO-BLI/PBP2 binder9 + β-lactam (carbapenem)	Intravenous	1	Meiji Seika	—	ESBL, KPC (2&3), OXA-48
MRX-8	Polymyxin	Intravenous	1	MicuRx	—	Gram-negative infections

BLI: β-lactamase inhibitor, DBO: diazabicyclooctane, cUTI: complicated urinary tract infection, cIAI: complicated intra-abdominal infection, ESBL: extended-spectrum β-lactamase, KPC: *Klebsiella pneumoniae* carbapenemase, OXA: oxacillinase, NDM: New Delhi metallo-beta-lactamase, —: no innovation.

1.5.3. Antibacterial agents in preclinical development

There are currently 217 products in the preclinical pipeline. The preclinical pipeline is highly diverse with 113 projects focused on direct and indirect-acting small molecules, 35 on direct and indirect-acting peptides, 19 on direct and indirect-acting large molecules, 28 on bacteriophage products, and 22 focused on other non-traditional antibacterial agents (including biotherapeutics, nucleic acid-based products, immunomodulators, microbiome modifying agents, and decolonization agents). Of the 217 products, only 58 have antibacterial activity against *K. pneumoniae* (WHO, 2022a).

1.6. Summary

Difficulties in discovering novel classes of antibiotics and finding new drug targets are well-known "rate-limiting steps in antibacterial development" (Silver, 2011), and it is evident in the current pipeline where the majority of antibacterial drugs are derivatives of known classes. This has led to the exploration of alternative strategies such as drug-potentiating and non-traditional antibacterial agents. Drug potentiating is a strategy explored to salvage existing antibacterial drugs by combating resistance mechanisms employed against them. It involves the use of antibiotic resistance breakers: these are drugs without direct or with insufficient antibacterial activity but are capable of restoring antibacterial activity (Brown, 2015, Torres et al., 2018, Laws et al., 2019, Theuretzbacher et al., 2020). Drug potentiation greatly increases efficacy, decreased toxicity, and preserves susceptibility of existing antibacterial drugs (Landahl, 1958, Foucquier and Guedj, 2015, Theuretzbacher et al., 2020), and these agents made up 75% of anti-carbapenemases presented in Table 1.1 and 1.2.

The global surge of antibacterial resistance generated renewed interest in non-traditional antibacterial drugs, involving novel antibacterial mechanisms and targets. Non-traditional antibacterial agents in the current pipeline include antibodies (neutralizing immune-evading toxins; targeting surface proteins facilitating adhesion – pili and membrane proteins – LPS) (Motley et al., 2019), bacteriophages and phage-derived enzymes (producing lytic proteins which lyse the bacterial cell wall) (Delbrück, 1940), microbiome-modulating agents (modulating intrinsic defense mechanisms against bacterial colonization and restoring disrupted microbiota) (Quigley and Gajula, 2020), immunomodulators (modifying host's immune response to infection by increasing immuno-stimulators) (Bascones-Martinez et al., 2014), and virulence disruptors – disrupting bacterial pathogenic mechanisms (Cegelski et al., 2008). About 32 of these unconventional antibacterial agents are in various phases of clinical development and about 50 are in preclinical development. Both Gram-

negative and Gram-positive bacteria are targeted, though the spectrum of their activity is mainly limited to one organism except for Bacteriophage (bacteriophages/phage-derived enzymes), Rhu-pGSN – rhu-plasma gelsolin (immunomodulating agent), and TRL1068 (antibodies), which have nonspecific target against both Gram-positive and Gram-negative pathogens. The updated clinical pipeline of non-traditional antibacterial agents has not responded favorably to *K. pneumoniae* infections, since none of the 32 have specific activity against it (WHO, 2022a).

Traditional antibacterial development relies heavily on scaffolds (using a common core structure for all compounds in a class of antibacterial drugs) on which different functional groups are attached (Dimova et al., 2017) e.g. the core structure of carbapenems consists of a 5-membered ring fused with a β-lactam ring, a structure similar to that of penicillins, except for an unsaturated bond between C2 and C3 and carbon at C1 instead of the sulfur molecule (Terico and Gallagher, 2014). The disadvantage of antibacterial scaffolding is the development of cross-resistance (resistance, against a new drug, acquired indirectly as a result of the pathogens' exposure to antibacterial drugs in the same class). Therefore, there's a high probability of resistance developing against 80% of the anti-carbapenemase drugs presented in Tables 1 and 2, since *K. pneumonia* has existing resistance against the β-lactam class of antibacterial drugs (Rice, 2008), and it continues to evolve its resistance mechanisms, with resistance already reported against the vaborbactama-meropenem combination (Gaibani et al., 2021, Findlay et al., 2023) and cefiderocol (Coppi et al., 2022, Lan et al., 2022).

A limitation identified in the latest WHO's antibacterial pipeline report was the predominance of intravenously administered drugs i.e., eleven out of fifteen *anti*-carbapenemase inhibitors are administered intravenously, restricting the treatment to a health-care facility (WHO, 2022a). However, this might also be an advantage for the application of restrictive antibacterial stewardship policies for new drugs, thus, preserving their susceptibility (WHO, 2022a).

1. 7. Rationale and benefits of the study

1.7.1. Rationale of the study

With the rapid global dissemination of carbapenem-resistant *K. pneumoniae*, there was an urgent need to develop a new and const-effective high-throughput screening platform that would speedup drug screening efforts to find potential drug candidates that will mitigate the threat posed by carbapenem-resistant *K.*

pneumoniae. Therefore, we proposed the development of a high-throughput agar-based microarray assay, to be used in the screening of compound libraries for anti-carbapenem-resistant *K. pneumoniae* activity.

1.7.2. Benefits of the study

The expected outcome of this study was the successful development of a simplistic and cost-effective high-throughput approach for antibacterial screening, that had a potential to accelerate drug discovery efforts against MDR *K. pneumoniae*.

1.8. Project aims and objectives

Aims

This study aimed to develop, optimize, and validate an agar-based microarray assay and to use the developed assay for screening compound libraries for anti-carbapenemase-resistant *K. pneumoniae* activity.

Objectives

The objectives of this study were:

1. To develop, optimize, and validate an agar-based microarray assay in the high-density microarray plate format.
2. To characterize the CNF film, spot sizes, and spot intensities.
3. To test the performance of the developed assay by printing a selected panel of antibacterial drugs and conducting an antibacterial screen.
4. To print and screen compound libraries against carbapenem-resistant *K. pneumoniae*.
5. To identify specific readout (identify potential hits from the primary screen data using computer data mining approaches).
6. To perform a secondary screen on the candidate hit(s) using a 96 well-plate format.
7. Determine the spectrum of activity of active compounds.

Chapter 2

Development, optimization, and validation of an agar-based *K. pneumoniae* assay in high-density (HD)-microarray plate format

2.1. Introduction

Miniaturization of biological assays is a widely adopted strategy in drug discovery research, aimed at cost-effectively accelerating compound screening (Mennen et al., 2019). By employing robotics, automation, and high-density plate formats, assay volumes were reduced from milliliteres to nanoliteres, and consequently increased throughput to approximately 100,000+ compounds' screening a day (Mayr and Fuerst, 2008, Murray and Wigglesworth, 2016). Advancements in HTS were always centered around the miniaturization of the multiwell plate to higher densities (i.e., 96-well, 382-well, 1536-well plates) (Pereira and Williams, 2007). This was enabled by the upgrades in screening infrastructure; however, the associated cost makes it inaccessible for most drug discovery research groups (Dreiman et al., 2021).

In recent years, there has been a notable shift to alternative technologies such as well-less screening methods called chemical microarrays, to increase throughput at a significantly low cost and efficiency (Burns et al., 2001, Hoever and Zbinden, 2004, Bailey et al., 2004, Cheng et al., 2005, Ma and Horiuchi, 2006). Most chemical microarray platforms are derivatives of genomic and proteomic microarray technologies, adapted to mechanically print hundreds of compounds at defined locations on an immobilized substrate (commonly glass slides) and screened against various biological targets including drug-resistant bacteria (Srinivasan et al., 2017, Lei et al., 2020).

This technology has been successfully applied in drug screening efforts including the droplet microarray (DMA) system developed by Lei and colleagues (Lei et al., 2020) for screening compounds against *P. aeruginosa*. The DMA technology is based on superhydrophilic-superhydrophobic patterning on a 7.5 x 2.5 cm glass substrate. The effect of discontinuous dewetting enables the formation of arrays of droplets trapped in superhydrophilic areas (Popova et al., 2017). A droplet of bacterial suspension is placed onto the superhydrophobic-hydrophilic array for 30 seconds before the slide is tilted to form 588 microdroplets containing bacteria. Following inoculation, a DMA slide is precisely sandwiched with antibiotic-printed fluorinated glass slides and incubated for 24 hours. Bacteria is subsequently stained, imaged, and quantified. Srinivasan and colleagues developed a nano-scale microarray platform for antimicrobial susceptibility testing

(AST) against community-acquired methicillin-resistant *S. aureus* (CA-MRSA) and called it an AST-Chip (Srinivasan et al., 2017). AST-Chip is characterized by printing 480 hydrogel-embedded antimicrobial drugs on a chemically modified microscope glass slide. Liquid growth media inoculated with CA-MRSA isolates is then printed on the previously printed drug spots and incubated for 12 hours to allow the growth (or inhibition) of CA-MRSA biofilms. Bacterial cell density in each spot is measured by fluorescence to obtain antimicrobial susceptibility. Both described technologies demonstrated the versatility and potential of microarray screening platforms for antibacterial screening.

Therefore, this chapter was aimed at demonstrating the development, optimization, and validation of an agar-based *K. pneumoniae* assay in high-density (HD)-microarray plate format to be used for screening compound libraries for anti-carbapenem-resistant *K. pneumoniae* activity. The assay was modeled based on the standard disc diffusion assay (Bauer et al., 1966) and adapted on a previously described microarray printing platform (Tantoh, 2014).

2.2. Materials and Methods

2.2.1. Antibacterial drugs

Polymyxin B sulfate (PMBS), aztreonam (ATM), cefotaxime acid (CTXA), erythromycin (ERY), gentamicin sulfate (GENS), trimethoprim (TMP), colistin sulfate (CSTS), doxycycline hyclate (DOX), and tobramycin (TOB) were procured from Sigma-Aldrich (United States of America – USA). Neomycin sulfate (NEOS), G418 sulfate (geneticin), and kanamycin sulphate (KANS) were obtained from Gibco (Invitrogen, USA). Antibacterial solutions (50 mg/mL) were prepared as per the manufacturers' recommendations. Antibiotic stock solutions were aliquoted and kept at -20ºC for a maximum of two weeks and dilutions were made as needed.

2.2.2. Bacterial strains and culture conditions

K. pneumoniae ATCC BAA-1705 – a multidrug-resistant carbapenemase-producer carrying a bla_{KPC+} gene, *K. pneumoniae* ATCC 700603 – a beta-lactamase-producer that carries SHV-18 gene, *K. pneumoniae* ATCC 33495 – drug-susceptible, *S. aureus* ATCC 25923 – drug-susceptible, and *E. coli* ATCC 25922 – drug-susceptible, are American Type Culture Collection (ATCC) quality control strains that were used in assay optimization and validation. *K. pneumoniae* ATCC 33495 was gifted by Dr Sekelwa Cosa from the University of Pretoria and *K. pneumoniae* ATCC 700603 was gifted by Marcelle Le Roux from Sefako Makgatho Health

Sciences University. Frozen stocks of test bacteria were cultured on tryptic soy agar (TSA) (prepared as described in Appendix B.1) overnight at 37ºC. A colony from an overnight culture plate was used to inoculate 10 mL of tryptic soy broth (TSB) (prepared as described in Appendix B.2) and subsequently incubated for 18 hours at 37ºC with shaking at 120 rpm. Following incubation, 100 µL of the overnight broth culture was sub-cultured into 10 mL of fresh TSB and incubated for 3 hours at 37ºC. Cultures were subsequently adjusted to McFarland No. 0.5 standard, equivalent to ~1 x 10^8 CFU/mL (0.08 to 0.1 absorbance at a wavelength of 600 nm), for susceptibility testing. All bacterial manipulations were carried out in a biosafety level two (BSL 2) cabinet.

2.2.3. High-density plate (HDP) coating with cellulose nanofibers

Glass substrates of HDPs were coated with biocompatible cellulose nanofibers (CNF) to form an absorbent matrix on which compounds were printed. For the compound immobilization matrix, the 20 x 60 mm glass substrate of the Persomics HDP (Povair Sciences), was coated with 2 mL of 1.5% (w/v) ultra-short (10〜50 nm width) CNF slurry (SUGINO, Japan), plasticised with 1% (v/v) of a 1.6 M sorbitol solution (prepared as described in Appendix B.10) and 1% (v/v) of dimethyl sulfoxide (DMSO). Plates were oven-dried at 37ºC for 2.45 hours with constant monitoring to ensure even drying. A thin transparent CNF film was obtained after drying. To prevent over-drying, plates were kept in an airtight container until further use.

2.2.4. Microarray printing

Before printing, printing solutions composed of optimally diluted test drugs in 1.6% (v/v) HPMC (with the viscosity of 6 centipoise) (HPMC-6 cP) (prepared as described in Appendix B.5), and 20 µM of sulforhodamine B (a xanthene fluorescent maker) (prepared as described in Appendix B.8) were prepared in the conical bottom 96-well prep-plates (Thermofisher Scientific) to a final volume of 25 µL. Printing solutions were loaded by capillary action, using micro-fluidic filling plates, into 330 µm diameter printing elements pre-mounted onto printing plates. Printing plates were mounted onto a custom-built Z-axis movable printing head. Using 15 milliseconds of contact time, ~5.1 nL solution per spot was printed on the CNF-coated HDPs using a custom-built contact microarray printer, forming an array of individual spots. Post printing, the HDPs were air dried at room temperature for 24 hours and subsequently sealed in polybags and stored at 4ºC (with desiccation) until further use. All array manipulations and drying were carried out in an ISO4 custom-built 2.5 m^3 clean bench with two down-facing high efficiency particulate air (HEPA) filters to maintain environmental sterility. Array printing was performed at 18ºC with 100% relative humidity in the printing chamber.

2.2.5. Drug susceptibility testing

For susceptibility testing, 2 mL of 0.8% (w/v) molten Muller-Hinton agar (MHA) (prepared as described in Appendix B.4 and cooled to 45ºC) was inoculated with 10 µL of McFarland 0.5 adjusted *K. pneumoniae* cultures, 20 µL and 15 µL were used for *S. aureus* 25923 and *E. coli* 25922, respectively. Inoculated agar (500 µL) was seeded over drug-printed HDPs (using a modified pour-plated method [Sharma et al., 2023]) and allowed to solidify for 5 minutes at room temperature. Once solidified, 2 mL of plain 1.5% (w/v) molten MHA (cooled to 45ºC) was poured over the seeded layer of agar and left for 10 minutes to solidify. Plates were then sealed with parafilm, placed in a humidified chamber, and incubated for 14 hours at 37ºC. Following incubation, the HDPs were imaged as described in section 2.2.8. All bacterial manipulations were carried out in a biosafety level two (BSL - 2) cabinet.

2.2.6. Proof of concept for the agar-based microarray assay

To verify the feasibility of the optimized assay, a panel of 12 FDA-approved antibacterial drugs (section 2.2.1) was prepared and printed as specified in section 2.2.4. Drugs were printed in quadruplicates and each print was repeated twice. Antibacterial susceptibility was carried out as outlined in section 2.2.5. HDPs were subsequently imaged and the data were extracted and analyzed as outlined in sections 2.2.8 – 2.2.10.

2.2.7. Broth microdilution assay

A standard broth microdilution assay was performed as described by Eloff (Eloff, 1998), with modifications, as a reference method for the agar-based microarray assay. A hundred microliters of antibacterial drugs' solutions were two-fold serially diluted in Muller-Hinton broth (MHB) (prepared as described in Appendix B.3) in 96-well round bottom microtiter plates (Greiner Bio-One, Germany) to obtain final concentrations ranging from 0.24 to 125 µg/mL for PMBS and CSTS, 0.98 to 500 µg/mL for G418 and DOX, and 0.49 to 250 µg/mL for ATM, CTXA, ERY GENS, TMP, TOB, NEOS, and KANS. A hundred microliters of McFarland No. 0.5 adjusted bacterial solution was added to each well. Plates were incubated at 37ºC for 18 hours. To determine bacterial viability, 40 µL of 0.2 mg/mL iodonitrotetrazolium chloride (INT) (prepared as described in Appendix B.11) was added to each well. Plates were further incubated at 37°C for 30-45 minutes for color development. Absorbance was read at 450 nm wavelength using the Infinite® F500 multimode microplate reader (Tecan, Switzerland).

2.2.8. Image acquisition

Imaging of assay HDPs was carried out with a Cytation3 automated digital microscopy (BioTek, USA) at 10X magnification. Bacterial colonies were captured with brightfield and the red fluorescent protein channel (RFP) / (excitation 531 nm, emission 593 nm) captured sulforhodamine B marked printed spots. Images were sequentially captured to generate separate image files for each channel. Images were captured as 1224 x 904 resolution TIF files.

2.2.9. Image processing and data extraction

Image sequences were imported into ImageJ (Java version No. 1.8.0_172), a free online image processing software for processing and spot extraction. Separate montages of the brightfield and RFP image files were created and subsequently merged to create a single-layered RGB image (the brightfield montage was used twice to create the green and blue components of the RGB image). Each spot of a layered image was manually extracted using ImageJ, annotated, and saved as ~500 x 500 RGB TIF files. Extracted spot images were imported into CellProfiler™, a free open-source cell image analysis software (version 4.2.1) (Broad Institute, USA) for further processing and extraction of quantitative data. A sequential set of image analysis modules (pipeline) were created to measure colony densities overlaying printed spots (in pixels – px) per printed spot. The extracted data were exported to Excel (Microsoft Office 365).

2.2.10. Data analysis

The percentage of bacterial inhibition for the agar-based microarray assay was calculated using the following equation:

$$\%\ \text{Bacterial inhibition} = \frac{\text{Colony densities on treated spots}}{\text{Colony densties on untreated spots}} \times 100$$

The percentage bacterial inhibition for the reference 96-well plate was determined using the following equation:

$$\%\ \text{Bacterial inhibition} = \frac{\text{Ab}_{450}\ \text{of treated wells} - \text{Ab}_{450}\ \text{of broth}}{\text{Ab}_{450}\ \text{of untreated wells} - \text{Ab}_{450}\ \text{of broth}} \times 100$$

Where Ab_{450} was the absorbance read at 450 nm wavelength.

Half-maximal inhibitory concentration (IC_{50}) was determined by plotting dose-response curves of percent bacterial inhibition against logarithms of drug concentration (Log) by non-linear regression model using the

equation "Log [Inhibitor] vs normalized response - Variable slope" in GraphPad Prism 9.4.1 (GraphPad Software Inc., San Diego, CA).

The performance of the agar-based microarray assay was assessed by calculating *Z*-factor for each test drug using the equation:

$$Z - \text{factor} = 1 - \frac{3\,(\sigma_s + \sigma_p)}{(\mu_s - \mu_p)}$$

Where σ_s was the standard deviation (SD) of the test drug, σ_p was the SD of the negative control, μ_s was the mean of the test drug, and μ_p was the mean of the positive control. A *Z*-score of 1 was indicative of an ideal assay. Scores ranging between 1 and 0.5 were indicative of an excellent assay. Scores between 0 and 0.5 were indicative of a marginal assay. A score of less than 0 meant the signal from the samples and negative controls overlapped, making the assay less useful for screening purpose (Zhang et al., 1999).

2.3. Results and Discussion

2.3.1. Assay development

The agar-based high-throughput microarray assay, developed to screen compound libraries against carbapenem-producing *K. pneumoniae*, was modeled based on the standard disc diffusion assay (Bauer et al., 1959). The disk diffusion method is "based on the principle that antibiotic-impregnated disk placed on inoculated agar, absorb moisture and the drug diffuse outward through the agar medium, producing a concentration gradient – a clear zone is formed around the disk after incubation if the test drug inhibits bacterial growth" (Figure 2.1 A). Figure 2.1 B shows the miniaturized microarray assay approach using a modified layout composed of (1) a CNF-coated HDPs glass substrate, printed with compounds, (2) a thin layer of inoculated agar, and (3) a top layer of plain agar to prevent the inoculated agar from drying out during the incubation process. In this layout, the CNF matrix absorbs moisture and allows the dissolution of compounds in the printed spots and their subsequent diffusion upward into the inoculated agar. Alternating columns of positive and negative control spots were printed and the clear zones observed on the positive control spots confirmed the performance of the method. The standard disk diffusion assay is usually carried out in a 60/90 mm by 15 mm circular petri dish containing 25 – 30 mL of agar, where compounds diffuse from a 6 mm disk impregnated with 20 µL of drug solution, resulting in zones of inhibition over 6 mm in diameter (EUCAST, 2000). The miniaturized assay, in comparison, was conducted on a 24 x 60 mm immobilized matrix, which accommodates a density of over 500 compounds per HDP. Compounds diffused from ~420

µm diameter spots, which resulted from ~5.1 nL of printing solution. Zones of inhibition were approximately 1 mm in diameter. The total volume of agar required for the assay was 2.5 mL, which formed a ~2 mm thick layer over printed spots.

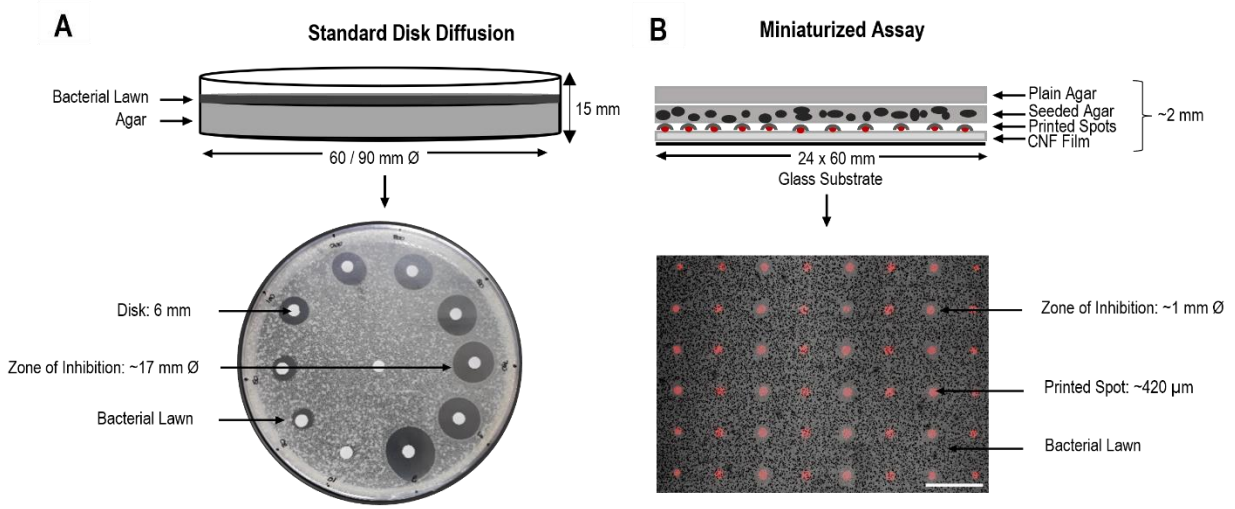

Figure 2.1. Comparative presentation of the miniaturized bacterial assay versus the standard disk diffusion assay. (A) Represents a standard disk diffusion assay, and (B) shows the high-throughput agar-based microarray assay. Scale bar = 3000 µm. Symbol: Ø = diameter.

2.3.2. Optimization of the agar-based microarray assay parameters

To achieve an effective performance for the agar-based high-throughput microarray assay described in section 2.3.1, the optimization of assay parameters including the test compound's immobilization matrix, printing solution, bacterial inoculum, agar volume, and agar concentration was undertaken as follows:

2.3.2.1. Determination of an optimal CNF concentration for HDP coating

The major purpose of the CNF matrix was to ensure that test compounds are stably immobilised in their respective positions on the array when seeded with molten agar. It was crucial to ensure that the CNF matrix had good light transmittance and was compatible with the bottom-up image-capturing mechanism of the automated microscope (Cytation3). To determine an optimal CNF concentration, HDPs were coated with CNF slurries of lower, intermediate, and high viscosities (0.5, 1, 1.5% w/v of a 2% w/v stock), plasticised with 1% (v/v) of a 1.6 M sorbitol solution and 1% (v/v) of dimethyl sulfoxide. CNF-coated HDPs were printed with 25 ng/spot of PMBS and CSTS and subsequently seeded with inoculated agar. Figure 2.2 shows a comparative analysis of matrix transparency, spot sizes, spot intensities, and sizes of zones of inhibition, conducted using Two-way ANOVA with Bonferroni post-test in GraphPad Prism (version 5.02).

2.3.2.1.1. Comparative analysis of CNF matrix transparency

Figure 2.2 (A – C) shows the three tested CNF films on HDP glass substrates. The tested CNF concentrations resulted in sufficiently transparent films and allowed fair visualization of opaque black lines that were placed under the glass substrate. The resulting transparency of the CNF matrixes enabled the acquisition of printed spots and bacterial colonies.

2.3.2.1.2. Comparative analysis of spot sizes and intensities

A spot maker, in the form of a fluorescent dye, was added to a printing solution to facilitate spot identification during imaging, re-boxing, and data extraction (Tantoh, 2014). Spot intensities and sizes from all tested CNF concentrations were measured using CellProfiler™ and comparative analyses were carried out (Figure 2.2 J and L). Spot sizes at 0.5, 1, and 1.5% CNF were ~356.6 (n = 64), ~435.9 (n = 64), and ~417 (n = 64) µm, respectively (Figure 2.2 J). Spot intensity at 0.5% was significantly different than intensities at 1 and 1.5% CNF ($p < 0.05$ and $p < 0.01$, respectively). No significant difference was observed at 1 and 1.5% CNF ($p > 0.05$) (Figure 2.2 D – F and L).

2.3.2.1.3. Comparative analysis of zones of inhibition

The diameters of zones of inhibition resulting from the three differently coated HDPs were measured from scaled image montages using ImageJ and comparative analyses were carried out as demonstrated in Figure 2.2 K and M. The susceptibility of *K. pneumoniae* 1705 to PMBS and CSTS resulted in the zone of inhibition diameters of ~806.2 and 930.3 µm at 0.5%, ~765.3 and 805.3 µm at 1%, and ~749.9 and 802.7 µm at 1.5%, respectively (Figure 2.2 K). A relatively similar outcome was obtained for *K. pneumoniae* 33495's susceptibility to PMBS and CSTS, with the zone of inhibition diameters of ~914.9 and 1058.7 µm at 0.5%, ~802.7 and 929.3 µm at 1%, and ~925.2 and 1091.8 µm at 1.5%, respectively (Figure 2.2 M). The difference in CNF concentration and spot sizes did not show a significant effect on the diameters of zones of inhibition ($p > 0.05$) (Figure 2.2 G – I).

In conclusion, varying degrees of film transparency resulting from 0.5, 1, and 1.5% CNF concentration did not affect the automated imaging of printed spots. Spot intensity increased with increasing CNF concentration. However, the susceptibility profiles of *K. pneumoniae* 1705 and 33495 to PMBS and CSTS (determined by diameters zones of inhibition) on differently coated HDPs was relatively similar. Therefore, due to the high spot intensity, the CNF concentration of 1.5% was selected as optimal for HDP coating.

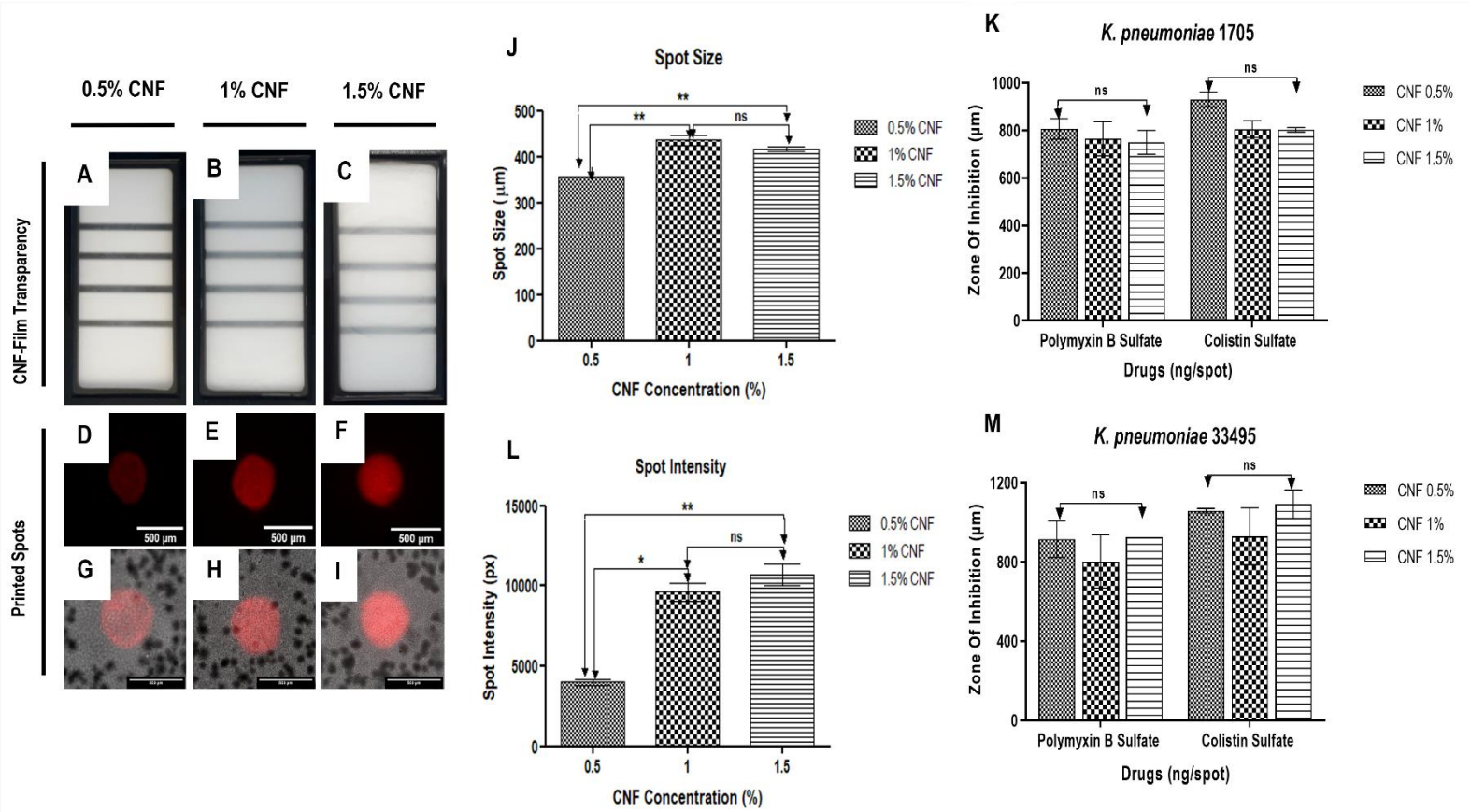

Figure 2.2. Optimization of CNF concentration for HDP glass substrate coating. HDP glass substrates were coated with 0.5%, 1%, and 1.5% CNF slurry and dried at 37ºC for 2.45 hours. Coated slides were printed with drugs and images were captured with an automated microscope at 10X magnification. Spot size, spot intensity, and resulting zones of inhibition were measured. (A – C) Degree of transparency of CNF films at 0.5%, 1%, and 1.5%, as indicated by the visibility of opaque black lines. (D – F) Spot intensities. (G – I) Zones of inhibition resulting from tested CNF concentrations. (J) Comparison of spot sizes. Spots at 0.5% were significantly smaller than spots at 1 and 1.5% CNF, with no significant difference between 1 and 1.5% CNF ($^{ns}p > 0.05$, $^{**}p < 0.01$). (L) Comparison of spot intensities. low spot intensity was measured at 0.5 as compared to 1 and 1.5% CNF ($^{ns}p > 0.05$, $^{*}p < 0.05$, $^{**}p < 0.01$). (K and M) Inhibition *K. pneumoniae* 1705 and 33495 (zone of inhibition) relative to CNF concentration. No significant difference was observed in zones of inhibition resulting from PMBC and CSTS spots printed on different CNF films ($^{ns}p > 0.05$). $n = 64$. Scale bar = 500 µm. Abbreviations: CNF = cellulose nanofibers, ns = not significant, px = pixel units.

2.3.2.2. Determination of an optimum microarray printing solution

A printing solution was made up of a combination of a polymer, a spot maker, and the compound. The polymer component of the printing solution served as a binding agent for compounds and prevented printed spots from washing off during seeding. An optimum polymer was determined by: (1) its compatibility with compounds – precipitation of the compounds, color change of the printing solution, gelation, or cloudiness were the incompatibility indicators that were considered (Marsilio et al., 2016), (2) ease of flow on microfluidic plates, efficient capillary loading, and printing, and (3) biocompatibility with the bacterial cultures. The diffusion rate of compounds from printed spots was another crucial parameter that was considered when choosing an appropriate polymer concentration. An optimal polymer would swell effectively upon exposure to moisture from the agar followed by an immediate diffusion of compounds from the printed spots into solidified agar to exert inhibitory effects.

To determine an optimal printing solution, four different water-soluble polymers were tested, including the ~86 kDa HPMC with the viscosity of 2,600+ cP (HPMC-2,600+ cP) (prepared as described in Appendix B.6) at 0.25%, 0.125%, and 0.0625% w/v, ~10,000 Mn HPMC-6 cP (at 1%, 0.5%, and 0.25% w/v), 400 cP methyl cellulose (prepared as described in Appendix B.7) at 0.5% and 0.25% w/v, and sucrose (prepared as described in Appendix B.9) at 50% and 25% w/v. Polymers were dissolved in water at different concentrations as specified above. A traceable fluorescent dye, sulforhodamine B (with an excitation and emission wavelength of 531 nm and 593 nm, respectively), was added to each solution for spot size and shape identification. Respective solutions were printed on CNF-coated HDPs as outlined in section 2.2.3. Printed plates were air-dried and imaged. Water-soluble polymers were preferred for biocompatibility purposes. Varying degrees of polymer viscosities necessitated printing at different concentrations (Figure 2.3). Observations on capillary loading, printability, and the spread of the solution on the CNF film were noted. HPMC-2,600+ cP (Figure 2.3 A: columns 1 – 3) and methyl cellulose (Figure 2.3 A: columns 9 – 10) were highly viscous and had to be diluted to concentrations less than 1% w/v. They also showed the lowest capillarity which resulted in plate-to-plate print variations during the print cycle. Similar observations were made with sucrose (Figure 2.3 A: columns 7 – 8). Further dilutions of these polymers resulted in size and morphological variable spots. Besides morphological differences, low polymer concentrations resulted in weak binding to the fibers of the CNF matrix, thus, resulting in some printed spots washing off while seeding (before agar solidification). With further optimization, a relatively consistent print, fitting the criteria above,

was obtained with a low molecular weight HPMC-6 cP (Figure 2.3 B). HPMC-6 cP, at a working concentration of 1.6% (v/v), was selected for all printing requirements of the study.

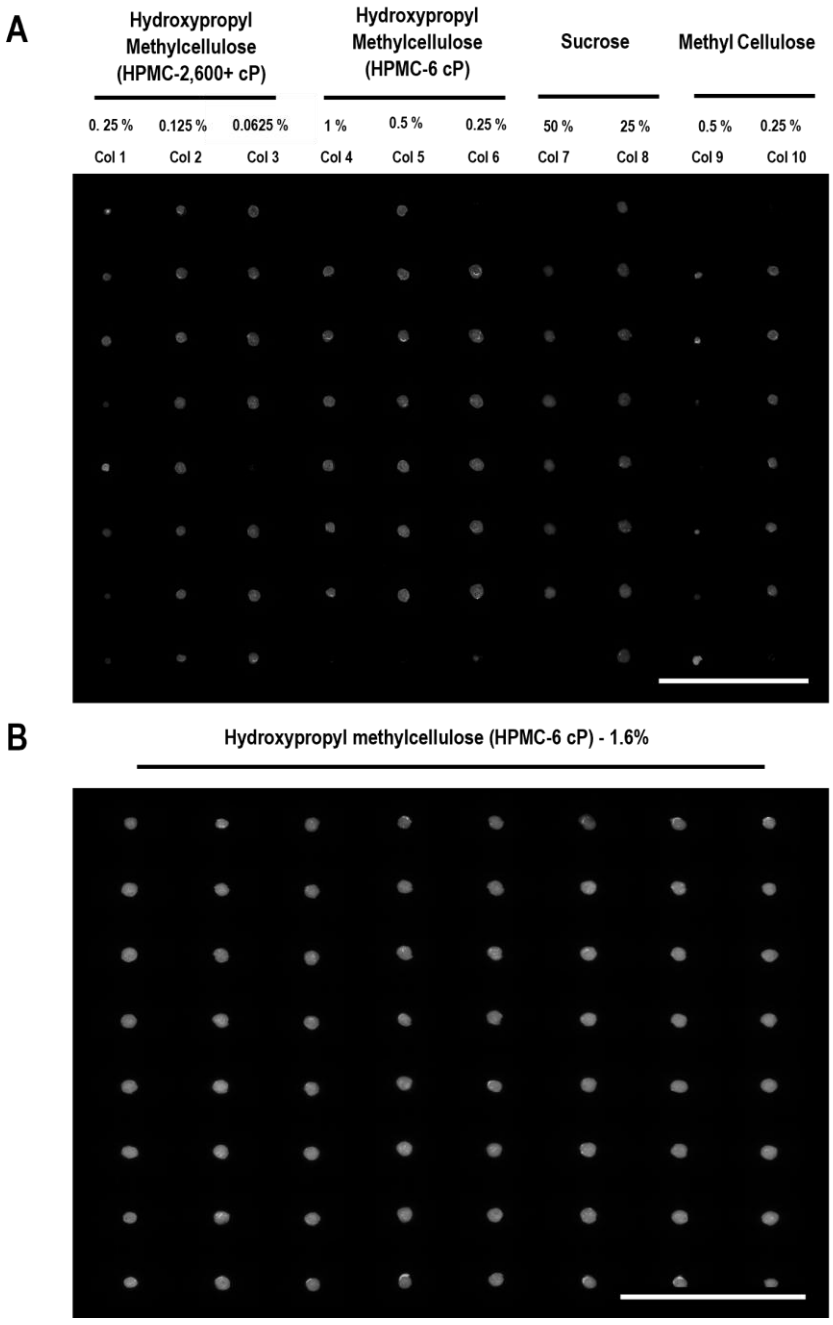

Figure 2.3. Optimization of the microarray printing solution. (A) An array of spots printed with HPMC-2,600+, HPMC-6 cP, sucrose, and methyl cellulose. (B) An array of spots printed with 1.6% HPMC-6 cP. Images were captured with an automated microscope at 10X magnification. Abbreviations: cP = centipoise, Col = column. Scale bar = 5000 µm.

2.3.2.3. Determination of an optimal inoculum volume

For this assay, antibacterial activity is measured by determining colony density over test printed spots relative to those on the negative control spots. An active compound inhibits or reduces bacterial growth proximal to the spot, indicated by zero or low colony density, while an inactive compound is indicated by high colony density over the spot. The accuracy of this assay's performance was dependent on a clear distinction in colony densities over active and inactive spots. This distinction was achieved when there was an adequate number of bacterial colonies covering inactive spots (negative controls). Therefore, to determine an optimal inoculum, different inoculum volumes were tested.

Optimization was carried out by inoculating molten agar with different volumes of McFarland 0.5 adjusted bacterial cultures (5, 7.5, and 10 µL which were equivalent to ~8.25×10^4, 1.13×10^5, and 1.10^5 CFU/mL and 1.33×10^5, 1.88×10^5, 1.98×10^5 CFU/mL, for *K. pneumoniae* 1705 and 33495, respectively) and seeded over HDPs printed with positive and negative controls. The resulting density and distribution of colonies over the array of printed spots are presented in Figure 2.4 (A and B). At 5 µL inoculum, colonies were sparsely distributed (Figure 2.4 A and B: panel 1), with an average of 3 and 5 colonies per negative control spot for *K. pneumoniae* 1705 *and* 33495, respectively (Figure 2.4 C and D). An average of 7 colonies resulted from 7.5 µL of inoculum of both tested strains. Adequate coverage was achieved with 10 µL inoculum (Figure 2.4 A and B: panel 3), with an average of 11 and 12 evenly distributed colonies over the negative control spots (Figure 2.4 C and D). The 5 and 7.5 µL inoculums present a high probability of producing false positives, thus compromising the reliability of the assay results.

Colonies at 10 µL were observed to be relatively smaller and slightly translucent compared to the sparsely distributed ones at 5 µL inoculum (Figure 2.4 A and B: panel 3 and 1, respectively). This was due to limited nutrients and limited by-products discharge area for bacterial cells (Cooper et al., 1968). The smallest of these colonies fell below the threshold smoothing scale (1.3488) differentiating foreground from the background during data extraction in CellProfiler™ (Figure 2.4 A and B). Therefore, a further increase of inoculum would heighten the aforementioned effect and affect the accuracy of measurements done for individual spots. For this reason, higher inoculum concentrations were not tested.

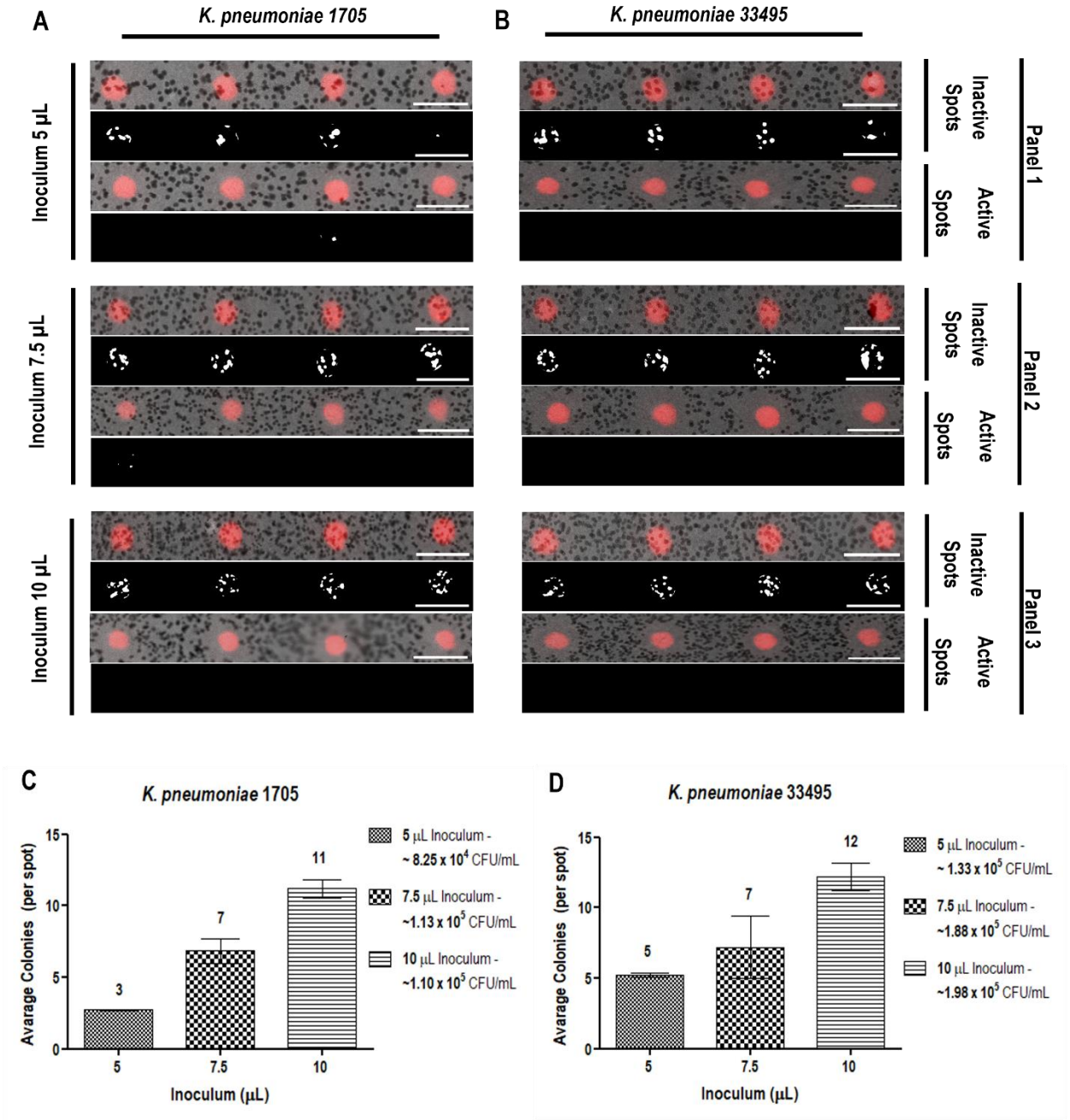

Figure 2.4. Optimization of bacterial inoculum. CNF-coated HDPs were printed and seeded with agar inoculated with three different concentrations (5 µL, 7.5 µL, 10 µL) of *K. pneumoniae* cultures. Following 14 hours of incubation, HDPs were imaged with an automated microscope at 10X magnification, and bacterial colonies over printed spots were quantified. (A and B) Top panel under each concentration – grayscale image showing colony density and distribution over an array of inactive spots; bottom panel – corresponding binary images of extracted spots and colony distribution. (C and D) An average number of *K. pneumoniae* 1705 and 33495 colonies resulting from 5 µL, 7.5 µL, and 10 µL of inoculum, respectively. *n* = 64. Scale bar = 1000 µm.

2.3.2.4. Determination of an optimal agar concentration

The moisture content in the seeding agar plays a crucial role in ensuring the swelling of both the CNF matrix and the polymer matrix of the printed spot, dissolving compounds embedded in the spot matrix and facilitating their diffusion into the agar. A certain degree of agar fluidity (in its molten state) was also required to ensure ease of spreading 500 µL of agar evenly over the 20 x 60 mm CNF-coated glass substrate of the HDP. Therefore, to determine an optimal agar concentration for seeding, different concentrations of MHA (0.8, 1, 1.2, 1.4%) were inoculated with McFarland 0.5 adjusted *K. pneumoniae* cultures and seeded over PMBS and CSTS (at 25.5 ng/spot) printed HDPs. Following incubation, HDPs were imaged and zones of inhibition around active spots were measured and comparative analysis was performed by Two-way ANOVA with Bonferroni post-test using GraphPad Prism (version 5.02).

Zones of *K. pneumoniae* 1705 inhibition decreased significantly with increasing agar concentration for both PMBS and CSTS ($^{ns}p > 0.05$, $^{*}p < 0.05$, $^{***}p < 0.001$) (Figure 2.5 A and C). Variation in agar concentrations had minimal effect on zones of inhibition for *K. pneumoniae* 33495 for both PMBS and CSTS ($^{ns}p > 0.05$, $^{*}p < 0.05$) (Figure 2.5 B and D). The observed decrease in zones of inhibition, especially for *K. pneumoniae* 1705, was attributed to partial swelling of the polymer matrix and subsequent dissolving and diffusion of compounds (Figure 2.5 B). The opposite effect observed in the *K. pneumoniae* 33495 screen was attributed to its high susceptibility to the test drugs, in that, the small amount of the drugs that diffused into the agar was sufficient to bring about the desired bioactivity. Regarding agar fluidity, 1.2 and 1.4% MHA had reduced fluidity due to increased viscosity. This led to a slow spread over the CNF matrix and solidified at a rate faster than 0.8 and 1% agar and resulted in an uneven layer of agar with poor coverage of the printed area. The 0.8% agar had sufficient moisture and maximum fluidity required for the efficiency of the assay. Moreover, a low concentration of agar did not compromise the solidity and stability in its solidified state (not prone to sliding off) and was selected as most suitable for use in the subsequent assays.

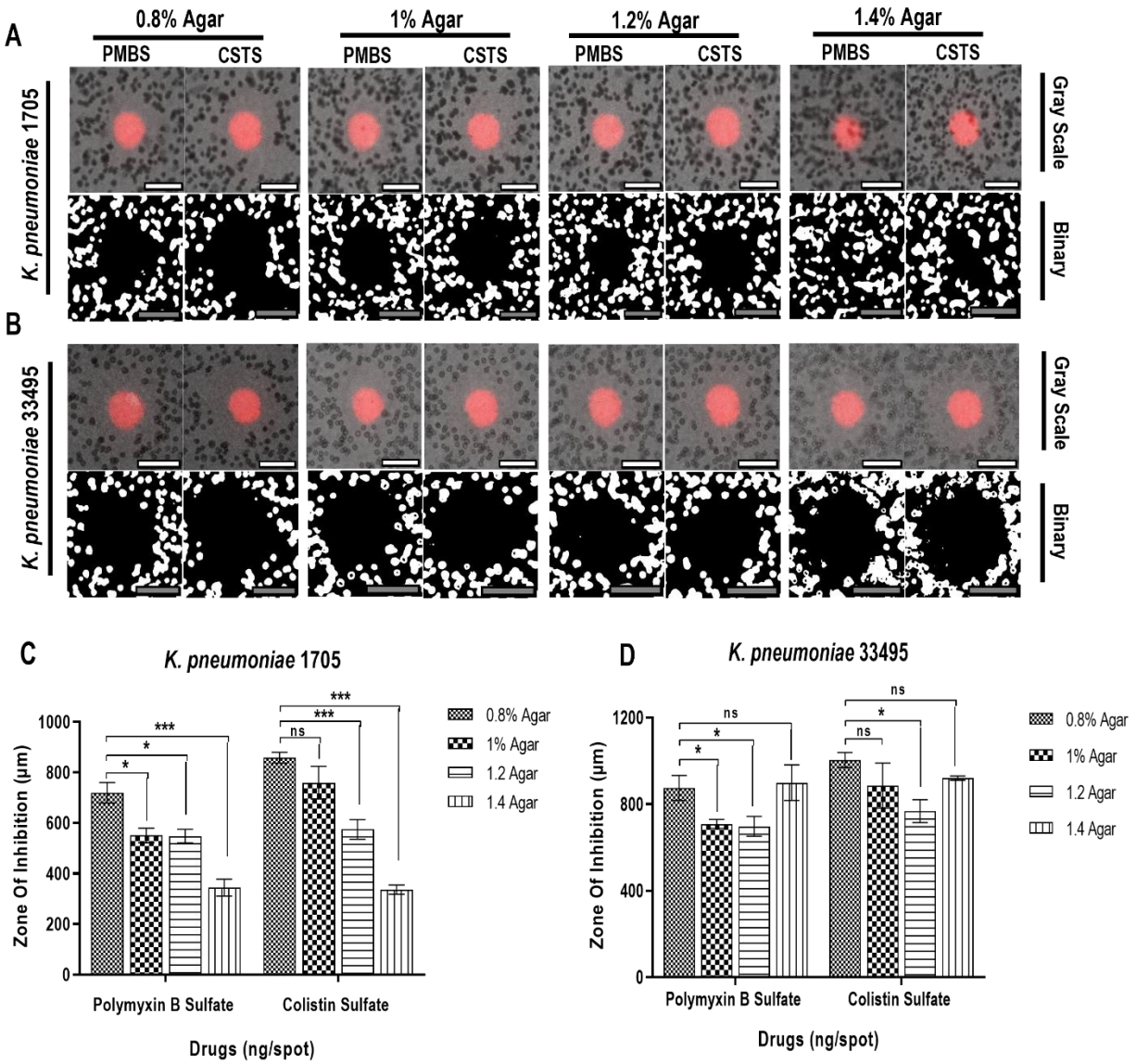

Figure 2.5. Optimization of agar concentration. CNF-coated HDPs were printed and subsequently seeded with 0.8%, 1%, 1.2%, and 1.4% MHA, and incubated for 14 hours. Brightfield images of HDPs were captured with an automated microscope at 10X magnification. Zones of inhibition were measured and compared to those obtained from the lowest concentration of agar. (A) The degree of *K. pneumoniae* 1705 inhibition at different agar concentrations, with zones of inhibition decreased with increasing agar concentrations. (B) The degree of *K. pneumoniae* 33495 inhibition at different agar concentrations, with relatively similar zones of inhibition at all concentrations. (C) Comparative analyses of *K. pneumoniae* 1705 inhibitions at different agar concentrations. Zones of inhibition decreased significantly with increasing agar concentrations for both PMBS and CSTS ($^{ns}p > 0.05$, $^{*}p < 0.05$, $^{***}p < 0.001$). (D) Comparative analyses of *K. pneumoniae* 33495 inhibitions at different agar concentrations. The zones of inhibition were relatively similar at all agar concentrations for both PMBS and CSTS ($^{ns}p > 0.05$, $^{*}p < 0.05$). $n = 64$. Scale bar = 500 µm. Abbreviations: PMBS = polymyxin b sulfate, CSTS = colistin sulfate, ns = not significant.

2.3.2.5. Optimization of agar volume

The volume of seed agar is directly proportional to the thickness of the agar covering the HDP's glass substrate, where a high agar volume would result in a thick layer and a low agar volume result in a thin layer. An optimal agar volume was expected to expose all agar-embedded bacterial colonies proximal to the printed spots to the strongest concentration of the test compound. The optimization was carried out by seeding different volumes (0.5, 1, and 1.5 mL) of *K. pneumoniae* 1705 and 33495 seeded MHA (0.8% w/v) over PMBS and CSTS (25.5 ng/spot) printed HDPs. Agar-embedded bacterial cells were exposed to the concentration gradient of the compound resulting from its radial diffusion from the printed spot into the agar. Brightfield images in Figure 2.6 (A and B) (panel 1) showed a monolayer of bacterial colonies resulting from 0.5 mL of agar and no colonies were observed over extracted spots of PMBS and CSTS, whilst 1 and 1.5 mL produced multi-layered colony arrangement within the agar, and colonies were observed over extracted spots of both PMBS and CSTS (Figure 2.6 A and B: panel 2 and 3). The assessment of the total area of active spots covered with colonies, following the culture period, showed partial bacterial inhibition with increasing agar volume (Figure 2.6 A and B). At 0.5 mL of agar, the total percent area of PMBS and CSTS spots covered with *K. pneumoniae* 1705 and 33495 colonies ranged between 1.9 and 0%, 30.45 and 15% at 1 mL, and 24.2 and 12.4 at 1.5 mL, respectively (Figure 2.6 C and D). Brightfield images presented in Figure 2.6 (A and B) show that bacterial growth observed over spots in 1 and 1.5 mL of agar occurred above the test compound's concentration gradient. As in the standard disc diffusion, the concentration of antibacterial drugs was highest closest to the printed spot and gradually decreased and lost inhibitory effects as the distance increased, hence, bacterial growth occurred from that point up (Tendencia, 2004, Hudzicki, 2009). A schematic diagram of an assumed test drug's concentration gradient relative to the thickness of the seed layer and the degree of bacterial inhibition is presented in Figure 2.7. The lowest volume of agar (0.5 mL) matches the aforementioned characteristic of an optimal seed layer, and therefore selected for further experiments. The 0.5 mL of agar (0.8% w/v) resulted in a relatively thin layer over the printed matrix and was prone to drying out. Therefore, to prevent this effect, an additional 2 mL of MHA (1.5 % w/v) was added over the seeded agar layer. Furthermore, the additional layer provided stability to the soft seed agar layer, preventing it from slight movements over the CNF matrix, caused by the high-water content in its composition (0.8% agar concentration).

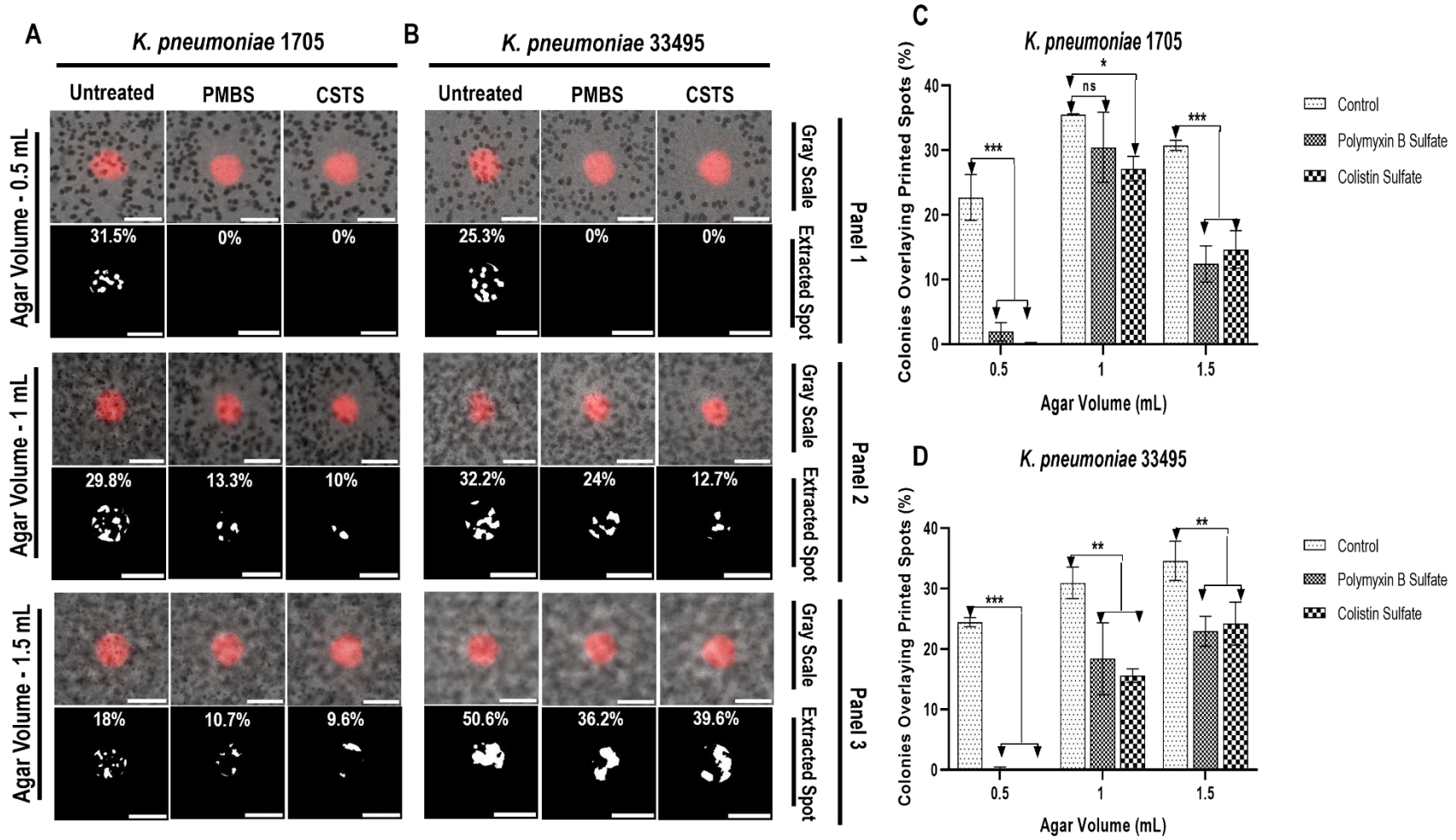

Figure 2.6. Optimization of seed agar volume. The drug-printed CNF-coated HDPs were seeded with 0.5 mL, 1 mL, and 1.5 mL of inoculated MHA and incubated for 14 hours. HDPs were subsequently imaged with an automated microscope at 10X magnification and the total bacterial growth over active and inactive spots was quantified and comparative analysis conducted. (A and B) The top panel of each agar volume: grayscale images showing colony densities over inactive and active spots; the bottom panel: binary images of corresponding extracted spots. (C) Comparison of *K. pneumoniae* 1705 growth over active and inactive spots. There was a significant increase in colony densities as the thickness of the inoculated agar increased PMBS and CSTS spots ($^{ns}p > 0.05$, $^{*}p < 0.05$, $^{***}p < 0.001$), signifying partial inhibition of bacterial growth. (D) Comparison of *K. pneumoniae* 33495 growth over active and inactive spots. There was a significant increase in colony

densities as the thickness of the inoculated agar increased over PMBS and CSTS spots ($^{ns}p > 0.05$, $^{**}p < 0.01$, $^{***}p < 0.001$), signifying partial inhibition of bacterial growth. *n* = 64. Scale bar = 500 µm. Abbreviations: PMBS = polymyxin b sulfate, CSTS = colistin sulfate, ns = not significant.

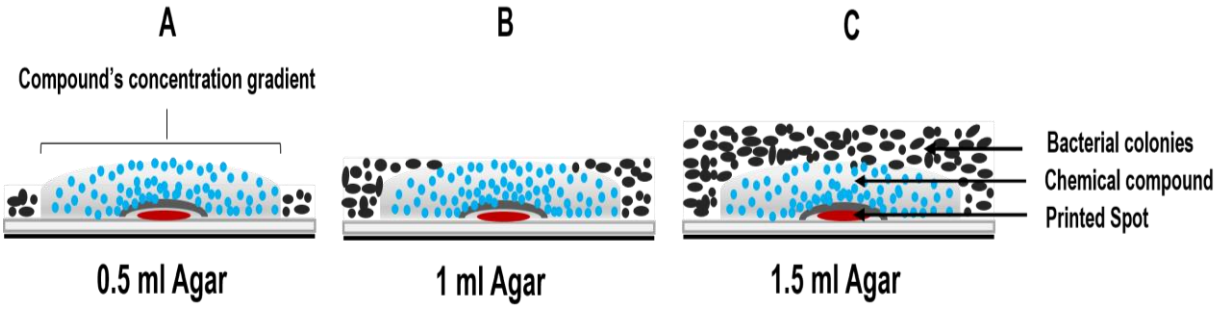

Figure 2.7. Diagrammatic illustration of the cross-section simulation of agar thickness relative to the test drug's concentration gradient (CG). (A) For the thinnest layer of agar (0.5 mL), CG is twice the height of seeded agar. (B) At 1 mL, the height of the seed layer is relatively similar to that of CG. This results in partial growth inhibition (resulting in a smaller zone of inhibition. (C) At 1.5 mL, the seed layer is twice the height of CG. Hence, the uninhibited bacterial growth above the CG.

2.3.3. Proof of concept

Once all assay parameters were fully optimized, the screening potential of the assay was demonstrated by screening a panel of 12 antibacterial drugs (Figure 2.9 A), comprising of polymyxins (PMBS, CSTS); β-lactam (ATM); diaminopyrimidines (TMP); third generation semisynthetic cephalosporin (CTXA); macrolide (ERY); aminoglycosides (GENS, TOB, NEOS, KANS, geneticin); and tetracycline (DOX), against both drug-susceptible and resistant strains of *K. pneumoniae* (BAA 1705, BAA 700603, 33495), drug-susceptible *E. coli* (25922) and *S. aureus* (25923) (Figure 2.9 B – F). This pilot screen was carried out following the step-by-step workflow demonstrated in Figure 2.8.

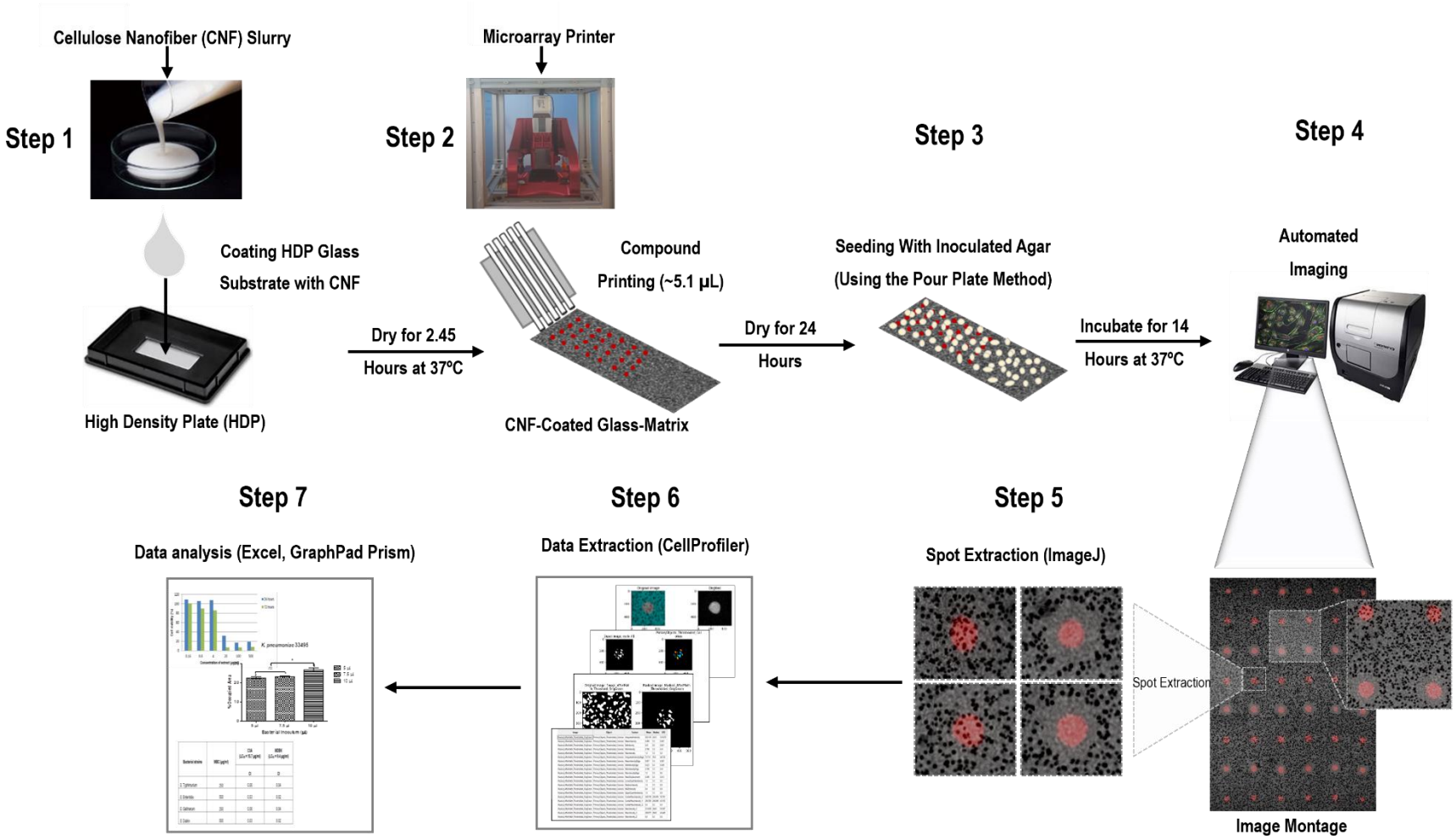

Figure 2.8. A schematic presentation of the agar-based microarray assay's workflow. Step 1 – coating of HDPs with a CNF slurry and drying: this resulted in thin transparent films over the HDP's glass substrate. Step 2 – approximately 5.1 nL of the printing solution containing drugs was printed into a CNF-coated glass substrate and allowed to dry for 24 hours before seeding. Step 3 – printed HDPs were seeded with inoculated agar and incubated for 14 hours at 37ºC for colony formation. Step 4 – HPSs were imaged with an automated microscope at 10X magnification. A montage showing printed spots overlayed with bacterial colonies was created. Step 5 – single spots were extracted from the montage using ImageJ. Steps 6-7 – extracted data was extracted from individual spots using CellProfiler, exported to Excel for processing, and analyzed in Prism.

2.3.3.1. Observations on assay performance

Bacteria grew and formed a layer of evenly distributed agar-embedded colonies, with zones of inhibition where there was antibacterial activity (Figure 2.9 B – F). Observed zones of inhibition were proof that drugs diffused from the printed spots into surrounding agar before colony formation. Variable susceptibility patterns of test bacterial were demonstrated on the platform with PMBS, CSTS, and GENS active against *K. pneumoniae* 1705 (Figure 2.9 B); PMBS and CSTS active against *K. pneumoniae* 700603 (Figure 2.9 C); PMBS, CSTS, GENS, KANS, G418 sulfate, and TOB active against *K. pneumoniae* 33495 (Figure 2.9 D); PMBS, CSTS, GENS, KANS, G418 sulfate, TOB, and NEOS active against *E. coli* 25922 (Figure 2.9 E); and GENS, KANS, G418 sulfate, TOB, and NEOS against *S. aureus* 25923 (Figure 2.9 F). Cross-contamination of zones of inhibition was observed in the screen against *S. aureus* (Figure 2.9 F), where zones crossed the periphery of active spots to inhibit the growth of neighbouring spots, and therefore, data could not be accurately captured. This is a common issue with well-less chemical screening platforms where the assay readout is a radial inhibitory effect (Bailey et al., 2004). To minimise cross-contamination, the vertical and horizontal centre-to-centre distance of the spots was set at ~1054 and 1553.5 µm, respectively. However, for highly susceptible strains like *S. aureus* 25923, additional adjustments of assay parameters would have to be applied to reduce the total area of the compound's concentration gradient. These adjustments could be a slight increase in the seed agar's concentration (to a maximum concentration of 1%, as demonstrated in section 2.3.2.4) or adjusting the effective drug concentration within printed spots. This would potentially reduce the size of zones of inhibition, thus, minimising cross-contamination without the need to further increase the centre-to-centre spot distance (which would result in decreased assay throughput).

2.3.3.2. Assessment of the quality of the agar-based microarray assay

A statistical parameter called *Z*-factor was used to assess the quality of the developed high-throughput assay (Zhang et al., 1999). *Z*-factors of test drugs were quantified by determining the degree of separation between the mean of the negative control (untreated spots with uninhibited growth) and the mean of bacterial density measured over the spot with the highest concentration of the serial dilution of test drugs, which is the dynamic range of the assay (Table 2.1). The dynamic range between active drugs and the negative control resulted in *Z*-factors of 1. For inactive drugs, the sample means and control means overlapped, implying that there was no dynamic range. Hence, *Z*-factors were either below or above the acceptable range of 0-1. The obtained results confirmed that this is an ideal assay for high-throughput screening and may lead to successful mining of potential hits (Zhang et al., 1999).

2.3.2.3. Comparison of antibacterial susceptibility in the agar-based microarray assay with the standard broth microdilution assay

The antibacterial activity of test bacteria obtained from the agar-based microarray assay (conducted as outlined section 2.2.6 with drug concentrations outlined in Figure 2.9 A) was compared to those of the standard broth microdilution assay (as outlined in section 2.2.7) to determine the accuracy and sensitivity of the HTS assay. For the agar-based microarray assay, the density of bacterial colonies on printed spots was measured and the obtained data was used to plot sigmoidal curves and determination of the IC_{50} of test drugs. A similar analysis was carried out for data obtained from the standard broth-microdilution assay. The IC_{50} values obtained from broth assays were variable, however, there was a similar pattern of susceptibility, where all drugs that showed activity in the microarray assay had a relatively low IC_{50} values (highly active) in the standard assay and those that had no activity in the microarray assay had a relatively high IC_{50} (less active) or no activity in the standard assay (Table 2.1, Appendix A 1 – 5). A combination of factors can be attributed to the observed variation, including a probability that there was either a minuscule amount of the drugs in the printed spots or varying degrees of drug dissolution in semi-solid media (Salmon et al., 1996, Hudzicki, 2009). As a result, the amount was either sufficient to show an inhibitory effect against susceptible bacteria or insufficient to exhibit a distinguishable antibacterial activity against drug-resistant bacteria. A conclusion drawn from this assessment was that the agar-based microarray assay, in its current state, is only suitable for primary antibacterial screening to identify hits, instead of being used as an antibacterial susceptibility screening method. Hits identified on this platform will be validated using a secondary low-throughput method, a procedural part of HTS and early drug discovery processes (Hughes et al., 2011).

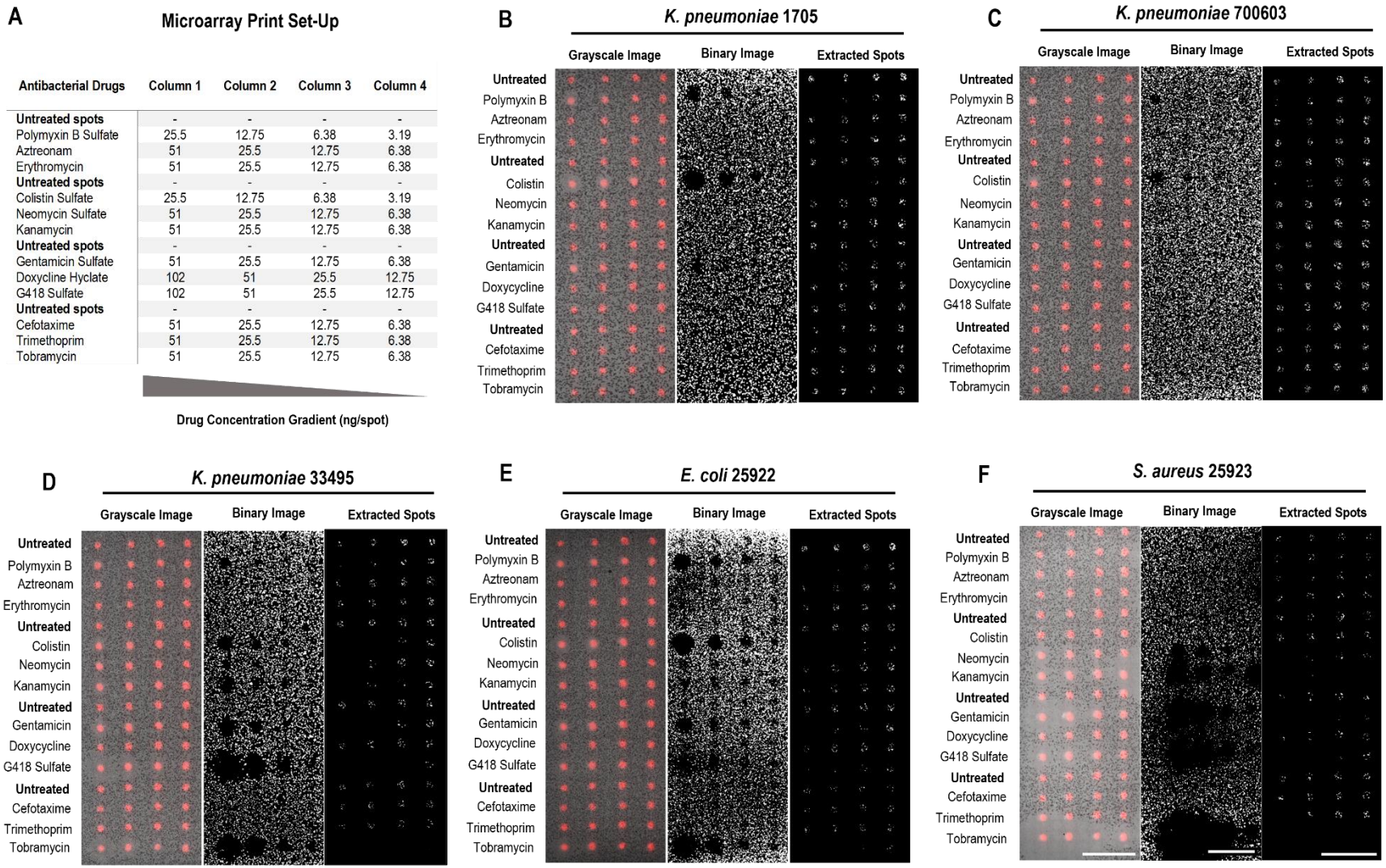

Figure 2.9. Antibacterial susceptibility profiles of tested bacteria to 12 antibacterial drugs. (A) A microarray print layout and drug concentrations. (B - F) Left panel, grayscale images showing layout of bacterial colonies over printed spots; middle panel, binary image converted from the grayscale showing zones of inhibition over active spots; right panel, binary images showing extracted spots and relative bacterial density over each spot. Scale bar = 3000 µm. Images were captured using an automated microscope at 10X magnification.

Table 2.1. Antibacterial activities of 12 FDA-approved drugs against *K. pneumoniae* 1705, *K. pneumoniae* 33495, *K. pneumoniae* 700603, *E. coli* 25922 and *S. aureus* 25923 and Z-factor scores of the agar-based microarray assay.

Antibacterial drugs	IC_{50} (ng/spot/mL) and Z-factor														
	K. pneumoniae 1705			*K. pneumoniae* 33495			*K. pneumoniae* 700603			*E. coli* 25922			*S. aureus* 25923		
	Z-factor	Microarray assay	Microdilution assay	Z-factor	Microarray assay	Microdilution assay	Z-factor	Microarray assay	Microdilution assay	Z-factor	Microarray assay	Microdilution assay	Z-factor	Microarray assay	Microdilution assay
Polymyxin B sulfate	1	10.96	4535	1	9.77	5481	1	18.76	1710	1	5.602	1338	-	-	14333
Aztreonam	-.8.3	UND	UND	1.9	UND	UND	3.4	UND	UND	4.1	UND	UND	-	-	130637
Erythromycin	3.4	UND	UND	-3.3	UND	34145	17.6	UND	159911	4.1	UND	10432	-	-	UND
Colistin sulfate	1	5.783	3441	1	6.891	5993	1	8.374	1392	1	7.024	1537	-	-	53874
Neomycin sulfate	-7.1	UND	60624	3.2	UND	4151	7.1	UND	30244	1.2	17.54	2642	-	-	1341
Kanamycin sulphate	-1.6	UND	UND	1.5	18.37	991.8	5.6	UND	55184	1.6	50.01	1031	-	-	340.7
Gentamicin sulfate	1	30.45	1257	1	14.71	709.2	6.2	UND	11329	1	15.91	866.9	-	-	UND
Doxycline hyclate	-1.1	UND	1898	2.4	UND	5701	3.4	UND	11305	3.1	UND	UND	-	-	UND
G418 sulfate	6.6	UND	29404	1	37.08	UND	5.4	UND	10016	1.3	77.01	UND	-	-	UND
Cefotaxime	1.6	UND	UND	7.8	UND	UND	5.2	UND	UND	3.8	UND	1253	-	-	1444
Trimethoprim	8.1	UND	UND	3.3	UND	5911	-6.9	UND	24012	8.6	UND	989.2	-	-	5934
Tobramycin	-8.5	UND	25376	1	13.27	846.7	4.4	UND	8694	1	12.1	780.5	-	-	UND

Abbreviations: UND = undefined, IC_{50} = half-maximal inhibitory concentration

2.4. Summary

A high-throughput agar-based microarray platform was developed for compound screening against carbapenem-resistant *K. pneumoniae.* The first step undertaken in developing the assay was optimising the assay parameters crucial for an efficiently running assay, ensuring the reliability of the end results. The parameters included the optimization of the test compound's immobilization matrix (CNF film), the polymer component of the printing solution, the density of the bacterial inoculum, agar thickness, and agar concentration. The optimized assay parameters were a 24 x 60 mm absorbent CNF immobilization matrix made from a 1.5% w/v CNF slurry, a printing solution containing 1.6% of HPMC-6 cP, an inoculum density ranging between ~1 x 10^5 and 2 x 10^5 CFU/mL, a 0.8% (w/v) concentration of seeding agar which formed a ~0.4 mm layer into which printed compounds diffused into and affected bacteria, and 1.5% (w/v) plain agar which formed a ~1.6 mm layer overlaying the thin seeded agar layer. The workflow of the optimized assay included the arraying of compounds into the CNF immobilization matrix, which generated spots ranging between ~270 and ~420 µm in size. This was followed by overlaying the drug-printed matrix with the 0.8% (w/v) inoculated molten agar. Incubating the seeded matrix resulted in the formation of agar-embedded bacterial colonies, which were subsequently imaged at 10X with an automated imaging system (Cytation3) to identify antibacterial activity in the form of zones of inhibition.

The screening potential of the assay was demonstrated by screening a panel of 12 FDA-approved antibacterial drugs against five ATCC quality control strains of bacteria. Different patterns and levels of susceptibility of tested bacteria were demonstrated on the platform. This was demonstrative of the assay's specificity. A statistical analysis of the proof-of-concept data was conducted using the *Z*-factor method, which yielded scores of 1 for active drugs and scores of 1 > or < 0 for non-active drugs. This result was indicative of an ideal assay for screening (Zhang et al., 1999). Following this assessment, a comparative assessment of the agar-based microarray assay's performance was carried out with the standard broth microdilution assay by comparing the susceptibility profiles of test bacteria to the 12 antibacterial drugs. The results (IC_{50} values) from these two assays differed. However, patterns of bacterial susceptibility were similar, drugs that showed activity in the microarray assay had a relatively low IC_{50} (highly active) in the standard assay and those that had no activity had a relatively high IC_{50} (less active) or no activity in the standard microdilution assay. It was then concluded that the agar-based microarray assay, in its current state, is suitable for primary antibacterial screening to identify hits, instead of being used as an antibacterial susceptibility screening method.

Overall, the miniaturised screening platform demonstrated here presents an efficient, cost-effective, and easily adaptable approach to HTS tor screening compound libraries for antibacterial activity. The established antibacterial screening assay workflow was achieved with minimum automation where the modification of the HDP's glass matrix with mechanically produced and biocompatible CNF required minimal effort. A repurposed custom-built microarray printing infrastructure (a genomic microarray technology) was adapted for mechanically printing compounds. A simplistic manual bacterial inoculation approach (pour-plated method (Sharma et al., 2023) was used. An image-based readout using brightfield imaging of agar-embedded colonies, using a standard automated imaging system, further simplified the screen, thus eliminating multiple fluorescent tagging processes. Moreover, no specialised software was required for data extraction, freely available software (i.e., CellProfiler™ and ImageJ) were utilised for this purpose. Additionally, the assay demonstrated a great potential to be adapted for bacteria other than *K. pneumoniae,* as demonstrated in the proof-of-concept experiments. This simplistic HTS approach provides accessibility and ease of use without investing in expensive automated HTS infrastructure.

Chapter 3

Screening compound libraries and FDA-approved drugs for anti-carbapenem-resistant *K. pneumoniae* activity

3.1. Introduction

Carbapenem-resistant *K. pneumoniae* was assigned a priority-one pathogen status in 2017 (WHO, 2017), due to its resistance to virtually all antibacterial drugs. The classification has positioned this pathogen to get first preference in drug discovery and development efforts. A few years following the classification, various basic drug discovery studies have been conducted to find novel therapies and alternative strategies to combat the resistance mechanisms of this pathogen. These include (1) screening of the FDA-approved drugs for antibacterial activity (drug repurposing) - a strategy characterized by fast development time-lines that are afforded by the pre-existing knowledge of a drug's pharmacology, formulation, potential toxicity, safety, and adverse drug reaction issues in humans (Ashburn and Thor, 2004); (2) the development of antibiotic resistance breakers (ARBs) - an approach aimed at re-sensitizing resistant bacteria to antibiotics by inhibiting their virulence factors/resistance mechanisms using drug hydrolyzing-enzyme inhibitors, membrane permeabilizers, and efflux pump inhibitors (Laws et al., 2019); (3) the exploration of the siderophore uptake mechanism with the aim of circumventing loss of porins (reduced membrane permeability) by creating an alternative antibacterial delivery system (Page, 2013) – a mechanism achieved by conjugating antibacterial drugs to a siderophore-mimicking small molecule to deliver the siderophore-compound complex into the cell's periplasmic space via the iron-siderophore uptake system (Halasohoris et al., 2021); (4) the exploration of alternative therapeutics such as the use of nanoparticles (Choi et al., 2019, Pareek et al., 2021), phage therapy characterized by lytic destruction of resistant bacteria (Anand et al., 2020), bacterial vaccines (WHO, 2022b), and clustered regularly interspaced short palindromic repeats (CRISPR) and CRISPR-associated proteins (Cas) based antibiotics (Mackow et al., 2019, Wang et al., 2020) which are characterized by removing plasmids carrying resistance genes from bacterial cells (i.e., genes coding for hydrolytic enzymes), thus re-sensitizing to antibacterial drugs (Gholizadeh et al., 2020, Tao et al., 2022), and (5) the screening of compound libraries for biological activities (Le Manach et al., 2021). The latter platform is one of the foundational approaches used for identifying hits with the potential to be developed into druggable antibacterial leads (Kwon et al., 2018, Semenov et al., 2021), post the Waksmann platform (Gajdács, 2019).

To date, these strategies yielded some success against *K. pneumoniae* including 4 FDA-approved drugs, 11 agents in clinical development, and 18 agents in preclinical development (WHO, 2022a). The latest WHO (WHO, 2022a) report on the state of the antibacterial pipeline indicated that it is still inadequate to sufficiently mitigate the impact of multidrug resistance in *K. pneumoniae*. Therefore, to contribute to the ongoing antibacterial discovery efforts, a diverse library of 4154 compounds comprising 99.1% new compounds and 0.9% FDA-approved drugs were screened for anti-carbapenem-resistant *K. pneumoniae* activity, using the developed high-throughput agar-based microarray assay described in Chapter 2.

3.2. Materials and Methods

3.2.1. Compound libraries

A total of 4526 compounds comprising 4406 compounds from the BioFocus proprietary library inhibitors (Livingston NJ, USA), 40 FDA-approved drugs (procured from Selleck Chemicals, Houston, TX, USA), and 80 compounds from Merck's proprietary library, obtained through a collaborative agreement between the Council of Scientific and Industrial Research (CSIR) and Merck, were chosen for the antibacterial screen against carbapenem-resistant *K. pneumoniae* (Table 3.1). Compounds were available as a 10 mM stock in DMSO and kept at -20ºC.

Table 3.1. Compound libraries selected for screening against carbapenem-resistant K. pneumoniae.

Compound libraries	Type of inhibitors	Number of compounds
BioFocus proprietary library	G-protein coupled receptors inhibitors (GPCR) – SFG and TPG	602
	Kinase inhibitors – SFK, TPF, and FFK	1449
	Protease inhibitors – SFP	142
	Ion-channel inhibitors – CNL, FFI, and SFI	827
	Alpha helix mimics – AZD and HM	1151
	Nuclear receptor mimic inhibitors – NNL	131
	Fragments – Series	104
Selleckchem	Anticancer drugs	16
	Antiviral drugs	8
	Steroids	2
	Immunosuppressants	2
	Hormone therapy drugs	3
	Glucocorticoid receptor agonist, antidiabetic, anti-rheumatic, and other drugs	9
Merck proprietary library	Undisclosed	80

3.2.2. Microarray printing

Before printing, compounds were thawed at room temperature for 30 minutes and 2.4 µL aliquots of each compound were subsequently pipetted into conical-shaped 96-well plates. The polymer solution (9.6 µL) prepared as described in section 2.2.3, was subsequently pipetted into each well to a final volume of 12 µL. Mixed solutions were loaded into capillaries and using a custom-built microarray printer, solutions of respective compounds were printed (at 2 mM per spot) on CNF-coated HDPs, and the HDPs were processed as described in section 2.2.4. A total of 512 compounds were printed on each HDP, including 480 library compounds (printed at 2 mM per spot), 16 positive control spots (8 PMBS and 8 CSTS spots), and 16

negative control spots (dissolution solvent - DMSO). Controls were positioned in columns F, K, V, and AA of the arrays (Figure 3.2). A total of 20 HDPs were preferably printed per print session.

3.2.3. High-throughput screen

The screening of compounds against the carbapenem-resistant *K. pneumoniae* was carried out using the agar-based microarray assay described in section 2.3.1. The primary screen was performed against the KPC-producing *K. pneumoniae* strain (ATCC BAA – 1705) at a single compound concentration of 2 mM per spot to ensure that the printed spots had sufficient quantity of the test compounds to achieve the desired biological effect. A separate screen against a carbapenemase-negative *K. pneumoniae* (ATCC 33495) strain was included as a control. Printed HDPs were seeded with inoculated agar, incubated, and processed as described in sections 2.2.2 and 2.2.5.

3.2.4. Secondary screen for determining the accuracy of primary screen results

To assess the accuracy of the results obtained in the primary screen, 5% of the compounds with *Z*-scores ranging between -1 and -2 SD were selected for each test organism and screened using the standard broth microdilution assay as described in section 2.2.7 to test the accuracy of the data analysis method and hit selection criteria. The assay was carried out by two-fold serial dilution of compounds in MHB in 96-well round bottom microtiter plates (Greiner Bio-One, Germany) to obtain final concentrations ranging from 0.25 to 1 mM. Fifty microliters of McFarland No. 0.5 adjusted cultures of *K. pneumoniae* 1705 and 33495 were added to respective wells, to make a final volume of 100 µL and subsequently incubated at 37ºC for 18 hours. Following incubation, INT was added to each well, and absorbance was recorded as described in section 2.2.7. The assay was run in duplicate.

3.2.5. Determination of the bactericidal activity of active compounds

The bactericidal activity of active compounds was performed as described by Parvekar and colleagues (Parvekar et al., 2020), with modifications. Fifty microliters of the 18 hours culture (of section 3.2.4) were sub-cultured into fresh 100 µL of MHB. Plates were incubated at 37ºC for 18 hours. Following incubation, INT was added to each well, and absorbance was recorded as described in section 2.2.7.

3.2.6. Image processing and data extraction

The HDPs of the high-throughput screen were imaged as outlined in section 2.2.8. Captured images were processed (montage building and spot extraction) and data were extracted (measured colony densities on printed spots) as outlined in section 2.2.9.

3.2.7. Data analysis

Primary screen data were normalized using the *Z*-score method, with the equation:

$$Z - \text{score} = \frac{\text{X}_{(\text{test sample})} - \overline{\text{X}}_{(\text{mean})}}{\text{S}_{(\text{standard deviation})}}$$

Where X was the colony density on test compound spots, $\overline{\text{X}}$ was the mean of the data set, and *S* was the SD of the data set.

The degree of spot size variation was determined by calculating the percent coefficient of variation (%CV) as:

$$\%\ \text{CV}_{\text{coefficient of variation}} = \frac{\sigma_{\text{standard deviation}}}{\mu_{\text{mean}}} \times 100$$

Where σ was the SD and μ was the mean of the data set.

Percent bacterial inhibition of compounds in the secondary screen was determined by normalizing the absorbance (Ab_{450}) data using the equation:

$$\%\ \text{Inhibition} = \frac{\text{Ab}_{450}\ \text{of treated wells} - \text{Ab}_{450}\ \text{of untreated wells}}{\text{Ab}_{450}\ \text{of untreated wells} - \text{Ab}_{450}\ \text{of broth}} \times 100$$

Where Ab_{450} was the absorbance read at 450 nm wavelength. The IC_{50} of active compounds was determined as described in section 2.2.10.

3.3. Results and Discussion

3.3.1. Assessment of compounds' compatibility with the HPMC-6 cp polymeric printing solution

The diversity of compounds in this screening campaign necessitated the assessment of the compounds' physical compatibility with the polymeric printing solution. The compound and polymer solution mixtures were visually observed for precipitation, color change, gelation, and cloudiness (Marsilio et al., 2016). Of the four indicators of physical incompatibilities, a slight color change from violet (color of sulforhodamine B in a polymer solution) to a pink-purple tint was observed in 4.89% of preparations (Figure 3.1 B). This observation was an indication that HPMC-6 cP did not have universal compatibility with compounds in this study, a commonly encountered phenomenon in drug-delivery systems, especially pharmaceutical excipients of polymeric nature (Mohamed et al., 2017). In pharmacology, these interactions are said to affect the "chemical nature, stability, and bioavailability of drugs, which consequently affect their efficacy and safety" (Bharate et al., 2010). The effect of the interaction between the polymeric solution and compounds was not investigated in this study.

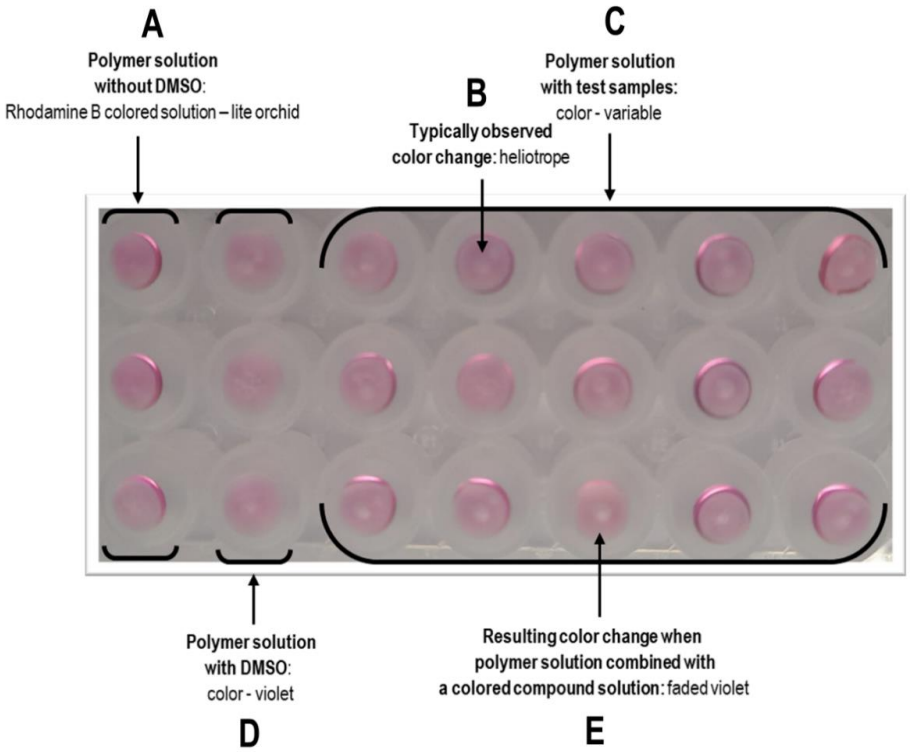

Figure 3.1. Physical compatibility of compounds with the polymeric printing solution. (A) Polymer solution without DMSO: sulforhodamine B colored solution – lite orchid, (B) typically observed color change: pink-purple tint, (C) polymer solution with test samples: variable colors, (D) polymer solution with DMSO: color – violet, (E) color change when polymer solution combined with a colored compound: faded violet.

3.3.2. Analysis of the microarray print

To conduct an antibacterial screening campaign using the high-throughput agar-based microarray assay described in section 2.3.1, compounds were printed in ten independent printing sessions, at a density of 512 compounds per HDP, arranged in 32 columns and 16 rows (except for the mini screen that had a density of 256 reactions) (Figure 3.2 A and B). The previously established microarray spot density for siRNA microarrays was over 3000 spots per HDP (Tantoh, 2014). However, for this chemical microarray assay, there had to be a consideration for the radial diffusion of compounds from printed spots and the possibility of the zones of inhibition contamination, as observed in section 2.3.3.1. This is a technical limitation associated with well-less screening platforms (Bailey et al., 2004). Therefore, to avoid the zone of inhibition contamination, the printed spots were vertically and horizontally interspaced at 1054 and 1553.5 µm, respectively.

Several assessments were carried out to determine the quality of microarray prints. Evaluating parameters included printability of printing solutions and spot uniformity. A total of 4526 compounds were prepared for microarray printing, but only 4281 were successfully printed, giving 5.4% missing spots. A spot diameter threshold of ≥ 100 px (> ~272.7 µm) was set for spot extraction on CellProfiler™ to exclude spots that were too small to derive any valid secondary measurements (Bajcsy, 2005). The excluded spots made-up 3.3% of the 4281 printed spots. The percentage of missing and excluded spots in this study was within the accepted range (1 – 10%) of microarray printing (de Brevern et al., 2004). The cause of these effects was attributed to either, (1) poor contact between printing elements and the immobilization matrix (CNF film), caused by sight unevenness (convex/concave) of the HDP's glass substrate, and/or (2) capillary recoiling which was characterized by printing solutions retracting within the glass capillary, an indication of a strong adhesive force to the cohesive force of compounds within the print solution, and therefore, causing printing solutions to keep rising to the top end of the glass capillaries. This effect was attributed to fluctuating climatic conditions (temperature and humidity) within the printing room during sample loading and printing.

To determine the degree of spot size variations, the total area of successfully printed spots was measured (in pixel units – px), grouped, and graphically presented in a bar graph (Figure 3.3 A). Variably sized spots were observed in all ten printed microarrays, with 4% spots ranging between 7 800 and 10 000 px (~272.7 ± 26,08 µm diameter), 23% spots between 10 000 and 15 000 px (~327.3 ± 19.01 µm diameter), 43% spots between 15 001 and 20 000 px (~382.7 ± 24.47 µm diameter), and 29% spots between 20 001 and 26 500 px (412.8 ± 29.89 µm diameter) (Figure 3.3 A and B). The %CV of spot areas was 22% (n = 4154). Spots

within the 7 800 and 10 000 px range were mostly located in rows 1 and 16, and columns A and B of the arrays (e.g., Figure 3.2 B). This effect was mainly attributed to poor contact between printing elements and the CNF-coated HDP glass substrate and the tendency of polymeric printing solution to lose moisture and become slightly viscous when the printing elements remained inactive for longer than ~2 hours. This resulted in partially printed spots (Figure 3.3 C1 – 4). Spots within the 10 000 – 26 500 range were fairly distributed across the arrays. A notable source of variation within this range was due to different drying patterns of the spots, where some spots presented with a homogeneous drying pattern (Figure 3.3 E1) and some presented with varying degrees of the Marangoni effect (a phenomenon where particles move towards the center of the spots, caused by surface tension gradient, generated either by a composition of the printing solution or a temperature variation on the CNF matrix) (Hu and Larson, 2005). This resulted in different spot outlines and area measurements (Figure 3.3 E2 – 5) and the observed impact of this effect was variable colony densities over differently sized spots (Figure 3.3 D1 – 5).

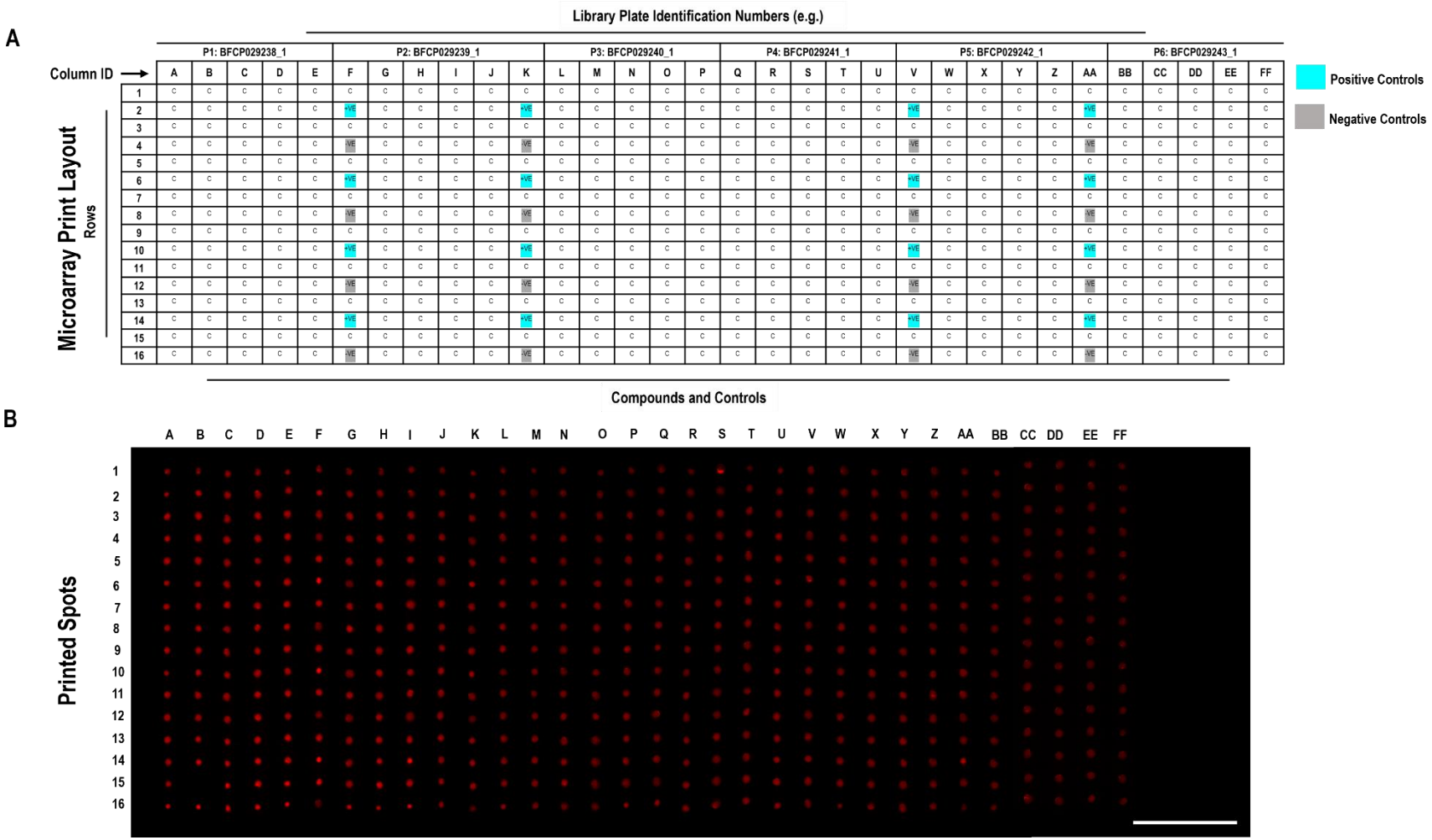

Figure 3.2. High-throughput microarray print layout. (A) Microarray print layout showing the arrangement of test samples and controls. (B) An array of printed spots on a 20 x 60 mm CNF-coated glass substrate. The array was generated by mechanically spotting printing solutions of the compounds on a CNF-coated HDP's glass substrate using a custom-built microarray printer at 15 milliseconds contact time. Abbreviations: C = compound, ID = identity, +ve = positive control, -ve = negative control. Scale bar = 5000 µm.

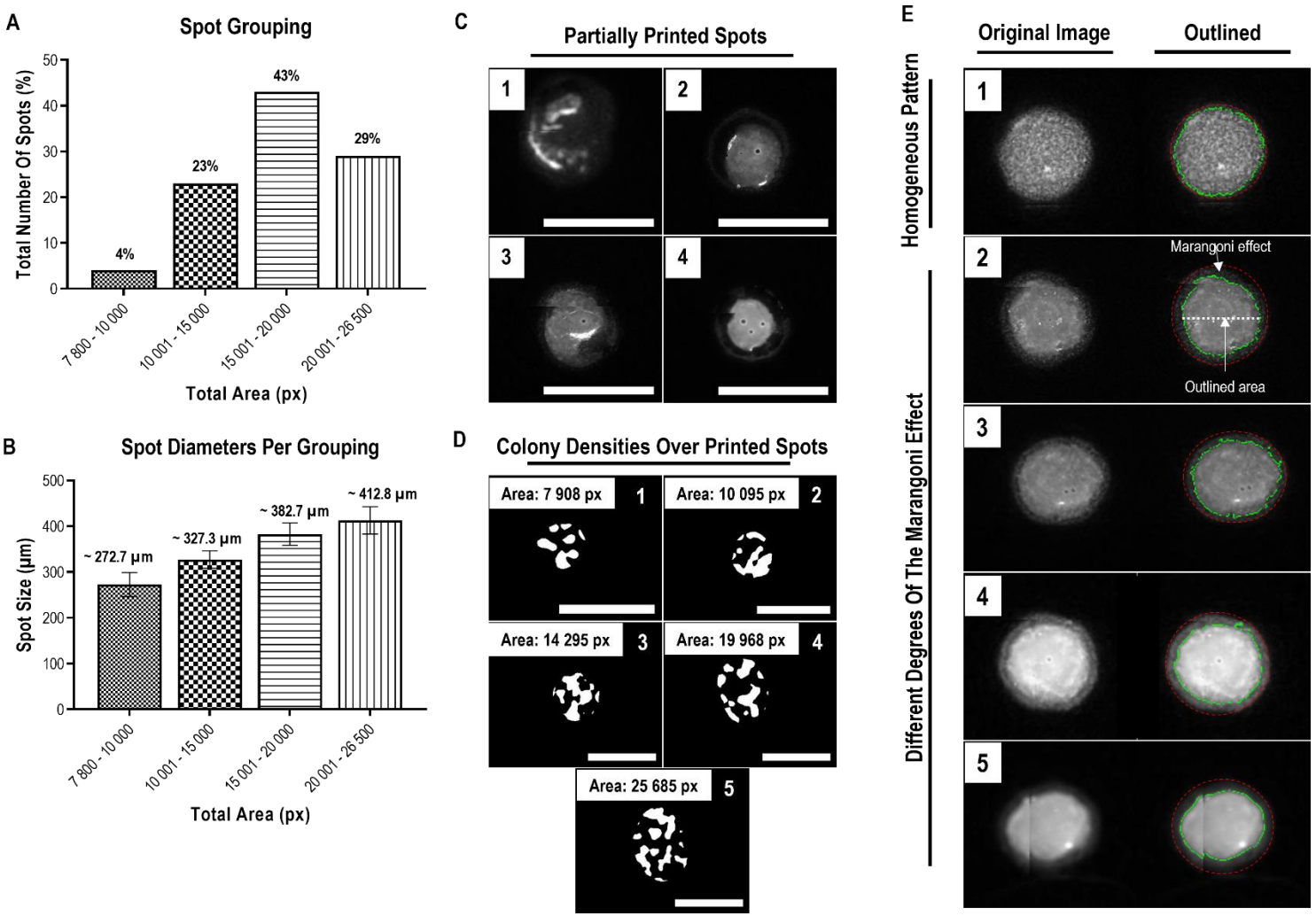

Figure 3.3. Assessment of printed spots for variabilities. A printing solution composed of compounds, HPMC-6 cP polymeric solution, and a fluorescent maker, was printed on CNF-coated HDPs, dried, and spots assessed for variabilities. (A) A bar graph showing the grouping of spots based on their total areas. (B) A bar graph showing the diameters of spots in each spot's total area groupings. (C 1-4) Binary images showing partially printed spots. (D) Binary images showing colony layered spots of different sizes. (E 1) A binary image showing a homogeneous drying pattern of a spot. (E 2-5) Binary images showing different degrees of the Marangoni effect (indicated by red dotted lines). Scale bar = 500 µm. Abbreviation: px = pixel units.

3.3.2. Primary antibacterial screen

To identify compounds with anti-carbapenem-resistant *K. pneumoniae* activity, randomly selected compounds were screened against a strain of *K. pneumoniae* harboring multiple resistance mechanisms including KPC-production, cephamycins, and ESBLs (Broberg et al., 2013). A diverse group of inhibitors (from the BioFocus library) and FDA-approved drugs with different mechanisms of action were chosen for screening, to increase the likelihood of finding active compounds against the test organism (Galloway et al., 2009). Compounds were tested at a concentration of 2 mM per spot. Primary screening concentration much higher than the recommended 1 – 10 µM (Hughes et al., 2011) was used to ensure that the nanoliter volumes (~5.1 nL) printed on HDPs had sufficient compound to show the desired biological effect. For screening, compound printed HDPs were seeded with *K. pneumoniae* (1705 and 33495) inoculated agar and incubated as previously described. Figure 3.4 represents a typical screen with the agar-based microarray assay, where an array of ~512 spots (Figure 3.4 A) was seeded with bacteria inoculated agar. Following incubation, uniform growth of agar-embedded colonies formed over the spots (Figure 3.4 B). The appearance of clear zones around positive control spots was an indication of antibacterial activity and confirmation of compounds diffusing from the printed spots into the agar and inhibiting the growth (Figure 3.4 C).

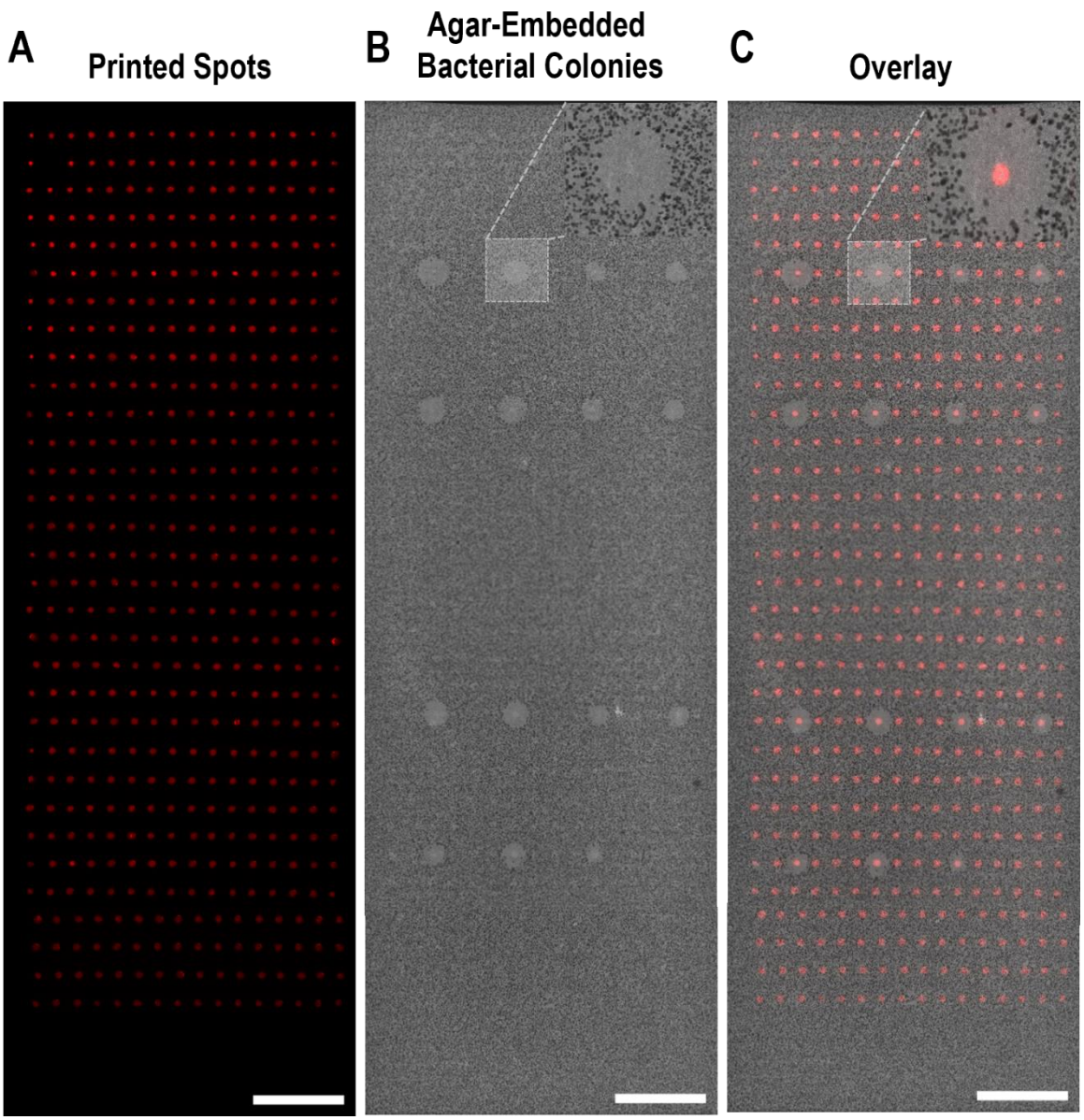

Figure 3.4. A demonstration of an antibacterial screening campaign using the agar-based microarray assay. Printed HDPs were seeded with *K. pneumoniae* inoculated agar and incubated for 14 hours. Following incubation, HDPs were imaged with an automated microscope at 10X magnification, and bacterial colony densities on individual spots were measured. (A) Printed spots on a 24 x 60 mm CNF matrix, (B) agar-embedded bacterial colonies, (C) an overlay image. Scale bar = 5000 µm.

3.3.2.1. Determination of an optimal data analysis method and hit selection approach

Data analysis and hit selection in HTS campaigns do not follow a universal approach, due to different assay formats and data outputs (Brideau et al., 2003). An assay-specific analysis method is carefully chosen to ensure a clear distinction between active and inactive compounds, thus preventing a high rate of false positive and negative hits (Brideau et al., 2003, Shun et al., 2011). Therefore, before the analysis of microarray assay

data, raw data (measured colony densities) of individual spots, extracted from a single HDP, was analyzed using three data normalization methods to determine an optimal data analysis method for the agar-based microarray assay. These include:

(1) Controls-based data normalization (% inhibition), to determine the degree of compounds' inhibitory effect, with high percentages indicative of none or low inhibitory effect and low percentages indicative of high inhibitory effect, was calculated using the equation:

$$\%\ \text{inhibition} = \frac{\mathrm{H}_{\text{(negative control)}} - \mathrm{X}_{\mathrm{i}\ \text{(test compound)}}}{\mathrm{H}_{\text{(negative control)}} - \mathrm{L}_{\text{(positive control)}}} \times 100$$

Where H was the measured colony density on negative control spots, $\mathrm{X_i}$ the colony density on test compound spots, and L the colony density on positive control spots.

(2) Non-controls-based statistical normalization (Z-score) calculated using the equation:

$$Z - \text{score} = \frac{\mathrm{X}_{\text{(test compound)}} - \overline{\mathrm{X}}_{\text{(mean)}}}{\mathrm{S}_{\text{(SD)}}}$$

Where X was the colony density overlaying test compound spots, $\overline{\mathrm{X}}$ the mean of the data set, and S was the SD of the data set. The scoring method determines the SD of the compounds relative to the mean of the whole data set. A positive score was obtained when the test value was above the mean and a negative score when the value was below the mean.

(3) Median-based % inhibition, where data was normalized using the median value of the whole data set, was calculated using the equation:

$$\%\ \text{Median inhibition} = 100 \times \left(1 - \frac{\mathrm{X}_{\text{i(compounds)}}}{\text{Median (of all } \mathrm{X}_i s)}\right)$$

Where $\mathrm{X_i}$ was the measured colony density on test compound spots which was divided by the median of data set. Percentages of inactive samples laid close to zero and active compounds laid close to 100% (Brideau et al., 2003). Analyzed data were plotted as scatter graphs and presented in Figure 3.5.

Similar to data analysis, the hit selection criterion is not universal in high-throughput screening. Hit selection thresholds are arbitrary and set based on what is deemed suitable for individual assays (Brideau et al., 2003, Asli et al., 2013). Therefore, for this test, generally used hit selection thresholds were used to test their

suitability and accuracy for the agar-based microarray assay. For the % inhibition methods, a threshold of 50% was selected. For the *Z*-score method, the threshold was set at -2 SD below the mean because the scores indicative of complete bacterial inhibition are below the mean (e.g., positive controls indicated by blue dots on the scatter graphs). The generally used threshold for the *Z*-score method is either 3 SD above or below the mean (Debnath et al., 2012), however, for this data set the lowest scores laid between -3 and -2 SD. These thresholds were indicated by red horizontal lines on the scatter graphs in Figure 3.5 (A – D).

Figure 3.5 A shows a scatter graph of raw intensity values of colony densities on printed spots, where positive controls (blue) are located at zero intensity, indicating 100% growth inhibition (no colony growth on the spots). Negative controls (red), with variable intensities, are randomly distributed among compounds (gray), and indication of a good screen. Figure 3.5 B shows an outcome of the controls-based data normalization, with 57 potential hits within the > 50% threshold. No hits were identified with the *Z*-score method when the threshold was set at < -2 SD below the mean (Figure 3.5 C). Twenty-four potential hits were identified with median-based normalization when the threshold was set at > 50% (Figure 3.5 D). To determine the accuracy of these analyses, a visual assessment of binary images corresponding to selected hits, showing colony distribution around and on printed spots, was conducted. It was observed that random spatial distribution of colonies (without any semblance of a zone of inhibition) and variably sized spots (with a plate-specific %CV of 24) were the cause of the low colony densities measurements, not antibacterial activity. The examples of the described effects are demonstrated in Figure 3.5 E.

The standard interpretation of % inhibition data (Figure 3.5 B) assumes that low colony densities are a result of bioactivity. However, when factoring in the previously identified systemic errors, the outcome of this analysis was misleading and had a high probability of generating false positive hits. In comparison, the median-based normalization and the *Z*-score method are based on the identification of outliers of the data set as hits (Brideau et al., 2003). In this case, it would be compounds with activity relatively similar to that of positive controls. Using any of the tested methods for data analysis would require setting the hit selection threshold relatively low and only selecting extreme outliers of the data set as hits, to circumvent the effect of identified systemic errors. Therefore, for primary screen data analysis, the *Z*-score method was selected as optimal for the agar-based microarray assay, with the hit selection threshold set at < -2 SD below the mean. The analysis was carried out in combination with a visual assessment of binary images of compounds with *Z*-scores of < -1. Thus, creating a two-step hit identification/data confirmation process.

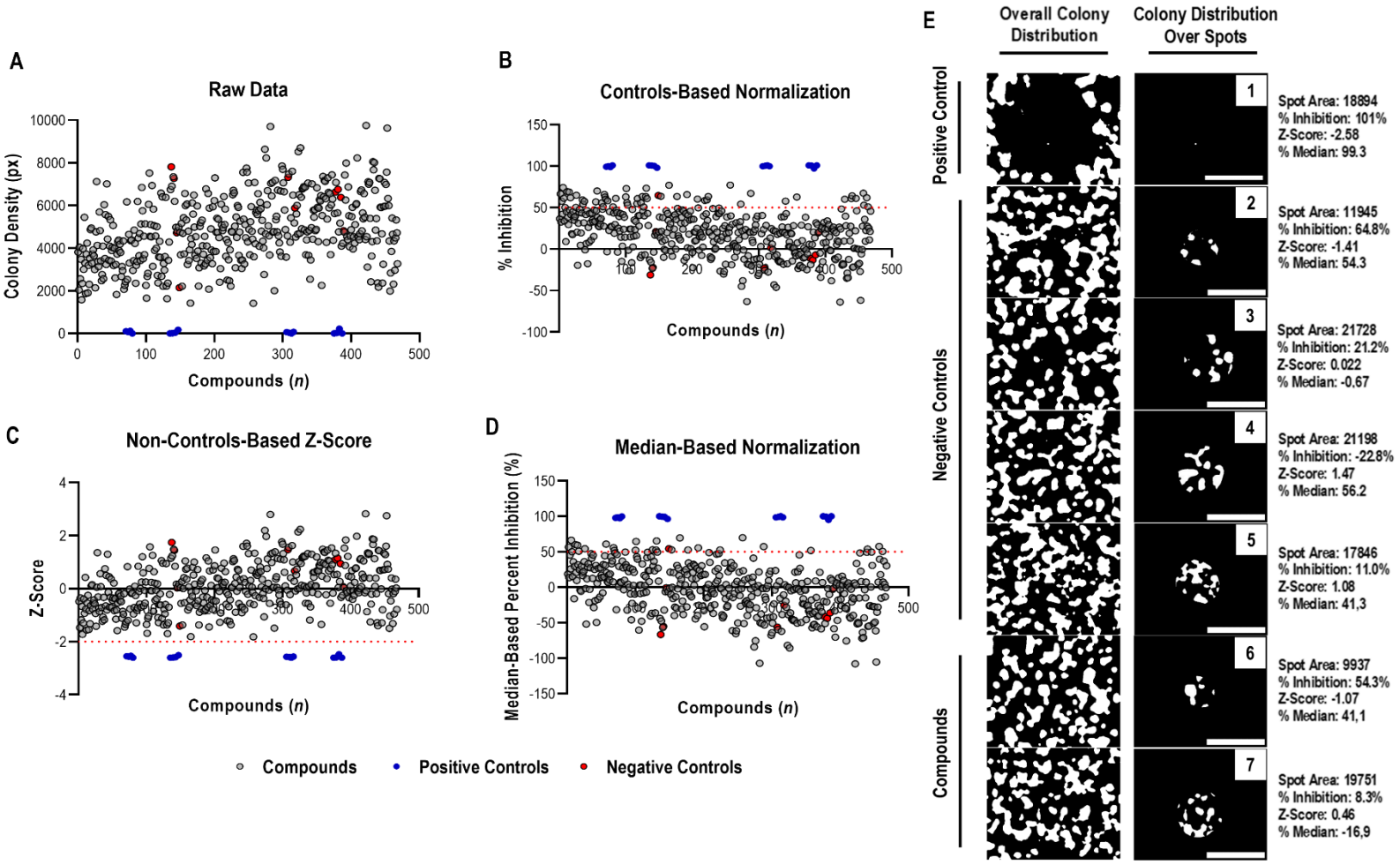

Figure 3.5. The determination of an optimal data analysis method and hit selection criteria. (A) A scatter graph of unnormalized data (colony densities in pixel), (B) a scatter graph of controls-based normalized data, (C) a scatter graph of non-controls-based *Z*-score normalized data, and (D) a scatter graph of median-based normalized data. Positive controls indicating 100% growth inhibition are shown in blue, negative controls indicating 0% growth inhibitory are shown in red, and compounds are shown in gray. Hit selection thresholds are indicated by red dotted horizontal lines on the scatter graphs, with hits identified by their proximity to the positive controls. (E) A display of binary images showing the distribution of colonies around and over the positive control (1) negative controls (2 – 5), and compounds (6 -7), with their corresponding spot size, % inhibition, *Z*-scores, and % median inhibition. Scale Bar = 500 µm.

3.3.2.2. Primary screen and hit selection

The raw data of the primary screen was normalized using the *Z*-score method, as established in section 3.3.2.1, and plotted as scatter graphs to demonstrate the effects of compounds against drug-resistant and control strains (Figure 3.6). A hit was defined as a compound with a *Z*-score of < -2 SD from the mean. The graphically presented outcome of the screen against *K. pneumoniae* 1705 did not show any compounds with *Z*-scores below the hit selection threshold (Figure 3.6 A). Four compounds with *Z*-scores ranging between -2.03 and -2.32 were identified in the screen against *K. pneumoniae* 33495 (Figure 3.6 B). A visual inspection of binary images of compounds with *Z*-scores of < -1 for spatial colony distribution and the effect of spot size on colony densities, confirmed the absence of antibacterial activity, including the hits identified against *K. pneumoniae* 33495.

The findings of this study are not uncommon in screening campaigns against Gram-negative bacteria, especially *K. pneumoniae,* where few or none of the compounds showed antibacterial activity. These include the drug repurposing study carried out by Younis and colleagues (Younis et al., 2017) that found only two (floxuridine and bleomycin) out of 1600 compounds with anti-*K. pneumoniae* activity, with MICs below 16 µM. An anti-colorectal cancer drug, 5-fluoro-2'-deoxyuridine (FdUrd) (van Laar et al., 1998), was identified as the only drug with anti-KPC-producing *K. pneumoniae* ATCC 1705 activity in a similar study involving the screening of National Institutes of Health's (NIH's) Clinical Collections 1 and 2, containing 727 FDA-approved drugs and small clinical compounds (Younis et al., 2015). A screening campaign of 140,000 small compounds carried out by Semenov and colleagues (Semenov et al., 2021) identified 2517 compounds with antibacterial activity against ESKAPE pathogens and only 23 of them had anti-*K. pneumoniae* activity, with MICs ranging between 0.25 and 1 µg/mL. This outcome was attributed to either the highly selective lipid bilayer outer membrane of bacteria which serves as a permeability barrier for ions and molecules, including antibacterial drugs whose site of action is beyond the periplasmic space (Darby et al., 2023). This could be a possible explanation behind the outcome of this screen, since over 75% of tested inhibitors targeted intracellular functions (Table 3.1) and would need to traverse the outer membrane to reach their targets (Miller, 2016, Muñoz and Hergenrother, 2021). A second possibility could be that the tested library lacked antibacterial properties against the *K. pneumoniae* strains.

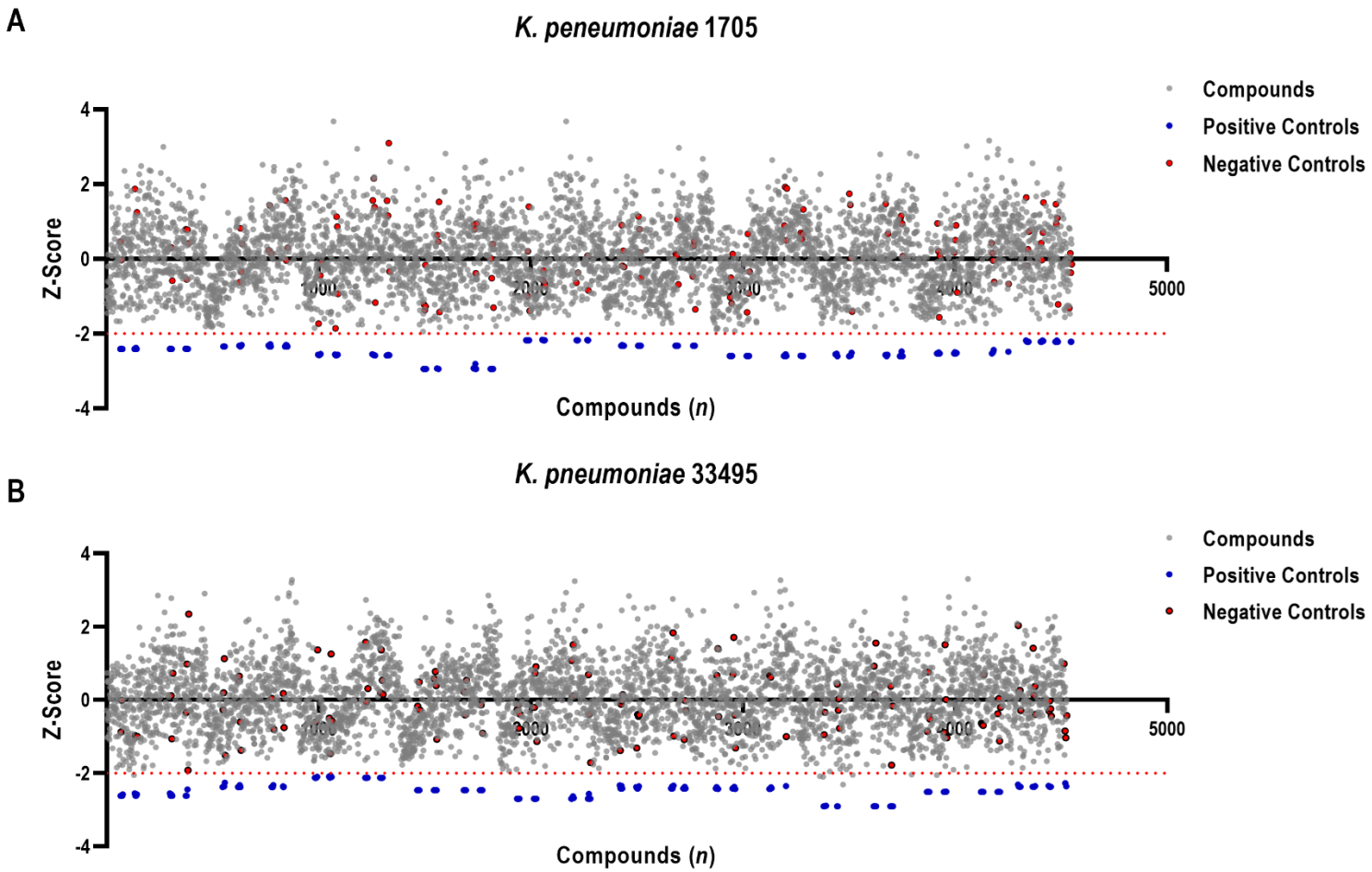

Figure 3.6. A primary screen of compound libraries and FDA-approved drugs for antibacterial activity, using the agar-based microarray assay. A library of 4154 compounds was successfully screened against a KPC-producing *K. pneumoniae* 1705 and a drug-susceptible *K. pneumoniae* 33495, at a single concentration of 2 mM per spot. Colony densities measured from 4154 spots were normalized using the Z-score method and the obtained scores were presented as scatter graphs. (A) A scatter plot of Z-scores obtained from the screen against *K. pneumoniae* 1705. (B) A scatter plot of Z-scores obtained from the screen against *K. pneumoniae* 33495. Positive controls indicating 100% growth inhibition are shown in blue, negative controls indicating 0% growth inhibitory are shown in red, and compounds are shown in gray. The hit selection threshold (< -2 SD) is indicated by a red horizontal line on the graphs.

3.3.3. Testing the accuracy and the reliability of the two-step data analysis method and the hit selection criteria

It was previously established that the agar-based microarray assay has two inherent systemic errors (spot size variabilities and random spatial distribution of bacterial colonies overlaying printed spots) that could not be compensated by any of the data analysis methods tested in section 3.3.2.1 (Brideau et al., 2003). As a result, a two-step data analysis method was established and the hit selection threshold for the primary screen data was set relatively low to only allow the selection of extreme outliers (with positive control-like activity) as potential hits, thus, minimizing false positive hits. Whilst these measures served the intended aim, there was a high probability that the set threshold could lead to a high number of false negatives within the -1 and -2 SD range of compounds, since the window of separation between these compounds and the positive controls was relatively small (Figure 3.6). Therefore, it was crucial, especially for a novel assay, to test the accuracy and the reliability of the two-step data analysis method and hit selection criteria established in section 3.3.2.1.

For this assessment, 5% (208 of 4154) of compounds that had *Z*-scores ranging between -1 and -2 SD from the mean in the primary screen against *K. pneumoniae* 1705, were screened using the standard broth microdilution assay. A similar screen was conducted for different compounds (within the -1 and -2 SD range) selected from the primary screen against *K. pneumoniae* 33495, including the four compounds that had *Z*-scores below < -2 SD (Figure 3.6 B). Two-fold serial dilutions of selected compounds were carried out as described in section 3.2.4, and the % inhibition of each compound was determined, and presented in line graphs in Figure 3.7 A and B. The highest concentration of the compound's serial dilution was intended to be 2 mM to emulate test concentrations used in the agar-based microarray. However, due to the limited amount of compound solutions available, a concentration of 1 mM (at 10% DMSO starting concentration) was used instead. It was noted that DMSO is toxic to bacterial cells at concentrations above 5% (Dyrda et al., 2019). Therefore, active compounds were identified as those showing antibacterial activity at < 0.5 mM (< 5% DMSO).

The results of the screen against *K. pneumoniae* 1705 revealed 1 active compound out of the 208 that were tested (Figure 3.7 A), and no active compounds were identified in the screen against *K. pneumoniae* 33495 (Figure 3.7 B). The results of the secondary screen were in perfect agreement with the results obtained in the primary screen (McHugh, 2012), with a percentage agreement (P%) of 99.52% for the screen against *K. pneumoniae* 1705 and 100% for the screen against *K. pneumoniae* 33495, which was calculated using the equation:

$$\mathrm{P\%} = \frac{\mathrm{Agreements}}{(\mathrm{Agreements} + \mathrm{Disagreements})} \times 100\%$$

Where “agreements“ were the number of compounds with similar results in both the microarray assay and the standard broth dilution assay and “disagreements were the number of compounds with different results between the two assay (Araujo and Born, 1985). The outcome of this screen demonstrated that the two-step data analysis method and the hit selection threshold were perfectly suited for reducing false positive hits and ensuring that a minimal number of false negative hits were generated.

The active compound identified in the screen against *K. pneumoniae* 1705 (an ion-channel inhibitor) was further screened, in an 8-concentration serial dilution screen, where it showed bactericidal activity against *K. pneumoniae* 1705 and *K. pneumoniae* 33495, with IC_{50} values of 174.5 and 112.2 μM, respectively (Figure 3.7 C and D). However, no further tests/screens (to determine the spectrum of antibacterial activity or cytotoxicity) were conducted for this compound because its potencies, both inhibitory and bactericidal, were way above the acceptable range of 100 nM to 5 μM (Hughes et al., 2011).

.

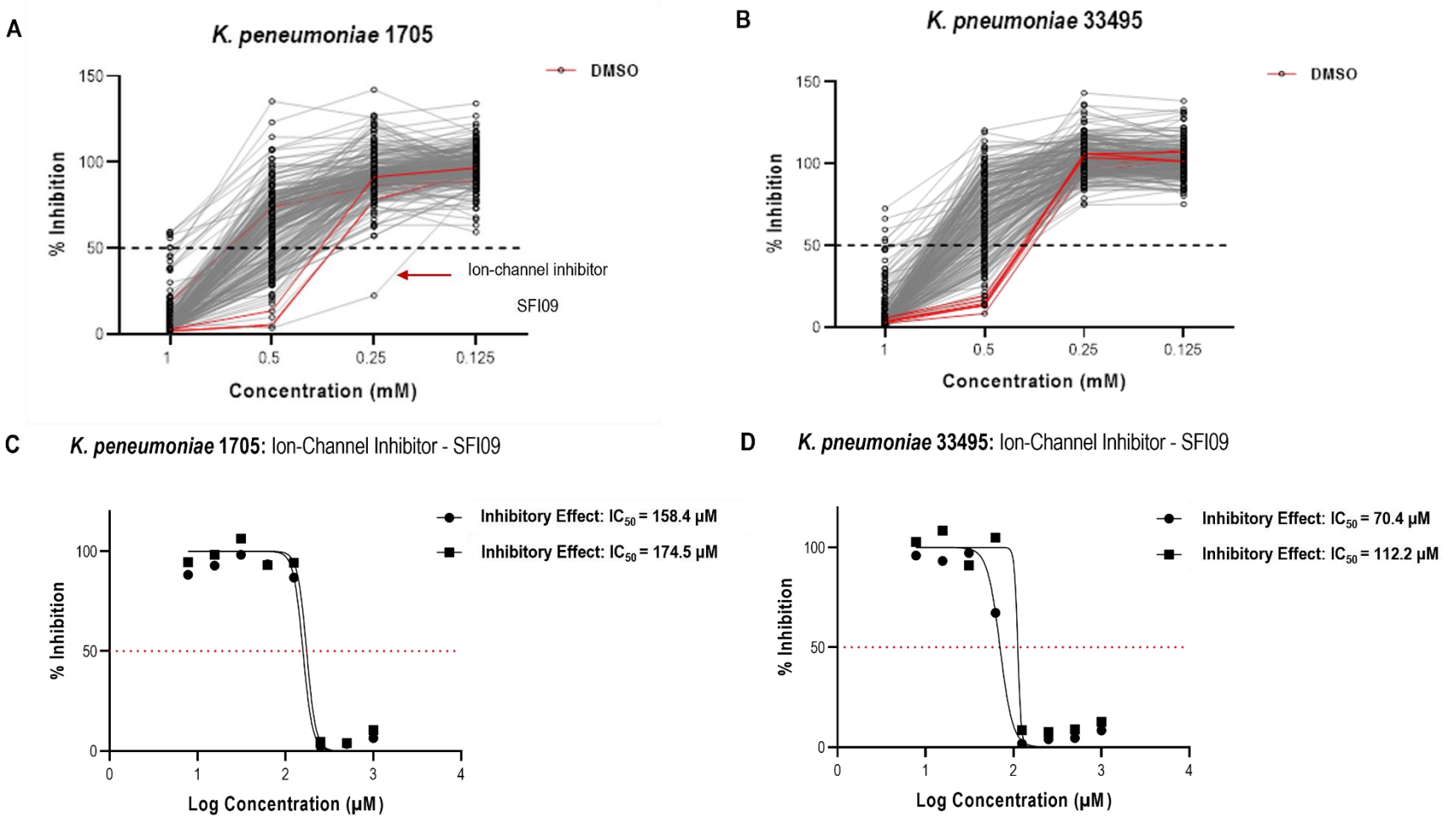

Figure 3.7. Secondary screen to determine the accuracy of the two-step data analysis method optimized for the agar-based microarray assay. A 2-fold serial dilution of 416 compounds (208 against each strain) was carried out against the drug-resistant and control strains using the standard broth microdilution assay. Percentage inhibition of the data set was determined and resulting data were presented as line graphs. (A) % inhibition of *K. pneumoniae* 1705, with one active ion-channel inhibitor. (B) % inhibition of *K. pneumoniae* 33495, with none of the compounds showing activity. (C and D) Dose-response of the ion-channel inhibitor against *K. pneumoniae* 1705 and *K. pneumoniae* 33495, respectively.

3.4. Summary

An HTS campaign was carried out using the agar-based microarray assay described in Chapter 2. The screening was undertaken with the hope of identifying hits with druggable properties for the development of antibacterial drugs with anti-carbapenem-resistant *K. pneumoniae* activity. The screening campaign involved screening 4154 compounds of diverse chemical classes, aimed to broaden the search for hits against the carbapenem-resistant *K. pneumoniae*. However, none of the compounds showed the desired antibacterial activity. This was attributed to either the virulence mechanism of Gram-negative strains used in this study (i.e., the selectively permeable cell membrane) (Darby et al., 2023) or the likelihood that none of the compounds have antibacterial properties. However, the outcomes of this screen do serve a purpose as a roadmap for future screening campaigns against MDR *K.* pneumoniae, especially when testing target-specific compound libraries. The finding also echoes the failures and challenges experienced in the discovery of new antibacterial drugs against Gram-negative bacteria (Jackson et al., 2018, Miethke et al., 2021).

The developed agar-based microarray assay enabled a screen of this study's compound library in ten printing sessions, with a density of 512 compounds printed per session. Mechanical errors and environmental conditions accounted for 5% of missing spots and 3.3% of partially printed spots, which was within the acceptable range (1 – 10%) of microarray printing (de Brevern et al., 2004). The high-throughput nature of this screening platform enabled the printing of compounds at a high concentration whilst using small amounts of the compound's stock solutions (which were available in limited amounts). Furthermore, the compound-loaded printing elements (glass capillaries) printed tens of HDPs in a single printing session (to repeat antibacterial screens), with more printing solution remaining to print hundreds more HDPs (Tantoh, 2014). Thus, saving the compounds solutions, consumables, and time that would be required for a repeat print. This simplistic screening approach was highly efficient, requiring minimum effort to conduct the antibacterial screening campaign (Figure 2.8). For data analysis, an assay-specific two-step data analysis method was successfully optimized for minimizing a probable number of false positive hits caused by the inherent systemic errors of the agar-based microarray assay (spot size variability and random spatial distribution of colonies) identified in section 3.3.2. This method demonstrated a robust hit mining capability with a low rate of false positives and false negatives (McHugh, 2012), as demonstrated by the percentage agreement of >99% between antibacterial results obtained in the primary screen (using the agar-based microarray assay) and those obtained in the secondary screen (using the broth microdilution assay). Overall, the assay

performed as intended and the chosen data analysis and hit selection methods ensured minimal false positive hits and a high degree of accuracy.

Chapter 4

General discussions and recommendations

4.1. Background

The emergence and continued spread of carbapenem-resistant *K. pneumoniae* is a major threat to human health, with increased risk of morbidity and mortality resulting from limited or ineffective treatment options (Li et al., 2020, Maraolo et al., 2021, Tesfa et al., 2022, Hu et al., 2020). The grand scale and impact of carbapenem-resistant *K. pneumoniae* necessitated its prioritisation for drug discovery and development (World Health, 2017). Therefore, to contribute to the ongoing drug discovery efforts, an agar-based microarray assay was developed to accelerate cost-effective drug screening campaign against the carbapenem-resistant *K. pneumoniae*.

4.2. Assay development

A high-throughput agar-based microarray platform was developed for compound screening against carbapenem-resistant *K. pneumoniae*. The optimised assay consisted of several key steps, including the arraying of compounds (mixed in a 1.6% w/v HPMC polymeric solution) into a 24 x 60 mm absorbent CNF immobilization matrix (made from a 1.5% w/v CNF slurry), thus, generating spots ranging between ~270 and ~420 µm in size. Overlaying the compound printed matrix with the inoculated agar (0.8% w/v) resulted in the swelling of the polymer matrix serving as a binder for compounds, the dissolution of compounds and their subsequent radial diffusion through the ~0.4 mm layer of agar (overlayed with a 1.5% w/v plain agar which formed a ~1.6 mm layer), thus forming a concentration gradient around each spot. Incubating the seeded matrix resulted in the formation of agar-embedded bacterial colonies, which were subsequently imaged with an automated imaging system to identify antibacterial activity in the form of zones of inhibition (Figure 2.1). This HTS method has a minimum throughput of 560 compounds per HDP when the vertical and horizontal centre-to-centre distance of the spots was ~1054 and 1553.5 µm, respectively.

To demonstrate the screening potential of the agar-based microarray assay, a panel of 12 FDA-approved antibacterial drugs (consisting of polymyxins, monobactam, macrolide, aminoglycosides, tetracycline, 3rd-generation cephalosporin, and a diaminopyrimidine) was screened against a panel of five ATCC quality control strains consisting of MDR and drug-susceptible strains of both Gram-positive and Gram-negative types. Varying patterns and levels of bacterial susceptibility were observed on the platform, with PMBS,

CSTS, and GENS active against *K. pneumoniae* 1705 (Figure 2.9 B); PMBS and CSTS active against *K. pneumoniae* 700603 (Figure 2.9 C); PMBS, CSTS, GENS, KANS, G418 sulfate, and TOB active against *K. pneumoniae* 33495 (Figure 2.9 D); PMBS, CSTS, GENS, KANS, G418 sulfate, TOB, and NEOS active against *E. coli* 25922 (Figure 2.9 E); and GENS, KANS, G418 sulfate, TOB, and NEOS against *S. aureus* 25923 (Figure 2.9 F). This outcome demonstrated the ideal degree of specificity of the assay and its adaptability to screen different types of bacteria. The statistical analysis of the proof-of-concept data with the *Z*-factor method yielded scores of 1 for active drugs and scores above 1 (1 >) or below zero (< 0) for inactive drugs (Table 2.1). This result was indicative of an ideal assay for screening (Zhang et al., 1999).

A comparative assessment of the agar-based microarray assay's performance was carried out with the standard broth microdilution assay by comparing the susceptibility profiles of five bacterial strains to 12 standard antibacterial drugs. The results (IC_{50} values) from these two assays did not coincide. However, all drugs that showed activity in the microarray assay had a relatively low IC_{50} in the standard broth dilution assay and those that had no activity in the microarray assay had a relatively high IC_{50} or no activity in the standard assay (Table 2.1). A combination of factors can be attributed to the observed variation, including a probability that there was either a minuscule amount of the drugs in the printed spots or varying degrees of drug dissolution in semi-solid media (Salmon et al., 1996). As a result, the amount was either sufficient to show an inhibitory effect against susceptible bacteria or insufficient to show a distinguishable antibacterial activity against resistant bacteria. A conclusion drawn from this assessment was that the agar-based microarray assay, in its current state, is suitable for primary antibacterial screening to identify hits, instead of being used as an antibacterial susceptibility screening method. Hits identified on this platform will be validated using a secondary low-throughput method, which is a procedural part of early drug discovery when using HTS platforms for primary screening (Hughes et al., 2011, Brideau et al., 2003).

Overall, the miniaturised screening platform demonstrated here presents an efficient, cost-effective, and easily adaptable approach to HTS, with easily accessible screening infrastructure and low operation costs. The established assay workflow was achieved with minimum automation where the modification of the HDP's glass matrix with mechanically produced and biocompatible CNF required minimal effort. A repurposed custom-built microarray printing infrastructure (a genomic microarray technology) was adapted for mechanically printing compounds. A simplistic manual bacterial inoculation approach – the pour-plate method – was used (Sharma et al., 2023). An image-based readout using brightfield imaging of agar-embedded colonies, using a standard Cytation3 automated imaging system, further simplified the screen, thus

eliminating multiple fluorescent tagging processes. Moreover, no specialised software was required for data extraction, a freely available software was utilised for this purpose (i.e., CellProfiler™, ImageJ). Whilst manual aliquoting of compounds and data extraction are possible, a liquid-handling facility and grid-fitting software could expedite these processes. This simplistic HTS approach provides accessibility and ease of use without investing in expensive automated HTS infrastructure.

4.3. Antibacterial screening campaign

An antibacterial screening campaign was conducted using the developed agar-based microarray assay. A library of 4154 compounds, comprised of GPCR inhibitors, kinase inhibitors, protease inhibitors, ion-channel inhibitors, alpha helix mimics inhibitors, nuclear receptor mimic inhibitors, fragments, and FDA-approved drugs of variable mechanisms, was screened for anti-carbapenem-resistant *K. pneumoniae* activity. Diversifying the library was aimed at increasing the likelihood of finding active compounds against the pathogen organism since it presents with multiple virulence factors and drug resistance mechanisms that could potentially enable the evasion of antibacterial activity (Podschun and Ullmann, 1998, Galloway et al., 2009, Davoudabadi et al., 2023). Before mining the primary screen data for hits, a thorough process was undertaken to optimise a stringent assay-specific data analysis method to minimise false positive and false negative hits. To this effect, various data analysis methods were tested (i.e., control-based data normalization, non-controls-based statistical normalization: *Z*-score, and median-based normalization method) and the *Z*-score method (with the hit selection threshold of < -2SD) coupled with visual assessment of binary images for colony sparsity/ random spatial distribution, zones of inhibition, and correlating spot sizes to colony densities, met the criteria of an optimal data analysis method for this assay (Figure 3.5). This two-step hit mining process was established to circumvent the erroneous selection of hits due to two systemic errors (i.e., spot size variabilities and random spatial distribution of bacterial colonies) which are inherent to the agar-based microarray assay (Brideau et al., 2003). The accuracy and the reliability of the two-step data analysis method and hit selection criteria was tested by conducting a secondary screen (using the standard broth microdilution method) on 5% (208 of 4154) of compounds that had Z-scores ranging between -1 and -2 SD (from the mean) in the primary screen against *K. pneumoniae* 1705, and a similar selection and screen was conducted against *K. pneumoniae* 33495 (Section 3.3.3). This method demonstrated a robust hit mining capability with a low rate of false positives and false negatives (McHugh, 2012), as demonstrated by the percentage agreement of >99% between antibacterial results obtained in the primary screen (using the agar-

based microarray assay) and those obtained in the secondary screen (using the broth microdilution assay) (Section 3.3.3 and Figure 3.7).

The screening effort did not yield a hit with antibacterial activity against carbapenem-resistant *K. pneumoniae* (Figure 3.6). This outcome was attributed to either the highly selective lipid bilayer outer membrane of bacteria which serves as a permeability barrier for ions and compounds, including antibacterial drugs whose site of action is beyond the periplasmic space (Darby et al., 2023). This justification was plausible for the outcome of this screen, since over 75% of tested inhibitors targeted intracellular functions (Table 3.1) and would need to traverse the outer membrane to reach their targets (Miller, 2016, Muñoz and Hergenrother, 2021). A second possibility could be that the tested library lacked antibacterial properties against the *K. pneumoniae* strains. Following this analysis, a confirmatory secondary screen was undertaken using 5% of the 4154 test compounds to prove the accuracy of the optimised data analysis method and confirmed the functionality of the assay as a viable primary antibacterial screening method. This screen only identified one false negative hit (ion-channel inhibitor), proving the stringency of the data analysis procedure (Figure 3.7).

The findings of this study are not uncommon in screening campaigns against Gram-negative bacteria, especially *K. pneumoniae*, where libraries of thousands of compounds yield few or no hits (Younis et al., 2015, Younis et al., 2017, Semenov et al., 2021, Lei et al., 2020). In the past six years since the publication of the WHO's priority list (WHO, 2017) there has been minimal success in finding new antibacterial drugs against MDR *K. pneumoniae* with only 4 FDA-approved drugs, 11 agents in clinical development, and 58 agents in preclinical development (WHO, 2022a). Multiple approaches are now being applied to find efficacious treatment including finding alternative therapies (Choi et al., 2019, Mackow et al., 2019, Anand et al., 2020, Wang et al., 2020, Pareek et al., 2021), establishing methods to re-sensitize MDR bacteria to existing antibiotics (Laws et al., 2019, Gholizadeh et al., 2020, Tao et al., 2022), and mechanisms to circumvent resistance mechanisms (Halasohoris et al., 2021). This platform, therefore, provides an avenue for continuing screening efforts against MDR *K. pneumoniae* with the hope of identifying druggable hits. The starting point in this case could be the further exploration of ion-channel inhibitors.

4.4. Future perspectives

The current study demonstrated the antibacterial screening capability of the high-throughput agar-based microarray screening approach. Despite its great potential, some experimental challenges were encountered. For instance, the capacity of the printed drug spots was restricted to 560 sports per HDP, though the platform has the flexibility to accommodate higher spot density (Tantoh, 2014). This limitation was caused by the

degree of radial spreading of the printed compound beyond the periphery of the printed spot which resulted in the zone of inhibition contamination (Figure 2.9 F). Identifying measures to restrict/limit the concentration gradient of compounds to within ~200 µm from the edge of the printed spot would enable a decrease in both the vertical and horizontal spot interspacing, thus increasing throughput. Some of these measures could be a slight increase in the agar concentration (from 0.8% to 1%) which could potentially increase throughput to 832 spots per HDP (Figure 2.5). Further optimization of the polymeric printing solution could achieve even higher throughput as suggested by Bailey et al. (2004). The next task would be to further optimize the bacterial inoculum densities. This parameter was identified as a contributor to colony sparsity/ random spatial distribution. The platform demonstrated good adaptability to screen different types of bacteria. Therefore, future studies will focus on optimising the platform for screening against other bacterial species.

4.5. Conclusion

This study was carried out to develop a high-throughput agar-based microarray assay for screening compound and drug libraries against carbapenem-resistant *K. pneumoniae*. Eight objectives were set out to fulfill the aims of the study. Of the seven, only five were completed. The completion of the subsequent objectives (i.e., which were (6^{th}) to perform a secondary screen on the candidate hit(s) for further validation, and (7^{th}) to determine the spectrum of activity of bioactive compounds/drugs) were reliant on the identification of hits with notable anti-carbapenem-resistant *K. pneumoniae* activity. However, no such compounds were identified, and therefore the remainder of the study objectives could not be completed. This being said, as demonstrated in the experimental chapters, the developed screening platform can still be utilized for future antibacterial screening campaigns.

Appendix

Appendix A: Dose-response curves

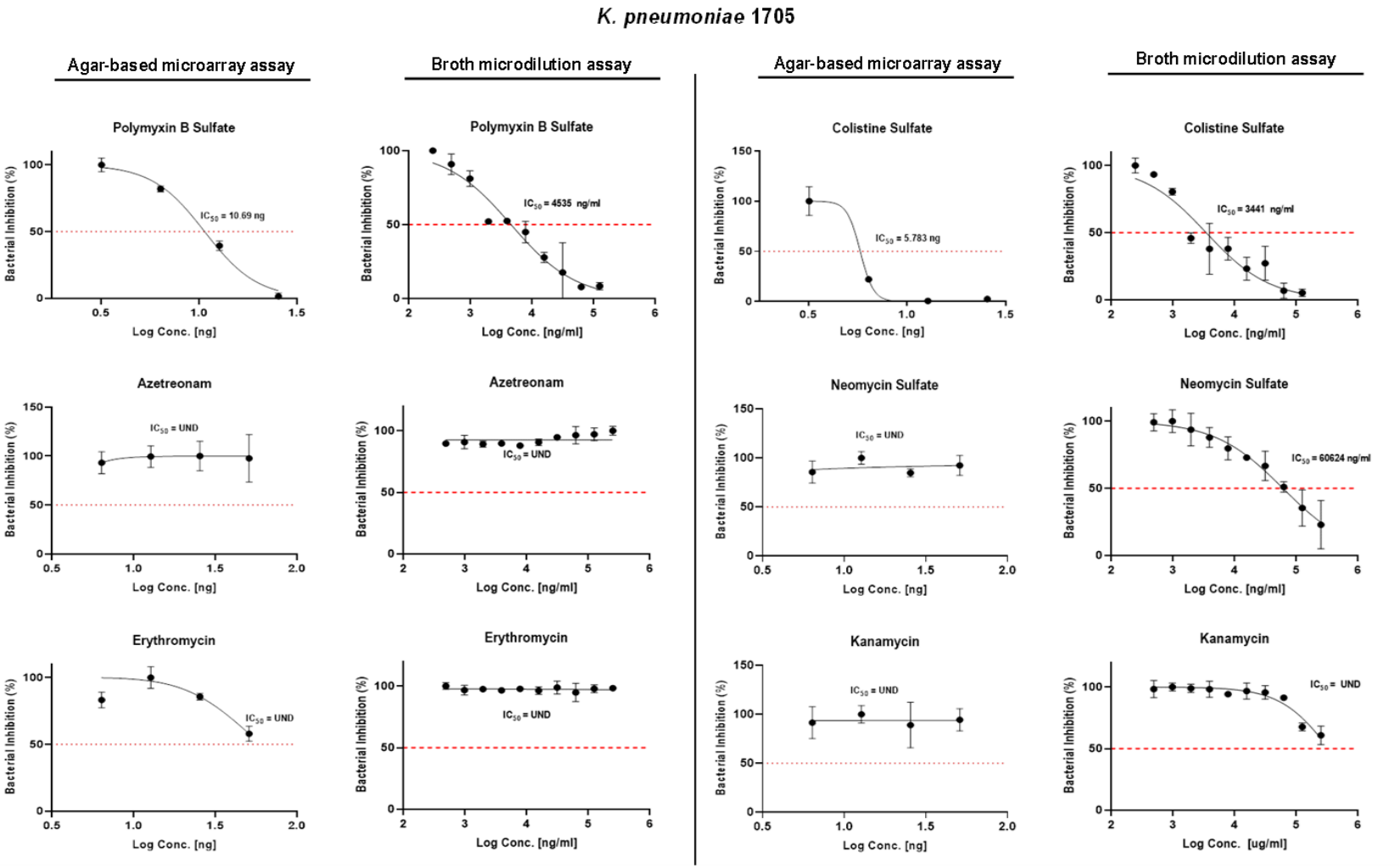

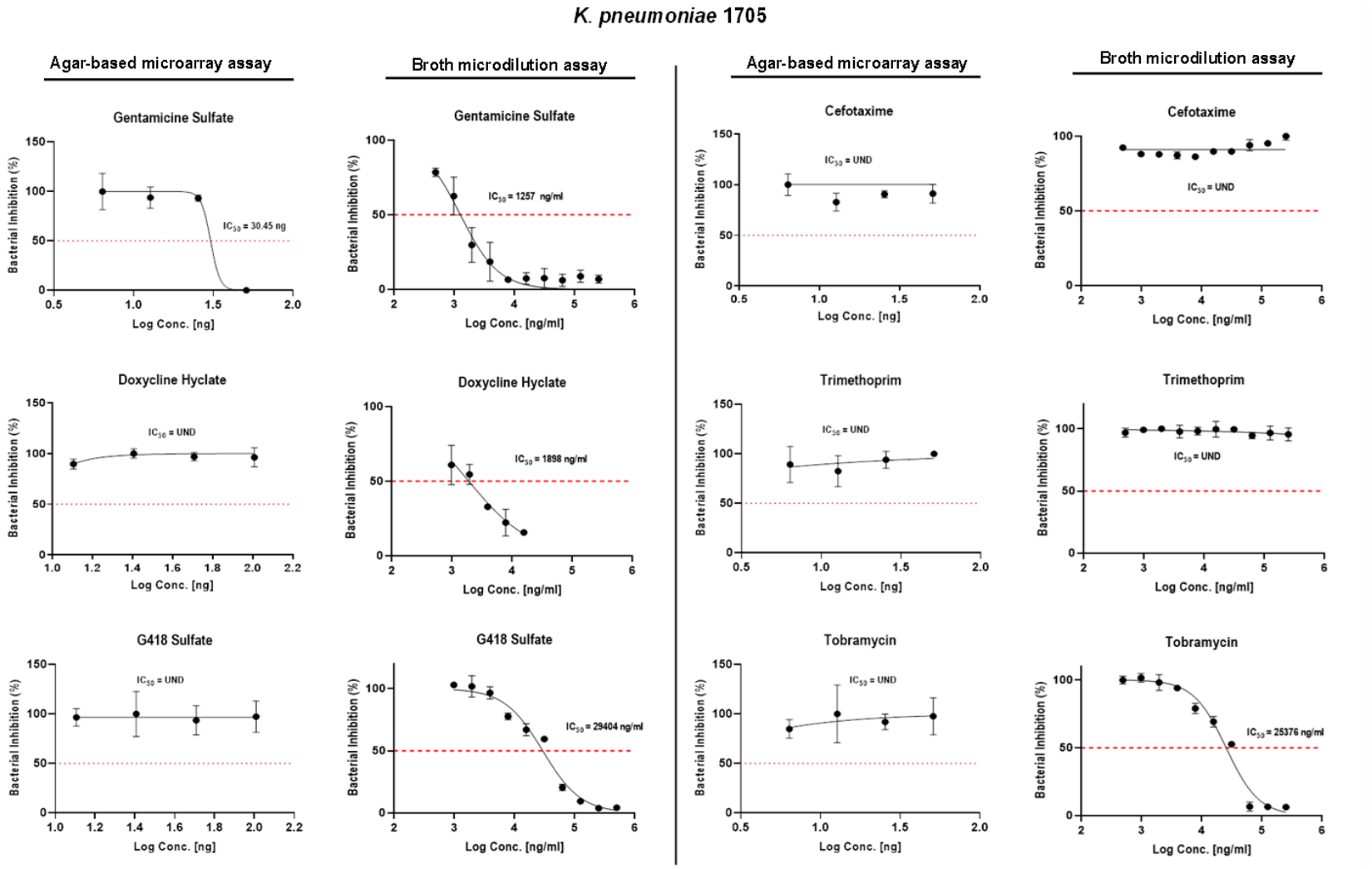

Figure A 1. Dose-response profile of *K. pneumoniae* 1705 obtained using the agar-based microarray and the standard broth microdilution assay.

K. pneumoniae 700603

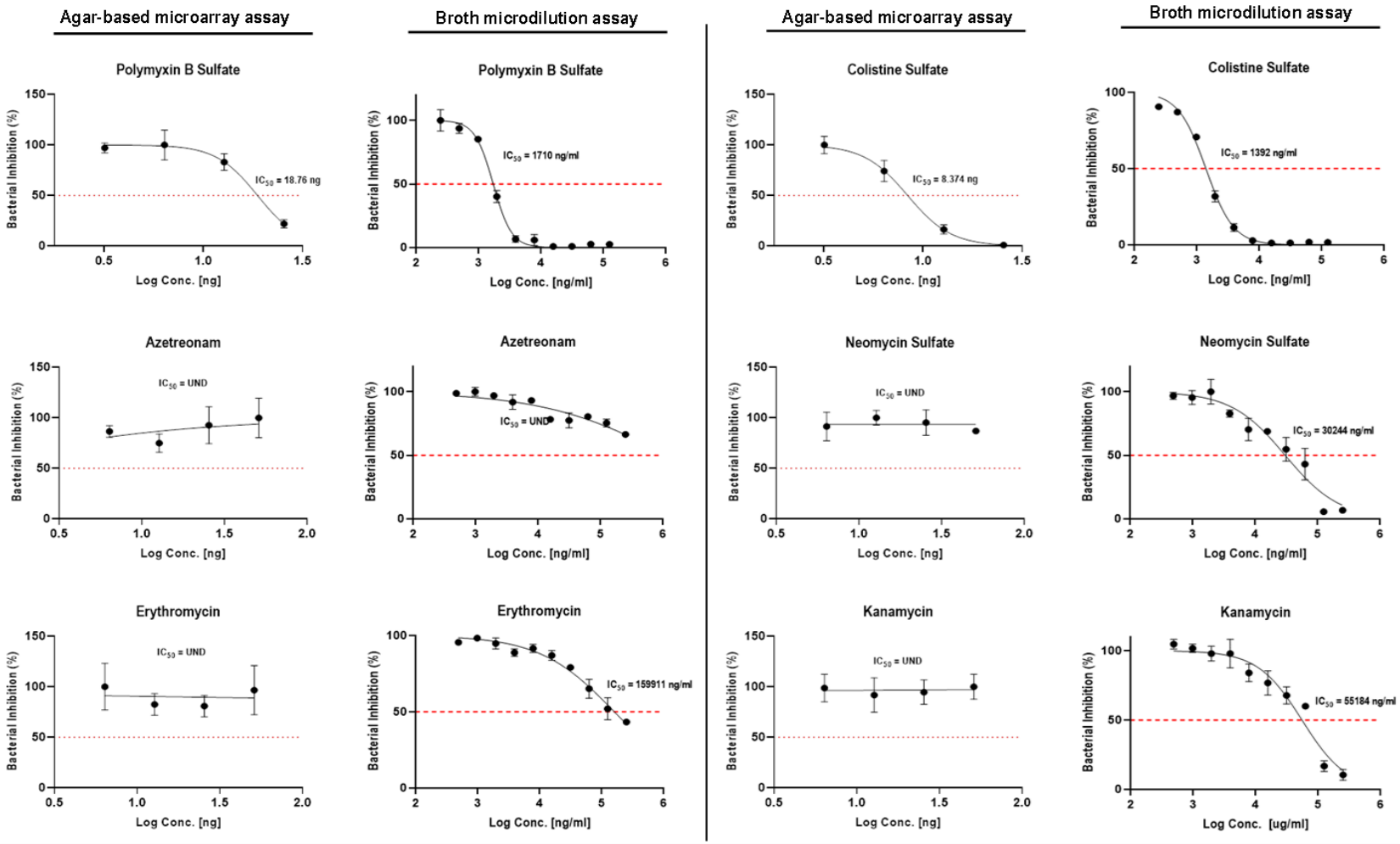

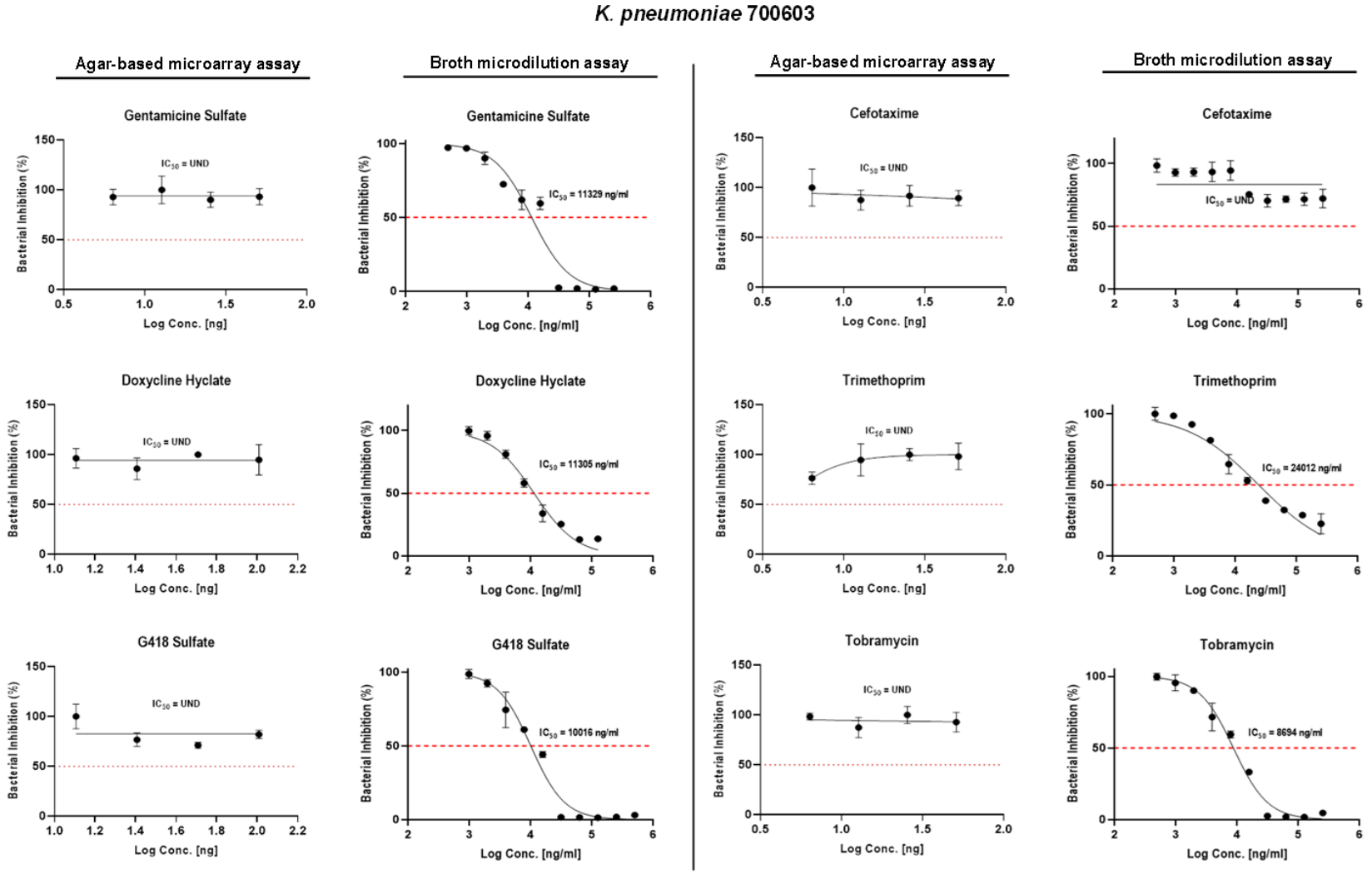

Figure A 2. Dose-response profile of *K. pneumoniae* 700603 obtained using the agar-based microarray and the standard broth microdilution assay.

K. pneumoniae 33495

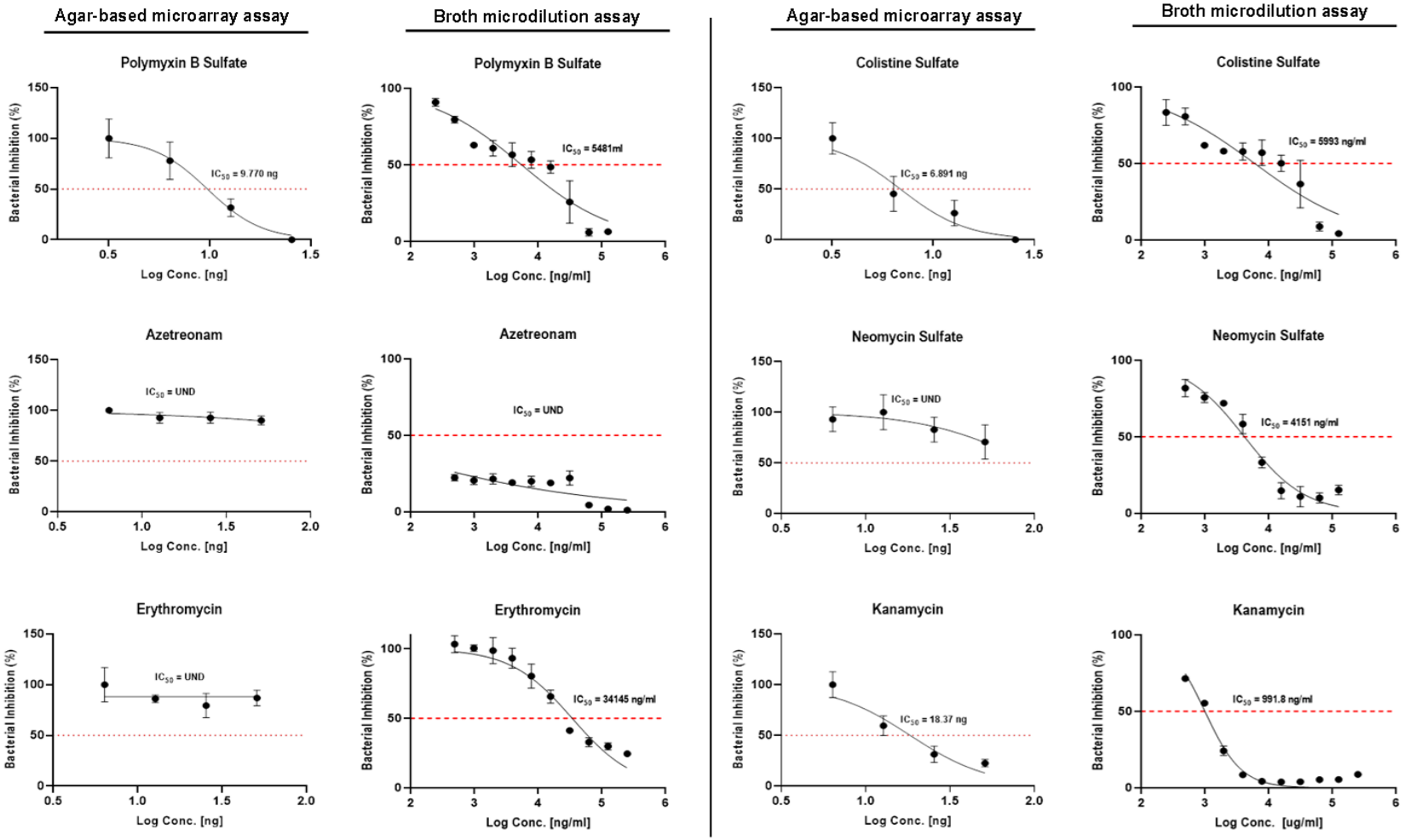

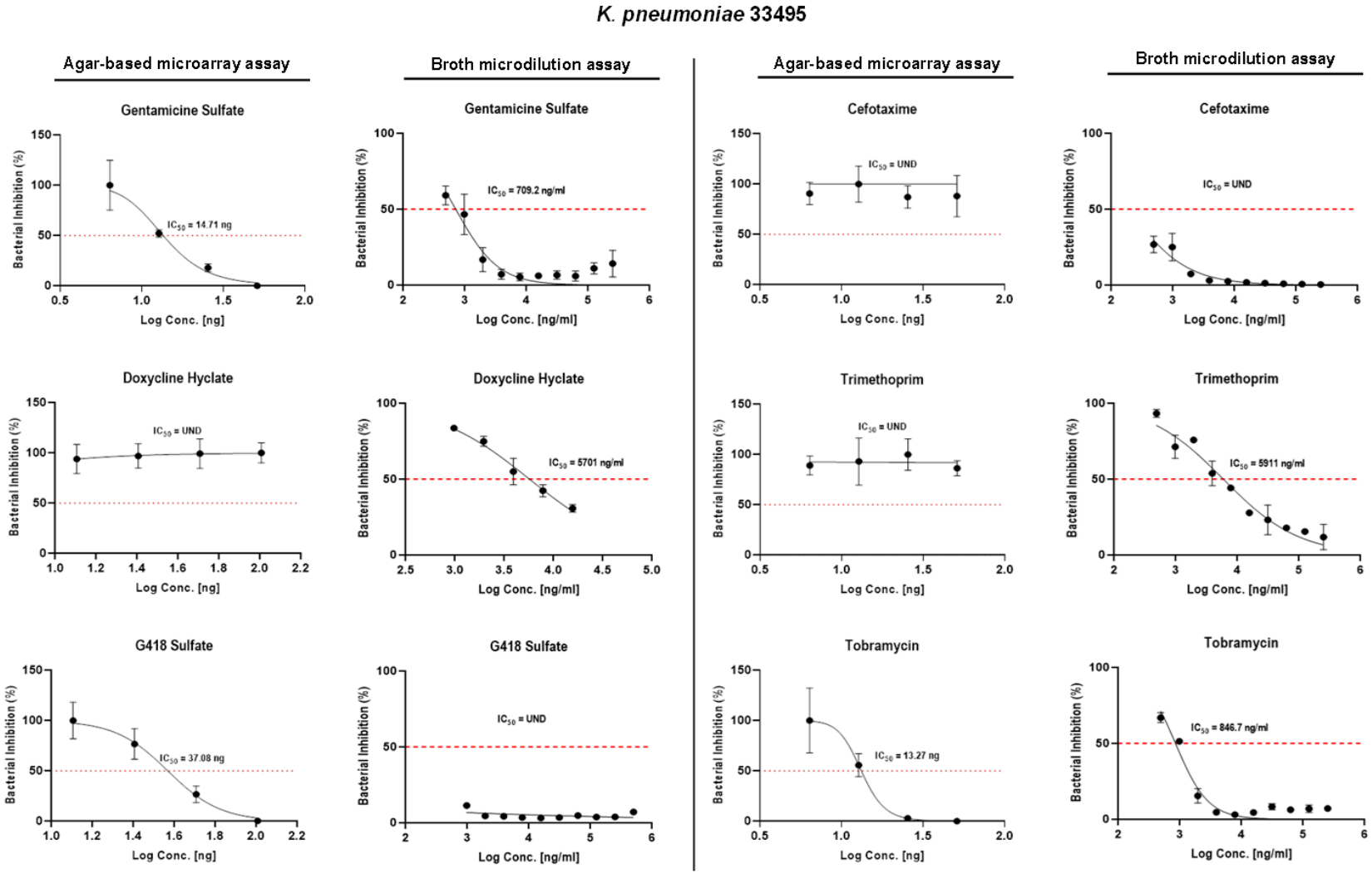

Figure A 3. Dose-response profile of *K. pneumoniae* 33495 obtained using the agar-based microarray and the standard broth microdilution assay.

E. coli 25922

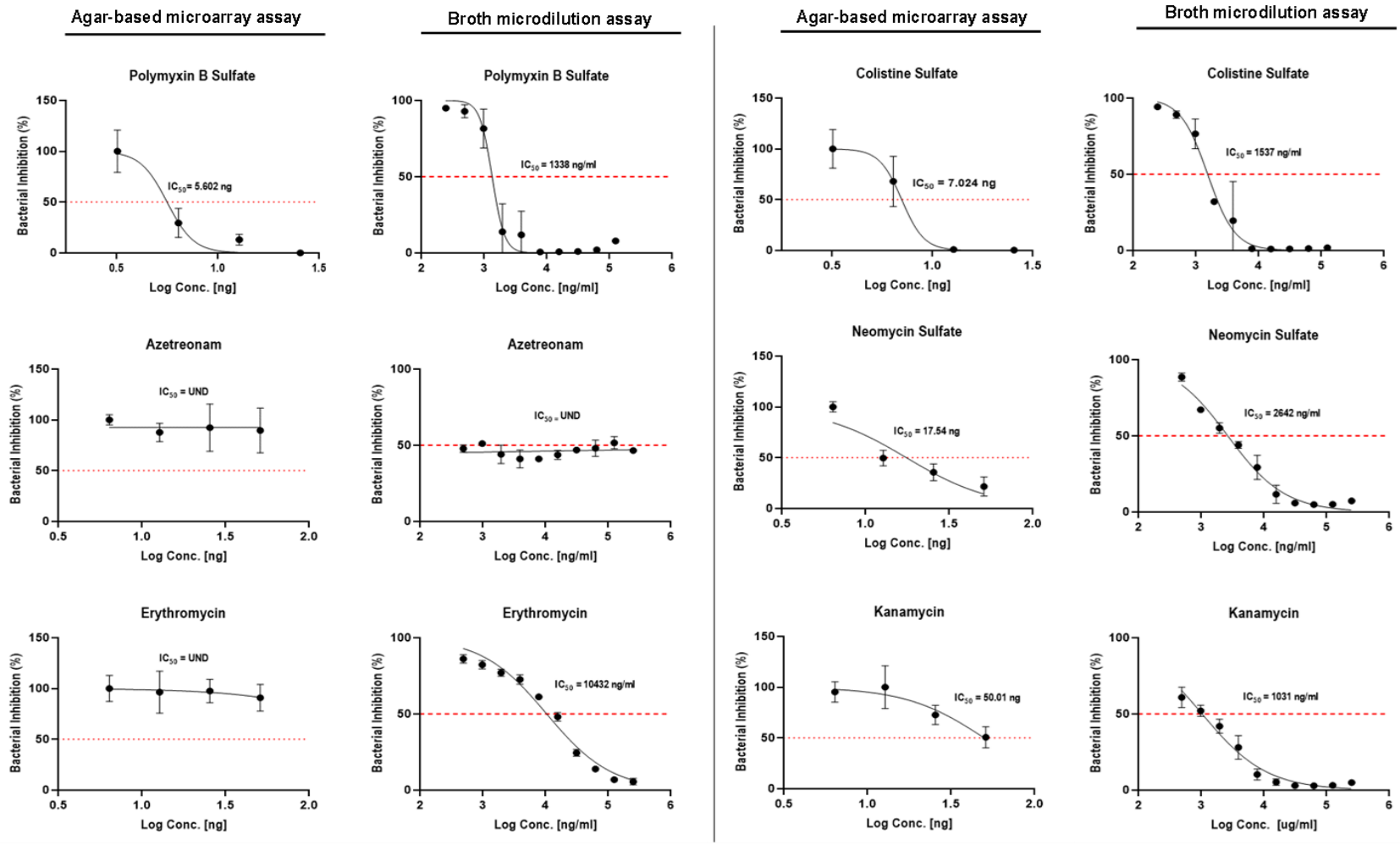
Agar-based microarray assay
Broth microdilution assay
Agar-based microarray assay
Broth microdilution assay
Polymyxin B Sulfate
Polymyxin B Sulfate
Colistine Sulfate
Colistine Sulfate
Bacterial Inhibition (%)
IC50= 5.602 ng
IC50 = 1338 ng/ml
IC50 = 7.024 ng
IC50 = 1537 ng/ml
Log Conc. [ng]
Log Conc. [ng/ml]
Azetreonam
Azetreonam
Neomycin Sulfate
Neomycin Sulfate
IC50 = UND
IC50 = UND
IC50 = 17.54 ng
IC50 = 2642 ng/ml
Erythromycin
Erythromycin
Kanamycin
Kanamycin
IC50 = UND
IC50 = 10432 ng/ml
IC50 = 50.01 ng
IC50 = 1031 ng/ml
Log Conc. [ug/ml]

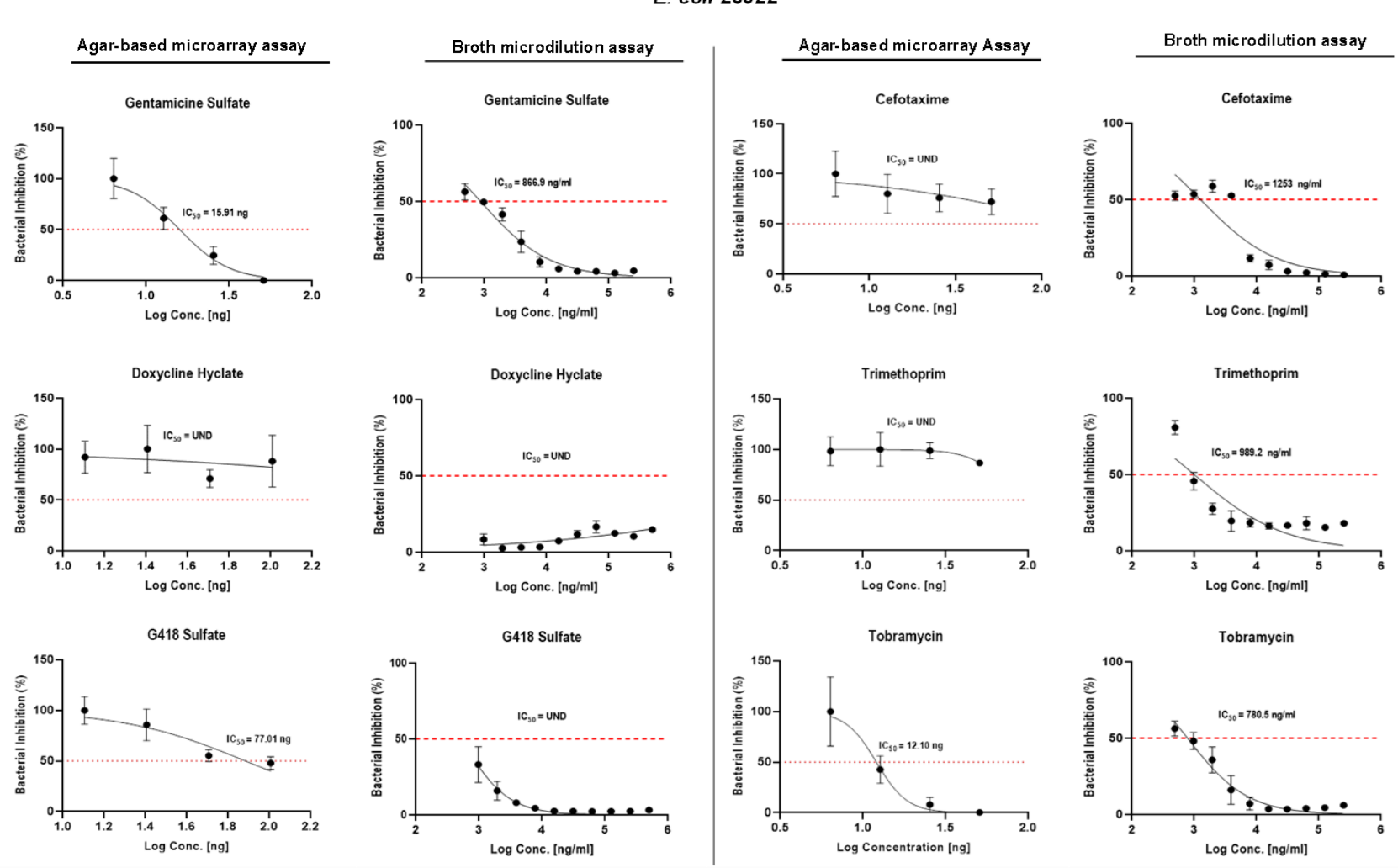

Figure A 4. Dose-response profile of *E. coli* 25922 obtained using the agar-based microarray and the standard broth microdilution assay.

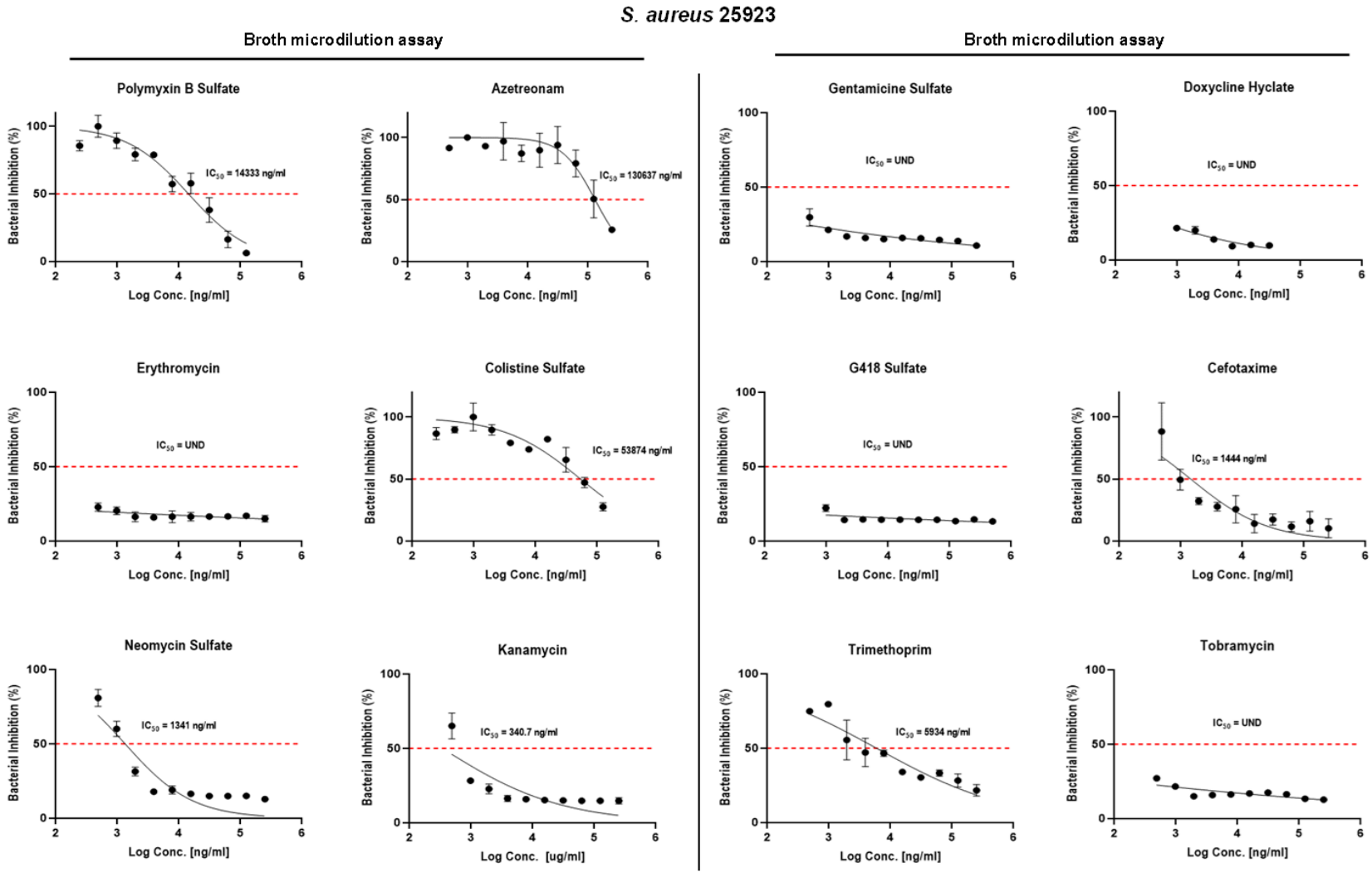

Figure A 5. Dose-response profile of *S. aureus* 25923 obtained using the standard broth microdilution assay.

Appendix B: Bacteria culture media and solutions

B.1. Tryptic soy agar (TSA)

Tryptic soy agar powder composition (Cat. No. 22091 – Sigma-Aldrich)

Agar	15 g/L
Casein peptone (pancreatic)	15 g/L
Sodium chloride	5 g/L
Soya peptone (papainic)	5 g/L

Preparation: agar medium was prepared as per manufacturer's instructions by suspending 40 g of dehydrated media in 1 liter of double distilled water (Milli-Q distilled). The suspension was heated with frequent agitation to completely dissolve the agar. The dissolved media was sterilized by autoclaving at 121°C for 15 minutes. Agar medium was cooled to 45-50°C (in a hot water bath), dispensed into sterile Petri dishes, and stored at 4ºC.

B.2. Tryptic soy broth (TSB)

Tryptic soy broth powder composition (Cat. No. 22092 – Sigma-Aldrich)

Casein peptone (pancreatic)	17 g/L
Dipotassium hydrogen phosphate	2.5 g/L
Glucose	2.5 g/L
Sodium chloride	5 g/L
Soya peptone (papain digest.)	3 g/L

Preparation: broth medium was prepared as per manufacturer's instructions by suspending 30 g of dehydrated media in 1 liter of double distilled water (Milli-Q distilled). The suspension was agitated to completely dissolve the media components. The dissolved media was sterilized by autoclaving at 121°C for 15 minutes. Media was cooled and stored at 4ºC.

B.3. Mueller Hinton broth

Mueller Hinton broth powder composition (Cat. No. 70192 – Sigma-Aldrich)

Beef infusion solids	2.0 g/L
Casein hydrolysate	17.5 g/L
Starch	1.5 g/L

Preparation: broth medium was prepared as per manufacturer's instructions by suspending 21 g of dehydrated media in 1 liter of double distilled water (Milli-Q distilled). The suspension was agitated to completely dissolve the media components. The dissolved media was sterilized by autoclaving at 121°C for 15 minutes. Media was cooled and stored at 4ºC.

B.4. Mueller Hinton Agar (0.8, 1, 1.2, 1.4, 1.5%)

Mueller Hinton agar powder composition (Cat. No. 70191 – Sigma-Aldrich)

Agar	17.0 g/L
Beef infusion solids	2.0 g/L
Casein hydrolysate	17.5 g/L
Starch	1.5 g/L

Preparation: dehydrated media (0.8, 1, 1.2, 1.4, and 1.5 g) was suspended in 100 mL of double distilled water (Milli-Q distilled). The suspension was heated with frequent agitation to completely dissolve the agar. The dissolved media was sterilized by autoclaving at 121°C for 15 minutes. Agar medium was cooled to 45-50°C (in a hot water bath), 10 mL was dispensed into sterile borosilicate glass bottles, and stored at 4ºC.

B.5. HPMC-6 cP (2% stock)

HPMC-6 cP (Cat. No. 423238 – Sigma-Aldrich)	0.4 g
DNase/RNase-free distilled water (Invitrogen)	20 mL

Preparation: one third (1/3) of the water was heated to 90 °C, following which the HPMC powder was added (with agitation) to wet and disperse the particles. Two-thirds of the water (cooled to 4ºC) was added to the mixture to lower the temperature. As the mixture cooled, it reached a temperature at which it became water soluble. The solution was further agitated for 30 minutes after the proper solubilization temperature was reached. The solution was kept at 4ºC.

B.6. HPMC-2,600+ cP (5% stock)

HPMC-2,600+ (Cat. No. H7509 – Sigma-Aldrich)	1 g
DNase/RNase-free distilled water (Invitrogen)	20 mL

Preparation: prepared and stored as described in section B.5.

B.7. Methyl cellulose (MC) – 400 cP (2% stock)

MC (Cat. No. M0262 – Sigma-Aldrich)	0.4 g
DNase/RNase-free distilled water (Invitrogen)	20 mL

Preparation: prepared as described in section B.5.

B.8. Sulforhodamine B solution (500 µM stock)

Sulforhodamine B (Cat. No. 230162 – Sigma-Aldrich)	4.79 mg
DMSO (Cat. No. D8418 – Sigma-Aldrich)	20 mL

Preparation: DMSO was added to the sulforhodamine B powder and vortexed until completely dissolved. The solution was aliquoted into microtubes (Eppendorf) and stored at -20ºC.

B.9. Sucrose solution (1.6 M stock)

Sucrose (Cat. No. S7903 – Sigma-Aldrich)	5.477 g
DNase/RNase-free distilled water (Invitrogen)	10 mL

Preparation: distilled water (heated to ~90ºC) was added to sucrose powder and vortexed until completely dissolved. The solution was incubated in a hot water bath at 65ºC for 1 hour. The solution was stored at 4ºC.

B.10. Sorbitol solution (1.6 M stock)

D-Sorbitol (Cat. No. S3889 – Sigma-Aldrich)	2.9147 g
DNase/RNase-free distilled water (Invitrogen)	10 mL

Preparation: the solution was prepared and stored as described in section B.9.

B.11. Iodonitrotetrazolium chloride (INT) solution (0.2 mg/mL working solution)

Iodonitrotetrazolium chloride (Cat. No. I8377 – Sigma-Aldrich)	6 mg
DNase/RNase-free distilled water (Invitrogen)	30 mL

Preparation: the INT powder was added to a sterilized borosilicate bottle containing distilled water. The mixture was gently heated to dissolve the powder. The solution was kept at 4ºC.

References

Abraham, E. P. and Chain, E. 1940. An enzyme from bacteria able to destroy penicillin. *Nature,* 146**,** 837.

Advisory-Board. 2020. *A crisis's: Why do antibiotics companies keep going 'belly up'?* [Online]. Available at: https://www.advisory.com/daily-briefing/2020/01/15/new-antibiotics [Accessed 14th August 2020].

Aggen, J. B., Armstrong, E. S., Goldblum, A. A., Dozzo, P., Linsell, M. S., Gliedt, M. J., Hildebrandt, D. J., Feeney, L. A., Kubo, A., Matias, R. D., Lopez, S., Gomez, M., Wlasichuk, K. B., Diokno, R., Miller, G. H. and Moser, H. E. 2010. Synthesis and spectrum of the neoglycoside achn-490. *Antimicrobial Agents and Chemotherapy,* 54**,** 4636-42.

Aghapour, Z., Gholizadeh, P., Ganbarov, K., Bialvaei, A. Z., Mahmood, S. S., Tanomand, A., Yousefi, M., Asgharzadeh, M., Yousefi, B. and Kafil, H. S. 2019. Molecular mechanisms related to colistin resistance in enterobacteriaceae. *Infection and Drug Resistance,* 12**,** 965-75.

Alberti, S., Alvarez, D., Merino, S., Casado, M. T., Vivanco, F., Tomas, J. M. and Benedi, V. J. 1996. Analysis of complement c3 deposition and degradation on *Klebsiella pneumoniae*. *Infection immunology,* 64**,** 4726-32.

Ambler, R. P. 1980. The structure of beta-lactamases. *Philosophical Transactions of the Royal Society of London. Series B: Biological Sciences,* 289**,** 321-31.

Amr-Industry-Alliance. 2022. *Progress report on amr industry alliance 2021 survey* [Online]. Available at: https://www.amrindustryalliance.org/wp-content/uploads/2022/01/AMRIA_progress-report_FINAL.pdf [Accessed 14th February 2023].

Anand, T., Virmani, N., Kumar, S., Mohanty, A. K., Pavulraj, S., Bera, B. C., Vaid, R. K., Ahlawat, U. and Tripathi, B. N. 2020. Phage therapy for treatment of virulent *Klebsiella pneumoniae* infection in a mouse model. *Journal of Global Antimicrobial Resistance,* 21**,** 34-41.

Araujo, J. and Born, D. G. 1985. Calculating percentage agreement correctly but writing its formula incorrectly. *The Behavior Analyst,* 8**,** 207-8.

Ashburn, T. T. and Thor, K. B. 2004. Drug repositioning: Identifying and developing new uses for existing drugs. *Nature Reviews Drug Discovery,* 3**,** 673-83.

Asli, N. G., Sergio, C. C. and Taosheng, C. 2013. Data analysis approaches in high throughput screening. *In:* Hany, A. E.-S. (ed.) *Drug discovery.* Rijeka: IntechOpen.

Bailey, S. N., Sabatini, D. M. and Stockwell, B. R. 2004. Microarrays of small molecules embedded in biodegradable polymers for use in mammalian cell-based screens. *Proceedings of the National Academy of Sciences,* 101**,** 16144-9.

Bajcsy, P. An overview of DNA microarray image requirements for automated processing. 2005 IEEE Computer Society Conference on Computer Vision and Pattern Recognition (CVPR'05) - Workshops, 21-23 Sept. 2005 2005. 147-.

Bascones-Martinez, A., Mattila, R., Gomez-Font, R. and Meurman, J. H. 2014. Immunomodulatory drugs: Oral and systemic adverse effects. *Medicina Oral, Patología Oral y Cirugía Bucal,* 19**,** e24-e31.

Bassetti, M., Nicolini, L., Esposito, S., Righi, E. and Viscoli, C. 2009. Current status of newer carbapenems. *Current Medicinal Chemistry,* 16**,** 564-75.

Bauer, A. W., Perry, D. M. and Kirby, W. M. 1959. Single-disk antibiotic-sensitivity testing of staphylococci; an analysis of technique and results. *A.M.A. Archives of Internal Medicine,* 104**,** 208-16.

Bauer, A. W., Kirby, W. M., Sherris, J. C. and Turck, M. 1966. Antibiotic susceptibility testing by a standardized single disk method. *American Journal of Clinical Pathology,* 45**,** 493-6.

Bharate, S. S., Bharate, S. B. and Bajaj, A. N. 2010. Incompatibilities of pharmaceutical excipients with active pharmaceutical ingredients: A comprehensive review. *Journal of Excipients and Food Chemicals; Vol 1 No 3 (2010)*.

Boucher, H. W., Talbot, G. H., Bradley, J. S., Edwards, J. E., Gilbert, D., Rice, L. B., Scheld, M., Spellberg, B. and Bartlett, J. 2009. Bad bugs, no drugs: No eskape! An update from the infectious diseases society of america. *Clinical Infectious Diseases,* 48**,** 1-12.

Bourque, G., Burns, K. H., Gehring, M., Gorbunova, V., Seluanov, A., Hammell, M., Imbeault, M., Izsvák, Z., Levin, H. L., Macfarlan, T. S., Mager, D. L. and Feschotte, C. 2018. Ten things you should know about transposable elements. *Genome Biology,* 19**,** 199.

Bowers, J. R., Kitchel, B., Driebe, E. M., Maccannell, D. R., Roe, C., Lemmer, D., De Man, T., Rasheed, J. K., Engelthaler, D. M., Keim, P. and Limbago, B. M. 2015. Genomic analysis of the emergence and rapid global dissemination of the clonal group 258 *Klebsiella pneumoniae* pandemic. *PloS One,* 10**,** e0133727.

Brideau, C., Gunter, B., Pikounis, B. and Liaw, A. 2003. Improved statistical methods for hit selection in high-throughput screening. *Journal of Biomolecular Screening,* 8**,** 634-47.

Broberg, C. A., Palacios, M. and Miller, V. L. 2013. Whole-genome draft sequences of three multidrug-resistant *Klebsiella pneumoniae* strains available from the american type culture collection. *Genome Announcements,* 1.

Brown, A. G., Butterworth, D., Cole, M., Hanscomb, G., Hood, J. D., Reading, C. and Rolinson, G. N. 1976. Naturally-occurring beta-lactamase inhibitors with antibacterial activity. *Journal of Antibiotics,* 29**,** 668-9.

Brown, D. 2015. Antibiotic resistance breakers: Can repurposed drugs fill the antibiotic discovery void? *Nature Reviews Drug Discovery,* 14**,** 821-32.

Bugg, T. D. and Walsh, C. T. 1992. Intracellular steps of bacterial cell wall peptidoglycan biosynthesis: Enzymology, antibiotics, and antibiotic resistance. *Natural Product Reports,* 9**,** 199-215.

Burns, D. J., Kofron, J. L., Warrior, U. and Beutel, B. A. 2001. Well-less, gel-permeation formats for ultra-hts. *Drug Discovery Today,* 6**,** 40-7.

Bush, K. and Jacoby, G. A. 2010. Updated functional classification of beta-lactamases. *Antimicrobial Agents and Chemotherapy,* 54**,** 969-76.

Capone, A., Giannella, M., Fortini, D., Giordano, A., Meledandri, M., Ballardini, M., Venditti, M., Bordi, E., Capozzi, D., Balice, M. P., Tarasi, A., Parisi, G., Lappa, A., Carattoli, A. and Petrosillo, N. 2013. High rate of colistin resistance among patients with carbapenem-resistant *Klebsiella pneumoniae* infection accounts for an excess of mortality. *Clinical Microbiology and Infection,* 19**,** E23-e30.

Carb-X. 2021. *5 years of progress - addressing the global antibacterial resistance threat: Innovation to prepare for the future* [Online]. Available at: chrome-extension://efaidnbmnnnibpcajpcglclefindmkaj/https://carb-x.org/wp-content/uploads/2021/06/Carb-X_FactSheet_7-31-21.pdf [Accessed 24th April 2023].

Carroll, J. 2015. *Whittled down to biotech size, astrazeneca's antibiotics crew starts over as entasis* [Online]. Available at: https://www.fiercebiotech.com/biotech/whittled-down-to-biotech-size-astrazeneca-s-antibiotics-crew-starts-over-as-entasis [Accessed 15th June 2020].

Castanheira, M., Rhomberg, P. R., Flamm, R. K. and Jones, R. N. 2016. Effect of the beta-lactamase inhibitor vaborbactam combined with meropenem against serine carbapenemase-producing enterobacteriaceae. *Antimicrobial Agents and Chemotherapy,* 60**,** 5454-8.

CDC. 2019. *Antibiotic resistance threats in the united states. Atlanta, ga: U.S. Department of health and human services* [Online]. Available at: Available at https://www.cdc.gov/drugresistance/Biggest-Threats.html [Accessed 8th March 2020].

Cegelski, L., Marshall, G. R., Eldridge, G. R. and Hultgren, S. J. 2008. The biology and future prospects of antivirulence therapies. *Nature reviews. Microbiology,* 6**,** 17-27.

Chang, A. and Knight, J. 2020. *Ushering in a new era of antibiotic innovation with a netflix-style subscription payment model* [Online]. Available at: https://www.xcenda.com/insights/htaq-winter-2020-new-era-antibiotic-subscription-model [Accessed 23rd January 2021].

Chen, H., Fang, L., Chen, W., Yang, Q., Li, D., Hu, D. and Zhang, J. 2022a. Pyogenic liver abscess-caused K*lebsiella pneumoniae* in a tertiary hospital in china in 2017: Implication of hypervirulent carbapenem-resistant strains. *BMC Infectious Diseases,* 22**,** 685.

Chen, L., Mathema, B., Chavda, K. D., Deleo, F. R., Bonomo, R. A. and Kreiswirth, B. N. 2014. Carbapenemase-producing K*lebsiella pneumoniae*: Molecular and genetic decoding. *Trends in Microbiology,* 22**,** 686-96.

Chen, X., Tian, J., Luo, C., Wang, X., Li, X. and Wang, M. 2022b. Cell membrane remodeling mediates polymyxin b resistance in K*lebsiella pneumoniae*: An integrated proteomics and metabolomics study. *Frontiers in Microbiology,* 13**,** 810403.

Cheng, X., Yan, B., Gao, L., Tang, H., Fan, Y., Anderson, S. N., Affleck, R. and Burns, D. J. 2005. Compound transfer efficiency from polystyrene surfaces: Application to microarrayed compound screening. *SLAS Discovery,* 10**,** 293-303.

Choi, S.-r., Britigan, B. E. and Narayanasamy, P. 2019. Dual inhibition of *Klebsiella pneumoniae* and *Pseudomonas aeruginosa* iron metabolism using gallium porphyrin and gallium nitrate. *ACS Infectious Diseases,* 5**,** 1559-69.

Cienfuegos-Gallet, A. V., Ocampo De Los Rios, A. M., Sierra Viana, P., Ramirez Brinez, F., Restrepo Castro, C., Roncancio Villamil, G., Del Corral Londono, H. and Jimenez, J. N. 2019. Risk factors and survival of patients infected with carbapenem-resistant K*lebsiella pneumoniae* in a kpc endemic setting: A case-control and cohort study. *BMC Infectious Diseases,* 19**,** 830.

Clark, J. A. and Burgess, D. S. 2020. Plazomicin: A new aminoglycoside in the fight against antimicrobial resistance. *Therapeutic Advances in Infectious Disease,* 7**,** 2049936120952604.

Codjoe, F. S. and Donkor, E. S. 2017. Carbapenem resistance: A review. *Journal of Medical Sciences (Basel),* 6.

Cooper, A. L., Dean, A. C. and Hinshelwood, C. 1968. Factors affecting the growth of bacterial colonies on agar plates. *Proceedings of the Royal Society B: Biological Sciences,* 171**,** 175-99.

Coppi, M., Antonelli, A., Niccolai, C., Bartolini, A., Bartolini, L., Grazzini, M., Mantengoli, E., Farese, A., Pieralli, F., Mechi, M. T., Di Pilato, V., Giani, T. and Rossolini, G. M. 2022. Nosocomial outbreak by ndm-1-producing *Klebsiella pneumoniae* highly resistant to cefiderocol, florence, italy, august 2021 to june 2022. *Euro Surveillance,* 27.

Cortes, G., Borrell, N., De Astorza, B., Gomez, C., Sauleda, J. and Alberti, S. 2002. Molecular analysis of the contribution of the capsular polysaccharide and the lipopolysaccharide o side chain to the virulence of *Klebsiella pneumoniae* in a murine model of pneumonia. *Infection and Immunity,* 70**,** 2583-90.

Dall, C. 2019. *Achaogen bankruptcy raises worry over antibiotic pipeline* [Online]. Available at: https://www.cidrap.umn.edu/antimicrobial-stewardship/achaogen-bankruptcy-raises-worry-over-antibiotic-pipeline [Accessed 15th June 2020].

Darby, E. M., Trampari, E., Siasat, P., Gaya, M. S., Alav, I., Webber, M. A. and Blair, J. M. A. 2023. Molecular mechanisms of antibiotic resistance revisited. *Nature Reviews: Microbiology,* 21**,** 280-95.

Darrow, J. J. and Kesselheim, A. S. 2020. Incentivizing antibiotic development: Why isn't the generating antibiotic incentives now (gain) act working? *Open Forum Infectious Diseases,* 7**,** ofaa001.

Davoudabadi, S., Goudarzi, M. and Hashemi, A. 2023. Detection of virulence factors and antibiotic resistance among *Klebsiella pneumoniae* isolates from iran. *BioMed Research International,* 2023**,** 3624497.

De Brevern, A. G., Hazout, S. and Malpertuy, A. 2004. Influence of microarrays experiments missing values on the stability of gene groups by hierarchical clustering. *BMC Bioinformatics,* 5**,** 114.

Debnath, A., Parsonage, D., Andrade, R. M., He, C., Cobo, E. R., Hirata, K., Chen, S., García-Rivera, G., Orozco, E., Martínez, M. B., Gunatilleke, S. S., Barrios, A. M., Arkin, M. R., Poole, L. B., Mckerrow, J. H. and Reed, S. L. 2012. A high-throughput drug screen for entamoeba histolytica identifies a new lead and target. *Nature Medicine,* 18**,** 956-60.

Delbrück, M. 1940. The growth of bacteriophage and lysis of the host. *The Journal of general physiology,* 23**,** 643-60.

Dimasi, J. A., Grabowski, H. G. and Hansen, R. W. 2016. Innovation in the pharmaceutical industry: New estimates of r&d costs. *Journal of Health Economics,* 47**,** 20-33.

Dimova, D., Stumpfe, D. and Bajorath, J. 2017. Computational design of new molecular scaffolds for medicinal chemistry, part ii: Generalization of analog series-based scaffolds. *Future science OA,* 4**,** FSO267-FSO.

Disarm. 2019. *Developing an innovative strategy for antimicrobial resistant microorganisms act of 2019* [Online]. Available at: https://www.congress.gov/bill/116th-congress/senate-bill/1712/text [Accessed 14th August 2020].

Doi, Y. and Paterson, D. L. 2015. Carbapenemase-producing enterobacteriaceae. *Seminars in Respiratory and Critical Care Medicine,* 36**,** 74-84.

Doi, Y., Wachino, J. I. and Arakawa, Y. 2016. Aminoglycoside resistance: The emergence of acquired 16s ribosomal rna methyltransferases. *Infectious Disease Clinics of North America,* 30**,** 523-37.

Doorduijn, D. J., Rooijakkers, S. H. M., Van Schaik, W. and Bardoel, B. W. 2016. Complement resistance mechanisms of *Klebsiella pneumoniae*. *Immunobiology,* 221**,** 1102-9.

Dreiman, G. H. S., Bictash, M., Fish, P. V., Griffin, L. and Svensson, F. 2021. Changing the hts paradigm: Ai-driven iterative screening for hit finding. *SLAS Discov,* 26**,** 257-62.

Drive-Ab. 2018. *Revitalizing the antibiotic pipeline: Stimulating innoation while driving sustainable use and global access* [Online]. Available at: chrome-extension://efaidnbmnnnibpcajpcglclefindmkaj/http://drive-ab.eu/wp-content/uploads/2018/01/CHHJ5467-Drive-AB-Main-Report-180319-WEB.pdf [Accessed 17 March 2021].

Durante-Mangoni, E., Andini, R. and Zampino, R. 2019. Management of carbapenem-resistant enterobacteriaceae infections. *Clinical Microbiology and Infection,* 25**,** 943-50.

Dyrda, G., Boniewska-Bernacka, E., Man, D., Barchiewicz, K. and Słota, R. 2019. The effect of organic solvents on selected microorganisms and model liposome membrane. *Molecular Biology Reports,* 46**,** 3225-32.

Egorov, A. M., Ulyashova, M. M. and Rubtsova, M. Y. 2018. Bacterial enzymes and antibiotic resistance. *Acta Naturae,* 10**,** 33-48.

Eisinger, R. W., Williams, M. P., Choe, S. H. and Krofah, E. 2023. A call to action-stopping antimicrobial resistance. *JAC-Antimicrobal Resistance,* 5**,** dlac142.

Eloff, J. N. 1998. A sensitive and quick microplate method to determine the minimal inhibitory concentration of plant extracts for bacteria. *Planta Medica,* 64**,** 711-3.

Elshamy, A. A. and Aboshanab, K. M. 2020. A review on bacterial resistance to carbapenems: Epidemiology, detection and treatment options. *Future Science OA,* 6**,** FSO438.

Eucast 2000. Determination of minimum inhibitory concentrations (mics) of antibacterial agents by agar dilution. *Clinical Microbiology and Infection,* 6**,** 509-15.

Falagas, M. E., Tansarli, G. S., Karageorgopoulos, D. E. and Vardakas, K. Z. 2014. Deaths attributable to carbapenem-resistant enterobacteriaceae infections. *Emerging Infectious Diseases,* 20**,** 1170-5.

Falcone, M., Russo, A., Iacovelli, A., Restuccia, G., Ceccarelli, G., Giordano, A., Farcomeni, A., Morelli, A. and Venditti, M. 2016. Predictors of outcome in icu patients with septic shock caused by *Klebsiella pneumoniae* carbapenemase-producing k. Pneumoniae. *Clinical Microbiology and Infection,* 22**,** 444-50.

Fernandez, J., Guerra, B. and Rodicio, M. R. 2018. Resistance to carbapenems in non-typhoidal salmonella enterica serovars from humans, animals and food. *Veterinary Sciences,* 5.

Fernández, L. and Hancock, R. E. 2012. Adaptive and mutational resistance: Role of porins and efflux pumps in drug resistance. *Clinical Microbiology Reviews,* 25**,** 661-81.

Findlay, J., Poirel, L. and Nordmann, P. 2023. In vitro-obtained meropenem-vaborbactam resistance mechanisms among clinical *Klebsiella pneumoniae* carbapenemase-producing k. Pneumoniae isolates. *Journal of Global Antimicrobial Resistance,* 32**,** 66-71.

Foucquier, J. and Guedj, M. 2015. Analysis of drug combinations: Current methodological landscape. *Pharmacology Research and Perspectives,* 3**,** e00149.

Founou, R. C., Founou, L. L. and Essack, S. Y. 2017. Clinical and economic impact of antibiotic resistance in developing countries: A systematic review and meta-analysis. *PloS One,* 12**,** e0189621.

Foxman, B. 2014. Urinary tract infection syndromes: Occurrence, recurrence, bacteriology, risk factors, and disease burden. *Infectious Disease Clinics of North America,* 28**,** 1-13.

Gaibani, P., Lombardo, D., Bussini, L., Bovo, F., Munari, B., Giannella, M., Bartoletti, M., Viale, P., Lazzarotto, T. and Ambretti, S. 2021. Epidemiology of meropenem/vaborbactam resistance in kpc-producing *Klebsiella pneumoniae* causing bloodstream infections in northern italy, 2018. *Antibiotics (Basel),* 10.

Gajdács, M. 2019. The concept of an ideal antibiotic: Implications for drug design. *Molecules,* 24.

Galloway, W. R. J. D., Bender, A., Welch, M. and Spring, D. R. 2009. The discovery of antibacterial agents using diversity-oriented synthesis. *Chemical Communications***,** 2446-62.

Gholizadeh, P., Köse, Ş., Dao, S., Ganbarov, K., Tanomand, A., Dal, T., Aghazadeh, M., Ghotaslou, R., Ahangarzadeh Rezaee, M., Yousefi, B. and Samadi Kafil, H. 2020. How crispr-cas system could be used to combat antimicrobial resistance. *Infection and Drug Resistance,* 13**,** 1111-21.

Govindaswamy, A., Bajpai, V., Khurana, S., Batra, P., Mathur, P. and Malhotra, R. 2019. Prevalence and characterization of carbapenemase-producing escherichia coli from a tertiary care hospital in india. *Journal of Global Infectious Diseases,* 11**,** 123-4.

Halasohoris, S. A., Scarff, J. M., Pysz, L. M., Lembirik, S., Lemmon, M. M., Biek, D., Hannah, B., Zumbrun, S. D. and Panchal, R. G. 2021. In vitro and in vivo activity of gt-1, a novel siderophore cephalosporin, and gt-055, a broad-spectrum β-lactamase inhibitor, against biothreat and eskape pathogens. *The Journal of Antibiotics,* 74**,** 884-92.

Hashizume, T., Ishino, F., Nakagawa, J., Tamaki, S. and Matsuhashi, M. 1984. Studies on the mechanism of action of imipenem (n-formimidoylthienamycin) in vitro: Binding to the penicillin-binding proteins (pbps) in escherichia coli and *Pseudomonas aeruginosa*, and inhibition of enzyme activities due to the pbps in *E. coli*. *Journal of Antibiotics,* 37**,** 394-400.

Hedges, R. W., Datta, N., Kontomichalou, P. and Smith, J. T. 1974. Molecular specificities of r factor-determined beta-lactamases: Correlation with plasmid compatibility. *Journal of Bacteriology,* 117**,** 56-62.

Hoever, M. and Zbinden, P. 2004. The evolution of microarrayed compound screening. *Drug Discovery Today,* 9**,** 358-65.

Holden, V. I. and Bachman, M. A. 2015. Diverging roles of bacterial siderophores during infection. *Metallomics,* 7**,** 986-95.

Hu, C. 2018. *Pharmaceutical companies are backing away from a threat that could kill 10 million a year by 2050* [Online]. Available at: https://www.sciencealert.com/pharmaceutical-companies-are-backing-away-from-a-threat-that-could-kill-10-million-a-year-by-2050 [Accessed 15th June 2020].

Hu, H. and Larson, R. G. 2005. Analysis of the effects of marangoni stresses on the microflow in an evaporating sessile droplet. *Langmuir,* 21**,** 3972-80.

Hu, Y., Liu, C., Shen, Z., Zhou, H., Cao, J., Chen, S., Lv, H., Zhou, M., Wang, Q., Sun, L., Sun, Q., Hu, F., Wang, Y. and Zhang, R. 2020. Prevalence, risk factors and molecular epidemiology of carbapenem-resistant *Klebsiella pneumoniae* in patients from zhejiang, china, 2008-2018. *Emerging Microbes and Infections,* 9**,** 1771-9.

Hudzicki, J. 2009. Kirby-bauer disk diffusion susceptibility test protocol. *American society for microbiology,* 15**,** 55-63.

Hughes, J. P., Rees, S., Kalindjian, S. B. and Philpott, K. L. 2011. Principles of early drug discovery. *British Journal of Pharmacology,* 162**,** 1239-49.

IDSA. 2004. *Bad bugs, no drugs: As antibiotic r&d stagnates, a public health crisis brews* [Online]. Available at: chrome-extension://efaidnbmnnnibpcajpcglclefindmkaj/https://www.idsociety.org/globalassets/idsa/policy--advocacy/current_topics_and_issues/antimicrobial_resistance/10x20/statements/070104-as-antibiotic-discovery-stagnates-a-public-health-crisis-brews.pdf [Accessed 17th February 2020].

IFPMA. 2020. *New amr action fund steps in to save collapsing antibiotic pipeline with pharmaceutical industry investment of us$1 billion* [Online]. Available at: https://www.ifpma.org/news/new-amr-action-fund-steps-in-to-save-collapsing-antibiotic-pipeline-with-pharmaceutical-industry-investment-of-us1-billion/#:~:text=Antimicrobial%20resistance-,New%20AMR%20Action%20Fund%20steps%20in%20to%20save%20collapsing%20antibiotic,needed%20long%2Dterm%20policy%20solutions. [Accessed 4th August 2020].

IFPMA. 2021. *Global principles on incentivizing antibiotic r&d* [Online]. Available at: https://www.ifpma.org/publications/global-principles-on-incentivizing-antibiotic-rd/ [Accessed 17th March 2021].

Ismail, H., Lowman, W., Govind, C. N., Swe Swe-Han, K., Maloba, M. R. B., Bamford, C. and Perovic, O. 2019. Surveillance and comparison of antimicrobial susceptibility patterns of eskape organisms isolated from patients with bacteraemia in south africa, 2016 - 2017. *South African Medical Journal,* 109**,** 934-40.

Jackson, N., Czaplewski, L. and Piddock, L. J. V. 2018. Discovery and development of new antibacterial drugs: Learning from experience? *Journal of Antimicrobial Chemotherapy,* 73**,** 1452-9.

Jeon, J. H., Lee, J. H., Lee, J. J., Park, K. S., Karim, A. M., Lee, C. R., Jeong, B. C. and Lee, S. H. 2015. Structural basis for carbapenem-hydrolyzing mechanisms of carbapenemases conferring antibiotic resistance. *International Journal of Molecular Sciences,* 16**,** 9654-92.

June, C. M., Vallier, B. C., Bonomo, R. A., Leonard, D. A. and Powers, R. A. 2014. Structural origins of oxacillinase specificity in class d beta-lactamases. *Antimicrobial Agents and Chemotherapy,* 58**,** 333-41.

Khan, A. U., Maryam, L. and Zarrilli, R. 2017. Structure, genetics and worldwide spread of new delhi metallo-beta-lactamase (ndm): A threat to public health. *BMC Microbiology,* 17**,** 101.

Kim, S. Y., Park, Y. J., Yu, J. K., Kim, H. S., Park, Y. S., Yoon, J. B., Yoo, J. Y. and Lee, K. 2007. Prevalence and mechanisms of decreased susceptibility to carbapenems in *Klebsiella pneumoniae* isolates. *Diagnostic Microbiology and Infectious Disease,* 57**,** 85-91.

Kwon, J., Mistry, T., Ren, J., Johnson, M. E. and Mehboob, S. 2018. A novel series of enoyl reductase inhibitors targeting the eskape pathogens, staphylococcus aureus and *Acinetobacter baumannii*. *Bioorganic and Medicinal Chemistry,* 26**,** 65-76.

Lan, P., Lu, Y., Chen, Z., Wu, X., Hua, X., Jiang, Y., Zhou, J. and Yu, Y. 2022. Emergence of high-level cefiderocol resistance in carbapenem-resistant *Klebsiella pneumoniae* from bloodstream infections in patients with hematologic malignancies in china. *Microbiology Spectrum,* 10**,** e0008422.

Landahl, H. D. 1958. Theoretical considerations on potentiation in drug interaction. *The bulletin of mathematical biophysics,* 20**,** 1-23.

Laws, M., Shaaban, A. and Rahman, K. M. 2019. Antibiotic resistance breakers: Current approaches and future directions. *FEMS Microbiology Reviews,* 43**,** 490-516.

Le Manach, C., Dam, J., Woodland, J. G., Kaur, G., Khonde, L. P., Brunschwig, C., Njoroge, M., Wicht, K. J., Horatscheck, A., Paquet, T., Boyle, G. A., Gibhard, L., Taylor, D., Lawrence, N., Yeo, T., Mok, S.,

Eastman, R. T., Dorjsuren, D., Talley, D. C., Guo, H., Simeonov, A., Reader, J., Van Der Watt, M., Erlank, E., Venter, N., Zawada, J. W., Aswat, A., Nardini, L., Coetzer, T. L., Lauterbach, S. B., Bezuidenhout, B. C., Theron, A., Mancama, D., Koekemoer, L. L., Birkholtz, L. M., Wittlin, S., Delves, M., Ottilie, S., Winzeler, E. A., Von Geldern, T. W., Smith, D., Fidock, D. A., Street, L. J., Basarab, G. S., Duffy, J. and Chibale, K. 2021. Identification and profiling of a novel diazaspiro[3.4]octane chemical series active against multiple stages of the human malaria parasite plasmodium falciparum and optimization efforts. *Journal of Medicinal Chemistry,* 64**,** 2291-309.

Leclerc, Q. J., Lindsay, J. A. and Knight, G. M. 2019. Mathematical modelling to study the horizontal transfer of antimicrobial resistance genes in bacteria: Current state of the field and recommendations. *Journal of The Royal Society Interface,* 16**,** 20190260.

Lei, W., Demir, K., Overhage, J., Grunze, M., Schwartz, T. and Levkin, P. A. 2020. Droplet-microarray: Miniaturized platform for high-throughput screening of antimicrobial compounds. *Advanced Biosystems,* 4**,** e2000073.

Li, Y., Li, J., Hu, T., Hu, J., Song, N., Zhang, Y. and Chen, Y. 2020. Five-year change of prevalence and risk factors for infection and mortality of carbapenem-resistant *Klebsiella pneumoniae* bloodstream infection in a tertiary hospital in north china. *Antimicrobial Resistance and Infection Control,* 9**,** 79.

Lin, Z., Yu, J., Liu, S. and Zhu, M. 2022. Prevalence and antibiotic resistance of *Klebsiella pneumoniae* in a tertiary hospital in hangzhou, china, 2006–2020. *Journal of International Medical Research,* 50**,** 03000605221079761.

Lobanovska, M. and Pilla, G. 2017. Penicillin's discovery and antibiotic resistance: Lessons for the future? *Yale Journal of Biology and Medicine,* 90**,** 135-45.

Lodise, T. P., Berger, A., Altincatal, A., Wang, R., Bhagnani, T., Gillard, P. and Bonine, N. G. 2019. Antimicrobial resistance or delayed appropriate therapy-does one influence outcomes more than the other among patients with serious infections due to carbapenem-resistant versus carbapenem-susceptible enterobacteriaceae? *Open Forum Infectious Diseases,* 6**,** ofz194.

Lomovskaya, O., Sun, D., Rubio-Aparicio, D., Nelson, K., Tsivkovski, R., Griffith, D. C. and Dudley, M. N. 2017. Vaborbactam: Spectrum of beta-lactamase inhibition and impact of resistance mechanisms on activity in enterobacteriaceae. *Antimicrobial Agents and Chemotherapy,* 61.

Ma, H. and Horiuchi, K. Y. 2006. Chemical microarray: A new tool for drug screening and discovery. *Drug Discovery Today,* 11**,** 661-8.

Mackow, N. A., Shen, J., Adnan, M., Khan, A. S., Fries, B. C. and Diago-Navarro, E. 2019. Crispr-cas influences the acquisition of antibiotic resistance in *Klebsiella pneumoniae*. *PloS One,* 14**,** e0225131.

Mahase, E. 2020. Uk launches subscription style model for antibiotics to encourage new development. *British Medical Journal,* 369**,** m2468.

Maraolo, A. E., Corcione, S., Grossi, A., Signori, A., Alicino, C., Hussein, K., Trecarichi, E. M., Viale, P., Timsit, J. F., Veeraraghavan, B., Villegas, M. V., Rahav, G., Daikos, G. L., Vardakas, K. Z., Roilides, E., Uhlemann, A. C., Ghafur, A. K., Mornese Pinna, S., Bassetti, M., Kohler, P. P. and Giacobbe, D. R. 2021. The impact of carbapenem resistance on mortality in patients with *Klebsiella pneumoniae* bloodstream infection: An individual patient data meta-analysis of 1952 patients. *Infectious Diseases and Therapy,* 10**,** 541-58.

Marsilio, N. R., Silva, D. and Bueno, D. 2016. Drug incompatibilities in the adult intensive care unit of a university hospital. *Revista Brasileira de Terapia Intensiva,* 28**,** 147-53.

Martin, A., Fahrbach, K., Zhao, Q. and Lodise, T. 2018. Association between carbapenem resistance and mortality among adult, hospitalized patients with serious infections due to enterobacteriaceae: Results of a systematic literature review and meta-analysis. *Open Forum Infectious Diseases,* 5**,** ofy150.

Marturano, J. E. and Lowery, T. J. 2019. Eskape pathogens in bloodstream infections are associated with higher cost and mortality but can be predicted using diagnoses upon admission. *Open Forum Infectious Diseases,* 6**,** ofz503.

Mayr, L. M. and Fuerst, P. 2008. The future of high-throughput screening. *Journal of Biomolecular Screening,* 13**,** 443-8.

Mcdermott, W. and Rogers, D. E. 1982. Social ramifications of control of microbial disease. *Johns Hopkins Medical Journal,* 151**,** 302-12.

Mchugh, M. L. 2012. Interrater reliability: The kappa statistic. *Biochemia Medica: Casopis Hrvatskoga Drustva Medicinskih Biokemicara,* 22**,** 276-82.

Mckenna, M. 2019. *The antibiotics business is broken—but there's a fix* [Online]. Available at: https://www.wired.com/story/the-antibiotics-business-is-broken-but-theres-a-fix/ [Accessed 15th June 2020].

Mennen, S. M., Alhambra, C., Allen, C. L., Barberis, M., Berritt, S., Brandt, T. A., Campbell, A. D., Castañón, J., Cherney, A. H., Christensen, M., Damon, D. B., Eugenio De Diego, J., García-Cerrada, S., García-Losada, P., Haro, R., Janey, J., Leitch, D. C., Li, L., Liu, F., Lobben, P. C., Macmillan, D. W. C., Magano, J., Mcinturff, E., Monfette, S., Post, R. J., Schultz, D., Sitter, B. J., Stevens, J. M., Strambeanu, I. I., Twilton, J., Wang, K. and Zajac, M. A. 2019. The evolution of high-throughput experimentation in pharmaceutical development and perspectives on the future. *Organic Process Research and Development,* 23**,** 1213-42.

Michael, C. A., Dominey-Howes, D. and Labbate, M. 2014. The antimicrobial resistance crisis: Causes, consequences, and management. *Frontiers in Public Health,* 2.

Miethke, M., Pieroni, M., Weber, T., Brönstrup, M., Hammann, P., Halby, L., Arimondo, P. B., Glaser, P., Aigle, B., Bode, H. B., Moreira, R., Li, Y., Luzhetskyy, A., Medema, M. H., Pernodet, J.-L., Stadler, M., Tormo, J. R., Genilloud, O., Truman, A. W., Weissman, K. J., Takano, E., Sabatini, S., Stegmann, E., Brötz-Oesterhelt, H., Wohlleben, W., Seemann, M., Empting, M., Hirsch, A. K. H., Loretz, B., Lehr, C.-M., Titz, A., Herrmann, J., Jaeger, T., Alt, S., Hesterkamp, T., Winterhalter, M., Schiefer, A., Pfarr, K., Hoerauf, A., Graz, H., Graz, M., Lindvall, M., Ramurthy, S., Karlén, A., Van Dongen, M., Petkovic, H., Keller, A., Peyrane, F., Donadio, S., Fraisse, L., Piddock, L. J. V., Gilbert, I. H., Moser, H. E. and Müller, R. 2021. Towards the sustainable discovery and development of new antibiotics. *Nature Reviews Chemistry,* 5**,** 726-49.

Miller, S. I. 2016. Antibiotic resistance and regulation of the gram-negative bacterial outer membrane barrier by host innate immune molecules. *mBio,* 7.

Moellering, R. C., Jr., Eliopoulos, G. M. and Sentochnik, D. E. 1989. The carbapenems: New broad spectrum beta-lactam antibiotics. *Journal of Antimicrobial Chemotherapy,* 24 Suppl A**,** 1-7.

Morales, S., Gallego, M. A., Vanegas, J. M. and Jiménez, J. N. 2018. Detection of carbapenem resistance genes in *Pseudomonas aeruginosa* isolates with several phenotypic susceptibility profiles. *CES Medicina,* 32**,** 203-14.

Morel, C. M., Lindahl, O., Harbarth, S., De Kraker, M. E. A., Edwards, S. and Hollis, A. 2020. Industry incentives and antibiotic resistance: An introduction to the antibiotic susceptibility bonus. *The Journal of Antibiotics,* 73**,** 421-8.

Motley, M. P., Banerjee, K. and Fries, B. C. 2019. Monoclonal antibody-based therapies for bacterial infections. *Current Opinion in Infectious Diseases,* 32**,** 210-6.

Munoz-Price, L. S., Poirel, L., Bonomo, R. A., Schwaber, M. J., Daikos, G. L., Cormican, M., Cornaglia, G., Garau, J., Gniadkowski, M., Hayden, M. K., Kumarasamy, K., Livermore, D. M., Maya, J. J., Nordmann, P., Patel, J. B., Paterson, D. L., Pitout, J., Villegas, M. V., Wang, H., Woodford, N. and Quinn, J. P. 2013. Clinical epidemiology of the global expansion of *Klebsiella pneumoniae* carbapenemases. *Lancet Infectious Diseases,* 13**,** 785-96.

Muñoz, K. A. and Hergenrother, P. J. 2021. Facilitating compound entry as a means to discover antibiotics for gram-negative bacteria. *Accounts of Chemical Research,* 54**,** 1322-33.

Murphy, C. N., Mortensen, M. S., Krogfelt, K. A. and Clegg, S. 2013. Role of *Klebsiella pneumoniae* type 1 and type 3 fimbriae in colonizing silicone tubes implanted into the bladders of mice as a model of catheter-associated urinary tract infections. *Infection immunology,* 81**,** 3009-17.

Murray, D. C. and Wigglesworth, M. J. Chapter 1:Hts methods: Assay design and optimisation. 2016.

Najafi, M. B. H. and Pezeshki, P. 2014. Bacterial mutation; types, mechanisms and mutant detection methods: A review. *European Scientific Journal, ESJ,* 9.

Narimisa, N., Goodarzi, F. and Bavari, S. 2022. Prevalence of colistin resistance of *Klebsiella pneumoniae* isolates in iran: A systematic review and meta-analysis. *Annals of Clinical Microbiology and Antimicrobials,* 21**,** 29.

Nhgri. 2023. *Plasmid* [Online]. Available at: https://www.genome.gov/genetics-glossary/Plasmid [Accessed 25th April 2023].

Nordmann, P. and Poirel, L. 2014. The difficult-to-control spread of carbapenemase producers among enterobacteriaceae worldwide. *Clinical Microbiology and Infection,* 20**,** 821-30.

Nordmann, P., Cuzon, G. and Naas, T. 2009. The real threat of *Klebsiella pneumoniae* carbapenemase-producing bacteria. *Lancet Infectious Diseases,* 9**,** 228-36.

O'neill, J. 2016. Tackling drug-resistant infections globally: Final report and recommendations.

Padilla, E., Llobet, E., Domenech-Sanchez, A., Martinez-Martinez, L., Bengoechea, J. A. and Alberti, S. 2010. *Klebsiella pneumoniae* acrab efflux pump contributes to antimicrobial resistance and virulence. *Antimicrobial Agents and Chemotherapy,* 54**,** 177-83.

Page, M. G. P. 2013. Siderophore conjugates. *Annals of the New York Academy of Sciences,* 1277**,** 115-26.

Papp-Wallace, K. M., Endimiani, A., Taracila, M. A. and Bonomo, R. A. 2011. Carbapenems: Past, present, and future. *Antimicrobial Agents and Chemotherapy,* 55**,** 4943-60.

Pareek, V., Devineau, S., Sivasankaran, S. K., Bhargava, A., Panwar, J., Srikumar, S. and Fanning, S. 2021. Silver nanoparticles induce a triclosan-like antibacterial action mechanism in multi-drug resistant *Klebsiella pneumoniae*. *Frontiers in Microbiology,* 12.

Parvekar, P., Palaskar, J., Metgud, S., Maria, R. and Dutta, S. 2020. The minimum inhibitory concentration (mic) and minimum bactericidal concentration (mbc) of silver nanoparticles against staphylococcus aureus. *Biomaterial Investigations in Dentistry,* 7**,** 105-9.

Pasteur. 2023. *Bennet, young, bipartisan house colleagues reintroduce bipartisan pasteur act to fight antimicrobial resistance* [Online]. Available at: https://www.bennet.senate.gov/public/index.cfm/2023/4/bennet-young-bipartisan-house-colleagues-reintroduce-bipartisan-pasteur-act-to-fight-antimicrobial-resistance [Accessed 24th April 2023].

Peleg, A. Y. and Hooper, D. C. 2010. Hospital-acquired infections due to gram-negative bacteria. *New England Journal of Medicine,* 362**,** 1804-13.

Pendleton, J. N., Gorman, S. P. and Gilmore, B. F. 2013. Clinical relevance of the eskape pathogens. *Expert Review of Anti-Infective Therapy,* 11**,** 297-308.

Pereira, D. A. and Williams, J. A. 2007. Origin and evolution of high throughput screening. *British Journal of Pharmacology,* 152**,** 53-61.

Petrosillo, N., Taglietti, F. and Granata, G. 2019. Treatment options for colistin resistant *Klebsiella pneumoniae*: Present and future. *Journal of Clinical Medicine,* 8.

Pew 2016. A scientific roadmap for antibiotic discovery: A sustained and robust pipeline of new antibacterial drugs and therapies is critical to preserve public health.

Piddock, L. J. V. 2018. The global antibiotic research and development partnership (gardp): A not-for-profit antibiotic development organisation. *The Lancet Infectious Diseases,* 18**,** 1304-5.

Podschun, R. and Ullmann, U. 1998. Klebsiella spp. As nosocomial pathogens: Epidemiology, taxonomy, typing methods, and pathogenicity factors. *Clinical Microbiology Reviews,* 11**,** 589-603.

Poirel, L., Bonnin, R. A. and Nordmann, P. 2012. Genetic features of the widespread plasmid coding for the carbapenemase oxa-48. *Antimicrobial Agents and Chemotherapy,* 56**,** 559-62.

Poirel, L., Heritier, C., Tolun, V. and Nordmann, P. 2004. Emergence of oxacillinase-mediated resistance to imipenem in *Klebsiella pneumoniae*. *Antimicrobial Agents and Chemotherapy,* 48**,** 15-22.

Popova, A. A., Depew, C., Permana, K. M., Trubitsyn, A., Peravali, R., Ordiano, J. Á. G., Reischl, M. and Levkin, P. A. 2017. Evaluation of the droplet-microarray platform for high-throughput screening of suspension cells. *SLAS Technology,* 22**,** 163-75.

Potter, R. F., D'souza, A. W. and Dantas, G. 2016. The rapid spread of carbapenem-resistant enterobacteriaceae. *Drug Resistance Updates,* 29**,** 30-46.

Quigley, E. M. M. and Gajula, P. 2020. Recent advances in modulating the microbiome. *F1000Research,* 9**,** F1000 Faculty Rev-46.

Ramsamy, Y., Essack, S. Y., Sartorius, B., Patel, M. and Mlisana, K. P. 2018. Antibiotic resistance trends of eskape pathogens in kwazulu-natal, south africa: A five-year retrospective analysis. *African Journal of Laboratory Medicine,* 7**,** 887.

Renwick, M. and Mossialos, E. 2018. What are the economic barriers of antibiotic r&d and how can we overcome them? *Expert Opinion on Drug Discovery,* 13**,** 889-92.

Rice, L. B. 2008. Federal funding for the study of antimicrobial resistance in nosocomial pathogens: No eskape. *Journal of Infectious Diseases,* 197**,** 1079-81.

Rodriguez-Martinez, J. M., Poirel, L. and Nordmann, P. 2009. Molecular epidemiology and mechanisms of carbapenem resistance in *Pseudomonas aeruginosa*. *Antimicrobial Agents and Chemotherapy,* 53**,** 4783-8.

Salmon, S. E., Liu-Stevens, R. H., Zhao, Y., Lebl, M., Krchňák, V., Wertman, K., Sepetov, N. and Lam, K. S. 1996. High-volume cellular screening for anticancer agents with combinatorial chemical libraries: A new methodology. *Molecular Diversity,* 2**,** 57-63.

Santajit, S. and Indrawattana, N. 2016. Mechanisms of antimicrobial resistance in eskape pathogens. *BioMed Research International,* 2016**,** 2475067.

Sawa, T., Kooguchi, K. and Moriyama, K. 2020. Molecular diversity of extended-spectrum beta-lactamases and carbapenemases, and antimicrobial resistance. *Journal of Intensive Care,* 8**,** 13.

Semenov, V. V., Raihstat, M. M., Konyushkin, L. D., Semenov, R. V., Blaskovich, M. A. T., Zuegg, J., Elliott, A. G., Hansford, K. A. and Cooper, M. A. 2021. Antimicrobial screening of a historical collection of over 140 000 small molecules. *Mendeleev Communications,* 31**,** 484-7.

Sharma, N., Sharma, N., Sharma, S., Sharma, P. and Devi, B. 2023. Chapter 3 - identification, morphological, biochemical, and genetic characterization of microorganisms. *In:* Bhatt, A. K., Bhatia, R. K. and Bhalla, T. C. (eds.) *Basic biotechniques for bioprocess and bioentrepreneurship.* Academic Press.

Sheng, Z. K., Li, J. J., Sheng, G. P., Sheng, J. F. and Li, L. J. 2010. Emergence of *Klebsiella pneumoniae* carbapenemase-producing proteus mirabilis in hangzhou, china. *Chinese Medical Journal (Engl.),* 123**,** 2568-70.

Sheppard, A. E., Stoesser, N., German-Mesner, I., Vegesana, K., Sarah Walker, A., Crook, D. W. and Mathers, A. J. 2018. Tetyper: A bioinformatic pipeline for classifying variation and genetic contexts of transposable elements from short-read whole-genome sequencing data. *Microbial Genomics,* 4.

Shun, T. Y., Lazo, J. S., Sharlow, E. R. and Johnston, P. A. 2011. Identifying actives from hts data sets: Practical approaches for the selection of an appropriate hts data-processing method and quality control review. *Journal of Biomolecular Screening,* 16**,** 1-14.

Silver, L. L. 2011. Challenges of antibacterial discovery. *Clinical Microbiology Reviews,* 24**,** 71-109.

Simpkin, V. L., Renwick, M. J., Kelly, R. and Mossialos, E. 2017. Incentivising innovation in antibiotic drug discovery and development: Progress, challenges and next steps. *The Journal of Antibiotics,* 70**,** 1087-96.

Smith, J. R., Rybak, J. M. and Claeys, K. C. 2020. Imipenem-cilastatin-relebactam: A novel β-lactam–β-lactamase inhibitor combination for the treatment of multidrug-resistant gram-negative infections. *Pharmacotherapy: The Journal of Human Pharmacology and Drug Therapy,* 40**,** 343-56.

Spaziante, M., Oliva, A., Ceccarelli, G. and Venditti, M. 2020. What are the treatment options for resistant *Klebsiella pneumoniae* carbapenemase (kpc)-producing bacteria? *Expert Opinion on Pharmacotherapy,* 21**,** 1781-7.

Spellberg, B. and Gilbert, D. 2009. *Rising plague: The global threat from deadly bacteria and our dwindling arsenal to fight them*, Prometheus.

Spellberg, B. and Gilbert, D. N. 2014. The future of antibiotics and resistance: A tribute to a career of leadership by john bartlett. *Clinical Infectious Diseases,* 59 Suppl 2**,** S71-5.

Srinivasan, A., Lee, G. C., Torres, N. S., Hernandez, K., Dallas, S. D., Lopez-Ribot, J., Frei, C. R. and Ramasubramanian, A. K. 2017. High-throughput microarray for antimicrobial susceptibility testing. *Biotechnology Reports (Amst),* 16**,** 44-7.

Stoesser, N., Sheppard, A. E., Peirano, G., Anson, L. W., Pankhurst, L., Sebra, R., Phan, H. T. T., Kasarskis, A., Mathers, A. J., Peto, T. E. A., Bradford, P., Motyl, M. R., Walker, A. S., Crook, D. W. and Pitout, J. D. 2017. Genomic epidemiology of global *Klebsiella pneumoniae* carbapenemase (kpc)-producing escherichia coli. *Scientific Reports,* 7**,** 5917.

Stoner, I. 2020. *Saving lives should be good business. Why doesn't that apply to finding new antibiotics?* [Online]. Available at: https://www.statnews.com/2020/03/18/saving-lives-should-be-good-business-why-doesnt-that-apply-to-finding-new-antibiotics/ [Accessed 15th June 2020].

Tang, Y., Li, G., Liang, W., Shen, P., Zhang, Y. and Jiang, X. 2017. Translocation of carbapenemase gene blakpc-2 both internal and external to transposons occurs via novel structures of tn1721 and exhibits distinct movement patterns. *Antimicrobial Agents and Chemotherapy,* 61.

Tantoh, A. L. A. 2014. *High throughput rna interference based screen for the identification of genes implicated in listeria monocytogenes infection.* University of Cape Town.

Tao, S., Chen, H., Li, N. and Liang, W. 2022. The application of the crispr-cas system in antibiotic resistance. *Infection and Drug Resistance,* 15**,** 4155-68.

Tendencia, E. 2004. Disk diffusion method. *Laboratory manual of standardized methods for antimicrobial sensitivity tests for bacteria isolated from aquatic animals and environment.* Aquaculture Department, Southeast Asian Fisheries Development Center.

Terico, A. T. and Gallagher, J. C. 2014. Beta-lactam hypersensitivity and cross-reactivity. *Journal of Pharmacy Practice,* 27**,** 530-44.

Tesfa, T., Mitiku, H., Edae, M. and Assefa, N. 2022. Prevalence and incidence of carbapenem-resistant k. Pneumoniae colonization: Systematic review and meta-analysis. *Systematic Reviews,* 11**,** 240.

Theuretzbacher, U., Outterson, K., Engel, A. and Karlén, A. 2020. The global preclinical antibacterial pipeline. *Nature Reviews Microbiology,* 18**,** 275-85.

Tofteland, S., Naseer, U., Lislevand, J. H., Sundsfjord, A. and Samuelsen, O. 2013. A long-term low-frequency hospital outbreak of kpc-producing *Klebsiella pneumoniae* involving intergenus plasmid diffusion and a persisting environmental reservoir. *PloS One,* 8**,** e59015.

Torres, N. S., Montelongo-Jauregui, D., Abercrombie, J. J., Srinivasan, A., Lopez-Ribot, J. L., Ramasubramanian, A. K. and Leung, K. P. 2018. Antimicrobial and antibiofilm activity of synergistic combinations of a commercially available small compound library with colistin against *Pseudomonas aeruginosa*. *Frontiers in Microbiology,* 9**,** 2541.

Van Laar, J. A., Rustum, Y. M., Ackland, S. P., Van Groeningen, C. J. and Peters, G. J. 1998. Comparison of 5-fluoro-2'-deoxyuridine with 5-fluorouracil and their role in the treatment of colorectal cancer. *European Journal of Cancer,* 34**,** 296-306.

Varela, M. F., Stephen, J., Lekshmi, M., Ojha, M., Wenzel, N., Sanford, L. M., Hernandez, A. J., Parvathi, A. and Kumar, S. H. 2021. Bacterial resistance to antimicrobial agents. *Antibiotics* [Online], 10.

Verma, N., Prahraj, A. K., Mishra, B., Behera, B. and Gupta, K. 2019. Detection of carbapenemase-producing *Pseudomonas aeruginosa* by phenotypic and genotypic methods in a tertiary care hospital of east india. *Journal of Laboratory Physicians,* 11**,** 287-91.

Wang, G., Song, G. and Xu, Y. 2020. Association of crispr/cas system with the drug resistance in *Klebsiella pneumoniae*. *Infection and Drug Resistance,* 13**,** 1929-35.

Wasfi, R., Rasslan, F., Hassan, S. S., Ashour, H. M. and Abd El-Rahman, O. A. 2021. Co-existence of carbapenemase-encoding genes in *Acinetobacter baumannii* from cancer patients. *Infectious Diseases and Therapy,* 10**,** 291-305.

WEF. 2018. *Antimicrobial resistance: Tackling the gap in r&d resources with pull incentives - in collaboration with wellcome trust* [Online]. Available at: https://www.weforum.org/reports/antimicrobial-resistance-tackling-the-gap-in-r-d-resources-with-pull-incentives-in-collaboration-with-wellcome-trust/ [Accessed 17th March 2021].

WHO. 2017. *Who publishes list of bacteria for which new antibiotics are urgently needed* [Online]. Available at: https://www.who.int/news/item/27-02-2017-who-publishes-list-of-bacteria-for-which-new-antibiotics-are-urgently-needed [Accessed 8th March 2017].

WHO. 2022a. *2021 antibacterial agents in clinical and preclinical development: An overview and analysis,* Geneva, World Health Organization.

WHO. 2022b. *Bacterial vaccines in clinical and preclinical development 2021: An overview and analysis,* Geneva, World Health Organization.

Wilson, B. R., Bogdan, A. R., Miyazawa, M., Hashimoto, K. and Tsuji, Y. 2016. Siderophores in iron metabolism: From mechanism to therapy potential. *Trends in Molecular Medicine,* 22**,** 1077-90.

WHO. 2017. Prioritization of pathogens to guide discovery, research and development of new antibiotics for drug-resistant bacterial infections, including tuberculosis. Geneva: World Health Organization.

Wu, J. Y., Srinivas, P. and Pogue, J. M. 2020. Cefiderocol: A novel agent for the management of multidrug-resistant gram-negative organisms. *Infectious Diseases and Therapy,* 9**,** 17-40.

Yang, Y., Bhachech, N. and Bush, K. 1995. Biochemical comparison of imipenem, meropenem and biapenem: Permeability, binding to penicillin-binding proteins, and stability to hydrolysis by beta-lactamases. *Journal of Antimicrobial Chemotherapy,* 35**,** 75-84.

Yigit, H., Queenan, A. M., Anderson, G. J., Domenech-Sanchez, A., Biddle, J. W., Steward, C. D., Alberti, S., Bush, K. and Tenover, F. C. 2001. Novel carbapenem-hydrolyzing beta-lactamase, kpc-1, from a carbapenem-resistant strain of *Klebsiella pneumoniae*. *Antimicrobial Agents and Chemotherapy,* 45**,** 1151-61.

Yong, D., Toleman, M. A., Giske, C. G., Cho, H. S., Sundman, K., Lee, K. and Walsh, T. R. 2009. Characterization of a new metallo-beta-lactamase gene, bla(ndm-1), and a novel erythromycin esterase gene carried on a unique genetic structure in *Klebsiella pneumoniae* sequence type 14 from india. *Antimicrobial Agents and Chemotherapy,* 53**,** 5046-54.

Younis, W., Thangamani, S. and Seleem, M. N. 2015. Repurposing non-antimicrobial drugs and clinical molecules to treat bacterial infections. *Current Pharmaceutical Design,* 21**,** 4106-11.

Younis, W., Abdelkhalek, A., Mayhoub, A. S. and Seleem, M. N. 2017. In vitro screening of an fda-approved library against eskape pathogens. *Current Pharmaceutical Design,* 23**,** 2147-57.

Yusof, N. Y., Norazzman, N. I., Hakim, S. N., Azlan, M. M., Anthony, A. A., Mustafa, F. H., Ahmed, N., Rabaan, A. A., Almuthree, S. A., Alawfi, A., Alshengeti, A., Alwarthan, S., Garout, M., Alawad, E. and Yean, C. Y. 2022. Prevalence of mutated colistin-resistant *Klebsiella pneumoniae*: A systematic review and meta-analysis. *Tropical Medicine and Infectious Disease* [Online], 7.

Zhang, J. H., Chung, T. D. and Oldenburg, K. R. 1999. A simple statistical parameter for use in evaluation and validation of high throughput screening assays. *Journal of Biomolecular Screening,* 4**,** 67-73.

Zhang, Y., Guo, L. Y., Song, W. Q., Wang, Y., Dong, F. and Liu, G. 2018. Risk factors for carbapenem-resistant k. Pneumoniae bloodstream infection and predictors of mortality in chinese paediatric patients. *BMC Infectious Diseases,* 18**,** 248.

Zhen, X., Lundborg, C. S., Sun, X., Hu, X. and Dong, H. 2019. Economic burden of antibiotic resistance in eskape organisms: A systematic review. *Antimicrobial Resistance and Infection Control,* 8**,** 137.

Zheng, R., Zhang, Q., Guo, Y., Feng, Y., Liu, L., Zhang, A., Zhao, Y., Yang, X. and Xia, X. 2016. Outbreak of plasmid-mediated ndm-1-producing *Klebsiella pneumoniae* st105 among neonatal patients in yunnan, china. *Annals of Clinical Microbiology and Antimicrobials,* 15**,** 10.